1985

Molecular beam photoionization spectrometry (1) photoionization studies of high temperature vapors (2) state-selected and state-to-state studies of electron transfer reactions

Chung-Lin Liao
Iowa State University

INFORMATION TO USERS

This reproduction was made from a copy of a manuscript sent to us for publication and microfilming. While the most advanced technology has been used to photograph and reproduce this manuscript, the quality of the reproduction is heavily dependent upon the quality of the material submitted. Pages in any manuscript may have indistinct print. In all cases the best available copy has been filmed.

The following explanation of techniques is provided to help clarify notations which may appear on this reproduction.

1. Manuscripts may not always be complete. When it is not possible to obtain missing pages, a note appears to indicate this.

2. When copyrighted materials are removed from the manuscript, a note appears to indicate this.

3. Oversize materials (maps, drawings, and charts) are photographed by sectioning the original, beginning at the upper left hand corner and continuing from left to right in equal sections with small overlaps. Each oversize page is also filmed as one exposure and is available, for an additional charge, as a standard 35mm slide or in black and white paper format.*

4. Most photographs reproduce acceptably on positive microfilm or microfiche but lack clarity on xerographic copies made from the microfilm. For an additional charge, all photographs are available in black and white standard 35mm slide format.*

***For more information about black and white slides or enlarged paper reproductions, please contact the Dissertations Customer Services Department.**

Liao, Chung-Lin

MOLECULAR BEAM PHOTOIONIZATION SPECTROMETRY. (1) PHOTOIONIZATION STUDIES OF HIGH TEMPERATURE VAPORS. (2) STATE-SELECTED AND STATE-TO-STATE STUDIES OF ELECTRON TRANSFER REACTIONS

Iowa State University PH.D. 1985

PLEASE NOTE:

In all cases this material has been filmed in the best possible way from the available copy. Problems encountered with this document have been identified here with a check mark __√__.

1. Glossy photographs or pages _____
2. Colored illustrations, paper or print _____
3. Photographs with dark background _____
4. Illustrations are poor copy _____
5. Pages with black marks, not original copy _____
6. Print shows through as there is text on both sides of page _____
7. Indistinct, broken or small print on several pages __√__
8. Print exceeds margin requirements _____
9. Tightly bound copy with print lost in spine _____
10. Computer printout pages with indistinct print _____
11. Page(s) _____ lacking when material received, and not available from school or author.
12. Page(s) _____ seem to be missing in numbering only as text follows.
13. Two pages numbered _____. Text follows.
14. Curling and wrinkled pages _____
15. Dissertation contains pages with print at a slant, filmed as received _____
16. Other _____

_____

_____

University
Microfilms
International

Molecular beam photoionization spectrometry

(1) photoionization studies of high temperature vapors

(2) state-selected and state-to-state studies of electron transfer reactions

by

Chung-Lin Liao

A Dissertation Submitted to the

Graduate Faculty in Partial Fulfillment of the

Requirements for the Degree of

DOCTOR OF PHILOSOPHY

Department: Chemistry

Major: Physical Chemistry

Approved:

Signature was redacted for privacy.

In Charge of Major Work

Signature was redacted for privacy.

For the Major Department

Signature was redacted for privacy.

For the Graduate College

Members of the Committee:

Signature was redacted for privacy.

Iowa State University
Ames, Iowa

1985

TABLE OF CONTENTS

GENERAL INTRODUCTION

Ionization and dissociation are usually the predominant processes when a molecule absorbs a vacuum ultraviolet (VUV) photon. The measurement of the ionization cross sections for a particular ionizing channel with variable photon excitation energies is the subject of photoionization experiments. Many of the most accurate ionization energies (IE) and appearance energies (AE) of fragment ions were obtained by the photoionization method. Reliable thermochemical information can be deduced from these measurements. This technique has proved to be a useful tool in the elucidation of the interaction of Rydberg states with continuum states. Information on potential energy surfaces can be explored by photoionization studies as well.[1,2]

The resolution achieved in photoionization experiments has been limited mainly by the low VUV light intensity which is partly due to the low reflectivity of diffraction gratings in this region. In order to circumvent this difficulty, conventional photoionization studies usually employ the gas-cell method with fairly high pressure in the gas-cell.[1,3] Unfortunately, the obtainable resolution was often limited by the rotational or low-frequency vibrational excitations of molecules at a given temperature. For gases with low condensation temperatures such as H_2, N_2, O_2, the hot-band effects can be overcome by cooling the sample gas in cell to lower temperatures.[4] Obviously, this method is not applicable to gas with high condensation temperatures.

An alternative to the gas-cell method is the supersonic molecular

beam technique. A supersonic molecular beam involves the expansion of a gas or the vapor of a liquid or solid at high pressure through a small orifice into an evacuated region at lower pressure. The molecules undergo many collisions during the expansion. The primary effect of the expansion is the conversion of random translational, rotational, and vibrational energies of the molecules into directed mass flow, and this causes the lowering of the translational, vibrational and rotational temperatures. In most cases, the translational temperature will reach nearly 0 K. Rotational and vibrational temperatures as low as 0.17 K and 20-50 K, respectively, have been reported for polyatomic molecules by this method.[5] Thus, in comparison to gas-cell experiments, supersonic expansion of the target gas can greatly improve the resolution while still providing a high constant flux of molecules at the ionization region. Further, if the molecule is sampled downstream in a collisionless environment, the secondary process encountered in gas-cell photoionization studies can be eliminated. For these reasons, the molecular beam method has been adapted for use in the present photoionization mass spectrometric studies. The advantages of this method have been demonstrated in a series of molecular-beam photoionization studies.[6-27]

Charge transfer reaction is one of the most interesting processes when an ion collides with a neutral atom or molecule. When such a reaction is exothermic, it is usually a dominant product channel in the outcome of ion-neutral interactions. Because of their large cross

sections, charge transfer reactions play a significant role in relaxation processes and reaction kinetics in ionized gases. Although the concentrations of ions in flames are low, thermal charge exchange processes are possible pathways for the conversion of ions into free radical chain carriers. Therefore, the microscopic understanding of these phenomena is of particular interest to gas discharges, lasers, flames, and controlled thermonuclear fusion research.

At the present stage, the theory of charge exchange between atomic ions and atoms is quite well-developed.[28-41] However, the detailed theoretical understanding of charge transfer processes involving molecular ions, in which energy can be transferred to or from internal motions of molecules and/or molecular ions, is still in a rudimentary state. The symmetric charge transfer reaction has been the subject of many theoretical studies.[33,42-47] The simplicity of this reaction makes it an important system for the detailed investigation of the dynamics of charge transfer processes.

The symmetric charge transfer reaction

$$H_2^+(v_o') + H_2(v_o'' = 0) \rightarrow H_2(v') + H_2^+(v'') \qquad (1)$$

has been chosen for the first study partly because of the availability of several theoretical calculations on this system.[43-47] This reaction was not observed in the state-selected studies of Koyano and Tonaka[48] and Anderson et al.[49] using the gas-cell arrangement. The relative total cross sections for Reaction (1) as a function of the

vibrational energy distribution of $H_2^+(v_o')$ reactant ions measured at collision energy $E_{c.m.}$ = 215 eV was reported by Chupka.[50] The only reported vibrational-state-selected total cross sections measurements for Reaction (1) was performed by Campbell et al.[51] using photoion-photoelectron coincidence (PIPECO) method and effusive H_2 sources. The relative total charge transfer cross sections for Reaction (1) were found to vary with v_o' in an abrupt way.

The work of Chupka and co-workers[52-55] shows that because of the dominance of autoionization with $\Delta v = -1$ over predissociation, H_2^+ at vibrational states v_o' = 0-5 can be prepared with high purity by the simple photoionization. This requires the photoionization at high resolution to select specific autoionization peaks and to minimize the contribution from direct photoionization processes. The fact that autoionization processes are much stronger than direct ionization in H_2 allows the preparation of $H_2^+(v_o' = 0\text{-}5)$ at higher intensities than can be prepared by the PIPECO method.

We have successfully combined the high resolution photoionization mass spectrometric method and the crossed ion-neutral beam technique to examine the internal and kinetic energy effect on the total cross sections for symmetric charge transfer reactions $H_2^+ + H_2$ and $Ar^+ + Ar$. By using the cross ion-neutral supersonic beam technique, we have not only minimized the secondary reactions of the charge transfer H_2^+ ions with background neutral H_2 molecules to form $H_3^+ + H$ at low kinetic energies, but also attained higher kinetic energy resolutions as compared

to using an ion beam-gas cell experiment arrangement. We have also developed a charge transfer detector to probe the vibrational state distribution of the product H_2^+ ions in $H_2^+ + H_2$ reaction and the spin-orbit state distribution of the product Ar^+ ions in $Ar^+ + Ar$ reaction.

Explanation of Thesis Format

This thesis consists of six sections which can be grouped into two main parts. Each section represents an independent article in a format ready for submission for publication with minor modifications. The figures, tables and references cited in each section refer only to those contained in that section. The references cited in the General Introduction and General Summary are contained in the reference section at the end of the dissertation.

PART 1. PHOTOIONIZATION STUDIES OF HIGH TEMPERATURE VAPORS

SECTION I. MOLECULAR BEAM PHOTOIONIZATION STUDY OF S_2

Abstract

Higher resolution photoionization efficiency data for the formation of S_2^+ and S^+ from S_2 in the wavelength region of 600-1350 Å have been obtained using the supersonic oven beam method. The ionization energy (IE) of S_2 is determined to be 9.356 ± 0.002 eV (1325.2 ± 0.3 Å). The measured appearance energy of 14.732 ± 0.005 eV (841.6 ± 0.3 Å) for the dissociative ionization process $S_2 + h\nu \rightarrow S^+ + S + e^-$, together with the IE of S_2, yields a value of 5.376 ± 0.005 eV for the bond dissociation energy of S_2^+. Two Rydberg series converging to the $\tilde{b}^4\Sigma_g^-$ state (13.20 eV) of S_2^+ are observed. Window resonances resolved in the wavelength region of 650-850 Å are assigned as members of the Rydberg series converging to the $\tilde{c}^4\Sigma_u^-$(17.70 eV) and $^2\Pi_u$ (or $^2\Sigma_u^-$) (18.66 eV) states of S_2^+.

Introduction

Due to the difficulty in the preparation of S_2, only a few spectroscopic studies of S_2 in the vacuum ultraviolet (VUV) region have been made. The VUV absorption[1] and photoelectron spectra of S_2[2-4] have provided information about the ground and excited states of S_2^+. The photoionization efficiency (PIE) spectrum for S_2^+ has been measured by Berkowitz and co-workers[5,6] using an effusive source of S_2 produced from heated HgS. In addition to giving a value of 9.36 ± 0.02 eV for

the ionization energy (IE) for the $\tilde{X}^2\Pi_{3/2g}$ state of S_2^+, the previous photoionization study reveals rich autoionization structure in the wavelength region of ∿ 950-1250 Å. No attempt was made by the authors to assign the autoionization peaks found in the PIE curve of S_2^+. Therefore, the nature of the Rydberg states at energies above the IE of S_2 is essentially unexplored.

The vapor produced by heating elemental sulphur may contain many higher molecular weight species other than S_2. Since moderately high temperatures are needed to produce pure S_2 vapor, the rotational and vibrational hot-band effects are expected to be severe. As demonstrated in previous studies[7,8] the supersonic oven beam method is a useful technique to overcome the rotational hot-band effects and allows higher resolution PIE spectra to be obtained for high temperature vapors. This report presents PIE data for S_2^+ measured using the supersonic oven beam method. The higher resolution PIE curve for S_2^+ obtained in this experiment has made possible the assignments of some autoionization peaks found in the wavelength region of 670-995 Å. Rydberg structures observed here in the wavelength region of ∿ 670-940 Å were unresolved in the previous photoionization mass spectrometric study.[6]

Experimental

The experimental procedures and arrangement are similar to those described previously.[7,8] Briefly, the apparatus consists of a windowless 3-m near normal incidence VUV monochromator (McPherson 2253 M),

an oven-type supersonic beam production system, a capillary discharge light source, a VUV light detector, and a quadrupole mass filter for ion detection. The grating is a Bausch and Lomb 1200 lines/mm MgF_2 coated aluminum grating blazed at 1360 Å. Either the hydrogen many-lined pseudocontinuum or the helium Hopfield continuum is used as the light source, depending on the wavelength region desired.

The oven beam source is a two-stage stainless steel oven. The temperature of the first stage (the main oven) is maintained at $\sim$ 450 K. The vapor pressure at this temperature was estimated to be a few Torr. In order to assure the predominance of S_2 in the sulphur vapor, the second stage of the oven (the nozzle) is kept at a temperature of $\sim$ 850 K. The relative concentrations of S_n, n = 1-10, species in the vapor depend critically on temperature and pressure.[9] At temperatures higher than 600 K and at pressures less than $\sim$ 1 Torr, the vapor phase of sulphur is dominated by S_2. The S_2 supersonic beam is formed by seeding the sulphur vapor in $\sim$ 500 Torr of He and then expanding the mixture through the nozzle. After the expansion, the S_2 beam is further collimated by a heated skimmer. Maintaining the skimmer at a temperature close to that of the main oven, eliminates the condensation problem. Under the conditions described above, S_4 and S_3 are the major impurities. The intensities for S_4^+ and S_3^+ observed at 800 Å are less than 5% that of S_2^+.

All of the PIE spectra presented here are based on at least two reproducible scans. The wavelength scales are calibrated by using

known atomic resonance lines, or H_2 emission lines[10] when the H_2 pseudo-continuum is used.

Results and Discussion

The PIE data for S_2^+ obtained with a wavelength resolution of 1.4 Å (FWHM) in the region of 610-1340 Å are plotted in Figures 1(a) and 1(b) at intervals of 0.5 Å. The general features of the S_2^+ spectrum recorded here are consistent with those reported by Berkowitz and Chupka.[6] High resolution [0.28 Å (FWHM)] PIE data in the region of 1340-1100 Å have also been accumulated. Since no new structure was found in the high resolution spectrum, only the portion near the ionization onset of S_2 (1320-1328 Å) is shown in the upper left hand corner of Figure 1(a). Figures 2(a) and 2(b) show the high resolution PIE spectrum for S_2^+ in the region of ∿ 840-1000 Å.

In the one-electron approximation, the ground state electronic configuration for S_2 is $...(3s\sigma_g)^2\ (3s\sigma_u)^2\ (3p\sigma_g)^2\ (3p\pi_u)^4\ (3p\pi_g)^2$ ($\tilde{X}\ ^3\Sigma_g^-$). The removal of an electron from the valence orbitals gives rise to the ionic states $\tilde{X}^2\Pi_g$, $\tilde{a}^4\Pi_u$, $\tilde{A}^2\Pi_u$, $\tilde{b}^4\Sigma_g^-$, $\tilde{B}^2\Sigma_g^-$, $^2\Pi_u$, $\tilde{c}^4\Sigma_u^-$, and $^2\Sigma_u^-$ etc. in the order of increasing energy.

The IE for the states of S_2^+ determined by photoelectron spectroscopy[2] are indicated in Figures 1(a)-(b) and 2(a)-(b). No apparent structures correlating to the onsets of these states can be seen except for the $\tilde{X}^2\Pi_{3/2g}$ and $^2\Pi_{1/2g}$ states. The IE for S_2^+ ($\tilde{X}^2\Pi_{3/2g}$) is marked by a sharp step at 1325.5 ± 1.5 Å in the low resolution spec-

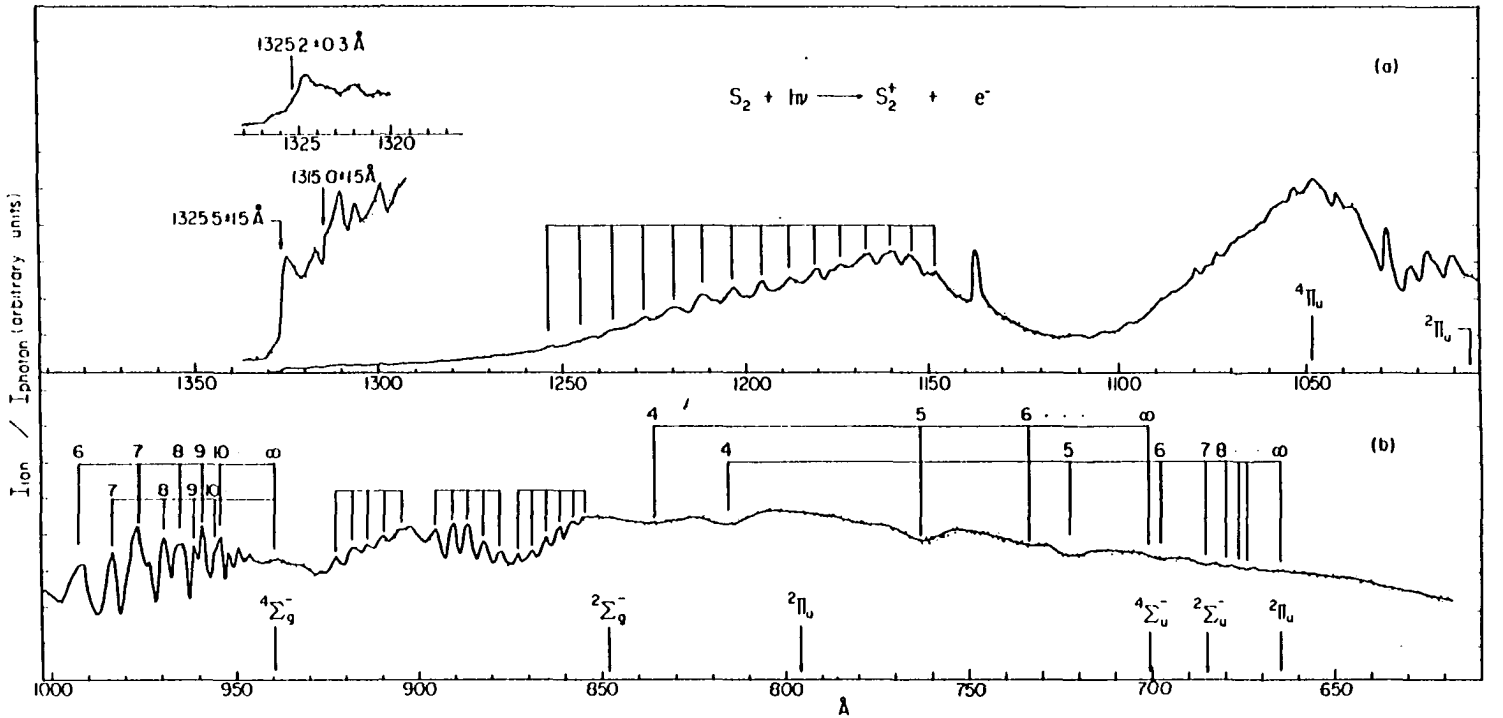

Figure 1. PIE curves for S_2^+ in the region of (a) 1000-1340 Å and (b) 620-1000 Å [wavelength resolution = 1.4 Å (FWHM)]

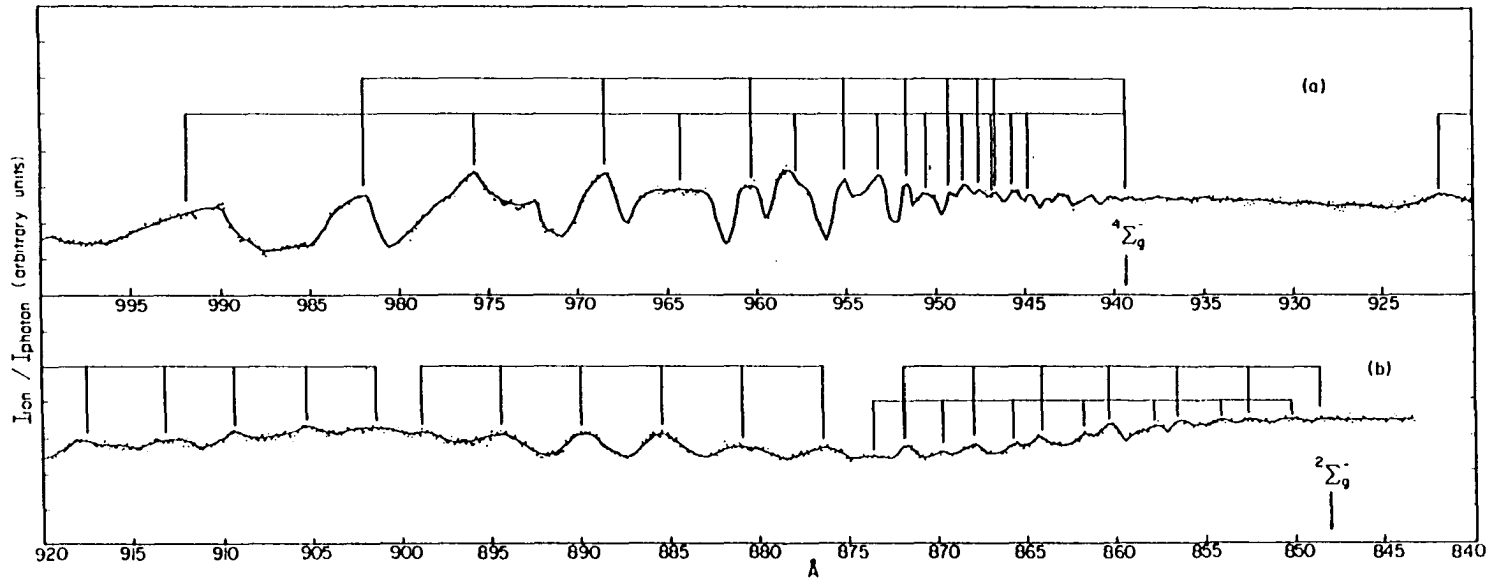

Figure 2. PIE curves for S_2^+ in the region of (a) 920-1000 Å and (b) 840-920 Å [wavelength resolution = 0.28 Å (FWHM)]

trum. A more accurate value of 1325.2 ± 0.3 Å (9.356 ± 0.002 eV) for the IE for $S_2^+(\tilde{X}^2\Pi_{3/2g})$ is determined from the high resolution PIE data (see Figure 1(a)). The latter value is in good agreement with the value of 9.36 ± 0.02 eV determined by the previous photoionization experiment[6] but slightly lower than that (9.38 ± 0.01 eV) found in the photoelectron spectroscopic study of Dyke et al.[2] The onset for the $^2\Pi_{1/2g}$ state of S_2^+ is less apparent. If the minor step at 1315 ± 1.5 Å is assigned to be the IE for the $^2\Pi_{1/2g}$ state of S_2^+, the spin-orbit splitting of the $^2\Pi_g$ state is estimated to be 600 ± 125 cm^{-1} from the low resolution PIE spectrum for S_2^+. Taking into account the experimental uncertainties, this value is consistent with the photoelectron result[2] of 470 ± 25 cm^{-1} and the value of 469.7 ± 2.3 cm^{-1} resulting from the rotational analysis[11] of the $\tilde{A}$ - $\tilde{X}$ bands of S_2^+. It is possible that autoionization features appearing at the ionization threshold have affected the position of the minor step associated with the IE for the $^2\Pi_{1/2g}$ state. The minor step is not discernible in the high resolution S_2^+ spectrum.

The positions of autoionizing vibrational bands superimposed on a strong and broad autoionization peak in the region of 1140-1260 Å, between the IE's of the $\tilde{X}^2\Pi_g$ and $\tilde{a}^4\Pi_u$ states of S_2^+, are summarized in Table 1. The spacing between adjacent vibrational bands varies in the range of ∿ 580-450 cm^{-1} with an average vibrational spacing of 525 cm^{-1}. It is likely that these vibrational bands can be grouped into more than one vibrational progression. The detailed assignment of these autoionizing vibrational features awaits a higher resolution study in

Table 1. Progression of vibrational bands of S_2 in the range of 1140-1260 Å

$\nu(cm^{-1})^a$	$\Delta\nu(cm^{-1})^b$
87,108	
	453
86,555	
	448
86,207	
	481
85,726	
	511
85,215	
	505
84,710	
	499
84,211	
	564
83,647	
	556
83,091	
	583
82,508	
	541
81,967	
	501
81,466	
	560
80,906	
	585
80,321	
	576
79,745	
	$\Delta\nu_{av}{}^c = 526$

[a] Estimated positions of the band centers.

[b] Spacings between adjacent vibrational bands.

[c] The average vibrational spacing.

the future. Similar autoionizing vibrational bands resolved in the PIE curve for O_2^+ below the IE of the $\tilde{a}^4\Pi_u$ state of O_2^+ are much stronger and have been attributed to vibrational progressions of Rydberg series converging to the $\tilde{a}^4\Pi_u$ state of O_2^+.[12,13]

Strong autoionization peaks appearing in the region of 945-1000 Å can be assigned as members of two Rydberg series converging to the $\tilde{b}^4\Sigma_g^-$ state of S_2^+ at 13.20 eV.[2] The positions of members of these Rydberg series, which are called Rydberg series I and II here, are listed in Table 2. According to the photoelectron spectrum of S_2 obtained by Dyke et al.,[2] the $S_2^+(\tilde{b}^4\Sigma_g^-) \leftarrow S_2(\tilde{X}^3\Sigma_g^-)$ electronic band is dominated by the (0,0) vibrational transition. It is likely that the positions of autoionizing peaks listed in Table 2 correspond to the (0,0) vibrational bands of the Rydberg transitions. In the case of O_2, two Rydberg series, one strong and one weak, were observed to converge to the $\tilde{b}^4\Sigma_g^-$ state of O_2^+.[12-15] It was suggested that the Rydberg states of the strong Rydberg series originated from the excitation of one of the $2p\sigma_g$ electron to a $np\sigma_u$ orbital.[16] Yoshino and Tanaka[14] speculate that the weak series might arise from the excitation of a $2p\sigma_g$ electron to a $ns\sigma$ or $nd\sigma$ orbital. The two Rydberg series of S_2 observed here are similar in intensity with Rydberg series I slightly stronger than Rydberg series II. The values for the effective principal quantum number, n^*, for Rydberg series I (Table 2) are similar to the n^*-values for the strong Rydberg series converging to the $\tilde{b}^4\Sigma_g^-$ state of O_2^+. The approximate quantum defects, δ, in the Rydberg series of the free atomic sulfur are δ = 2.0 for ns, 1.6 for np, and 0.3 for nd orbitals.[17] If the first members of Rydberg series I and II are assumed to have the values of 6 and 7 for n, the quantum defects for Rydberg series I and II are calculated to be $\sim$ 1.6 and $\sim$ 2.1, respectively. Therefore, it is logical

Table 2. Rydberg series I and II of S_2 observed in the region of 935-1000 Å

n	E(n) (eV) Series I	E(n) (eV) Series II	n* [a]		δ [b]	
6	12.501 (991.8 Å)	...	4.412	...	1.88	...
7	12.715 (975.1 Å)	12.626 (982.0 Å)	5.300	4.868	1.70	2.13
8	12.858 (964.3 Å)	12.802 (968.5 Å)	6.303	5.845	1.70	2.16
9	12.945 (957.8 Å)	12.911 (960.3 Å)	7.301	6.862	1.70	2.14
10	13.906 (953.3 Å)	12.980 (955.2 Å)	8.372	7.864	1.63	2.14
11	13.044 (950.5 Å)	13.028 (951.7 Å)	9.345	8.887	1.66	2.11
12	13.073 (948.4 Å)	13.061 (949.3 Å)	10.353	9.882	1.65	2.12
13	13.095 (946.8 Å)	13.086 (947.5 Å)	11.392	10.900	1.61	2.10
14	13.112 (945.6 Å)	...	12.419	...	1.58	...
15	13.123 (944.8 Å)	...	13.404	...	1.60	...
Series limit	IE($\tilde{b}^4\Sigma_g^-$) 13.20[c]	IE($\tilde{b}^4\Sigma_g^-$) 13.20[c]				

[a] Effective principal quantum number.

[b] Quantum defect.

[c] Reference 2.

to associate Rydberg series I with Rydberg transitions $X^3\Sigma_g^- \rightarrow \ldots (3s\sigma_g)^2 (3s\sigma_u)^2 (3p\sigma_g) (3p\pi_u)^4 (3p\pi_g)^2 np\sigma_u \, ^3\Sigma_u^-$, n = 6 ..., and Rydberg series II with transitions $X^3\Sigma_g^- \rightarrow \ldots (3s\sigma_g)^2 (3s\sigma_u)^2 (3p\sigma_g) (3p\pi_u)^4 (3p\pi_g)^2 ns\sigma_u \, ^3\Sigma_u^-$, n = 7 .... The satisfactory fits obtained

for Rydberg series I and II using 13.20 eV as the convergence limit suggest that the value for the IE for S_2^+ ($\tilde{b}^4\Sigma_g^-$) determined by Dyke et al.[2] is accurate.

The low resolution PIE curve for S_2^+ [Figure 1(b)] shows three autoionizing vibrational progressions in the region of 850-930 Å. The high resolution spectrum of S_2^+ for the same region [Figures 2(a)-(b)] reveals an additional progression. The positions of the vibrational bands belonging to progressions I, II, III, and IV are listed in Table 3. The average vibrational spacings of progressions I, II, III, and IV are 498, 568, 527, and 529 cm^{-1}, respectively. These progressions most likely belong to Rydberg states converging to the $\tilde{B}^2\Sigma_g^-$ state of S_2^+ at 14.62 eV. The $\tilde{B}^2\Sigma_g^-$ photoelectron band of S_2^+ was found previously[2] to have a progression of six vibrational bands with an average vibrational spacing of 546 cm^{-1}.

In the wavelength region of $\sim$ 650-850 Å, the PIE curve for S_2^+ shows a series of autoionizing states appearing as window resonances. These resonances are broadened, due in part to fast predissociation of S_2^+ to form $S^+ + S$ in this region. The analysis of the window resonances is summarized in Table 4. Using the values of 17.70 and 18.66 eV for the IE's of the $\tilde{c}^4\Sigma_u^-$ and $^2\Pi_u$ (or $^2\Sigma_u^-$)[18] states, we have satisfactorily grouped these features into two Rydberg series, series III and IV, converging to the $\tilde{c}^4\Sigma_u^-$ and $^2\Pi_u$ (or $^2\Sigma_u^-$) states, respectively. The n^*-values calculated for series III and IV are similar to those observed by Codling and Madden[16] for Rydberg series of O_2 converging

Table 3. Progressions of vibrational bands of S_2 observed in the region of 845-925 Å

Progression I		Progression II		Progression III		Progression IV	
$\nu(cm^{-1})^a$	$\Delta\nu(cm^{-1})^b$	$\nu(cm^{-1})^a$	$\Delta\nu(cm^{-1})^b$	$\nu(cm^{-1})^a$	$\Delta\nu(cm^{-1})^b$	$\nu(cm^{-1})^a$	$\Delta\nu(cm^{-1})^b$
108,460		111,247		114,456		114,679	
	520		560		526		541
108,980		111,807		114,982		115,220	
	513		565		531		521
109,493		112,372		115,513		115,741	
	482		558		537		511
109,975		112,930		116,050		116,252	
	486		590		527		530
110,461		113,520		116,577		116,782	
	490		570		505		534
110,951		114,090		117,082		117,316	
					537		539
				117,619		117,855	
$\Delta\nu_{av}{}^c = 498$		$\Delta\nu_{av}{}^c = 568$		$\Delta\nu_{av}{}^c = 527$		$\Delta\nu_{av}{}^c = 529$	

[a]Estimated positions of the band centers.

[b]Spacings between adjacent vibrational bands.

[c]The average vibrational spacing.

Table 4. Rydberg series III and IV of S_2 observed in the region of 660-850 Å

n	E(n) (eV) Series III	E(n) (eV) Series IV	n^* [a]	b
4	14.840(835.5 Å)		2.181	1.819
		15.204(815.4 Å)	1.985	2.015
5	16.271(762.0 Å)		3.086	1.914
		17.161(722.5 Å)	3.012	1.988
6	16.915(733.0 Å)		4.163	1.837
		17.788(697.0 Å)	3.951	2.049
7	...		...	...
		18.100(685.5 Å)	4.929	2.071
8	...		...	...
		18.273(678.5 Å)	5.932	2.068
Series limit	IE($c^4\Sigma_u^-$) 17.70[c]	IE($^2\Pi_u$ or $^2\Sigma_u^-$) 18.66[c]		

[a] Effective principal quantum number.

[b] Quantum defect.

[c] Reference 2.

to the $c^4\Sigma_u^-$ state of O_2^+. The PIE spectrum of O_2^+ obtained by Dehmer and Chupka[13] shows that the first members of one of the Codling and Madden's Rydberg series in the region of 580-596 Å appear as broad window resonances. These Rydberg states of O_2 have been assigned[19,20] to Rydberg transitions of a $2s\sigma_u$ electron to an $ns\sigma_g$ orbital. Assuming n = 4 for the first members of Rydberg series III and IV, the δ-values are found to be close to that for a free sulfur atom in the ns orbital. This observation suggests that Rydberg series III and IV involved tran-

sitions to ns -type Rydberg orbitals.

The PIE curve for S^+ from S_2 in the region of 730-850 Å obtained using a wavelength resolution of 1.4 Å (FWHM) is shown in the lower part of Figure 3. The low resolution S^+ spectrum is consistent with that reported by Berkowitz and Chupka.[6] The appearance energy (AE) for S^+ formed by the process

$$S_2 + h\nu \rightarrow S^+ + S + e^- \qquad (2)$$

is determined to be 841.5 ± 1.5 Å from the low resolution spectrum. The high resolution [0.28 Å (FWHM)] PIE data for S^+ in the region of 825-845 Å are plotted in the upper part of Figure 3, showing that the value of 14.732 ± 0.005 eV (841.6 ± 0.3 Å) for the AE of S^+ can be obtained directly without the correction for hot-band effects. The AE for S^+ determined here is in good agreement with a value of 14.74 ± 0.01 eV deduced in the previous photoionization study.[6] The latter value was obtained by correcting for the shift of the measured AE for S^+ due to initial thermal energy of S_2. Combining the IE of S_2 and AE for process (2) measured in this experiment, we obtain a value of 5.376 0.005 eV for the bond dissociation energy of S_2^+. The AE for S^+, together with the known IE (10.360 eV)[21] for the sulfur atom, allows the calculation of a value of 4.372 eV for the bond dissociation energy of S_2. Taking into account the experimental uncertainties, the latter value is in accord with the spectroscopic value of 4.3693 eV deduced by Ricks and Barrow.[22]

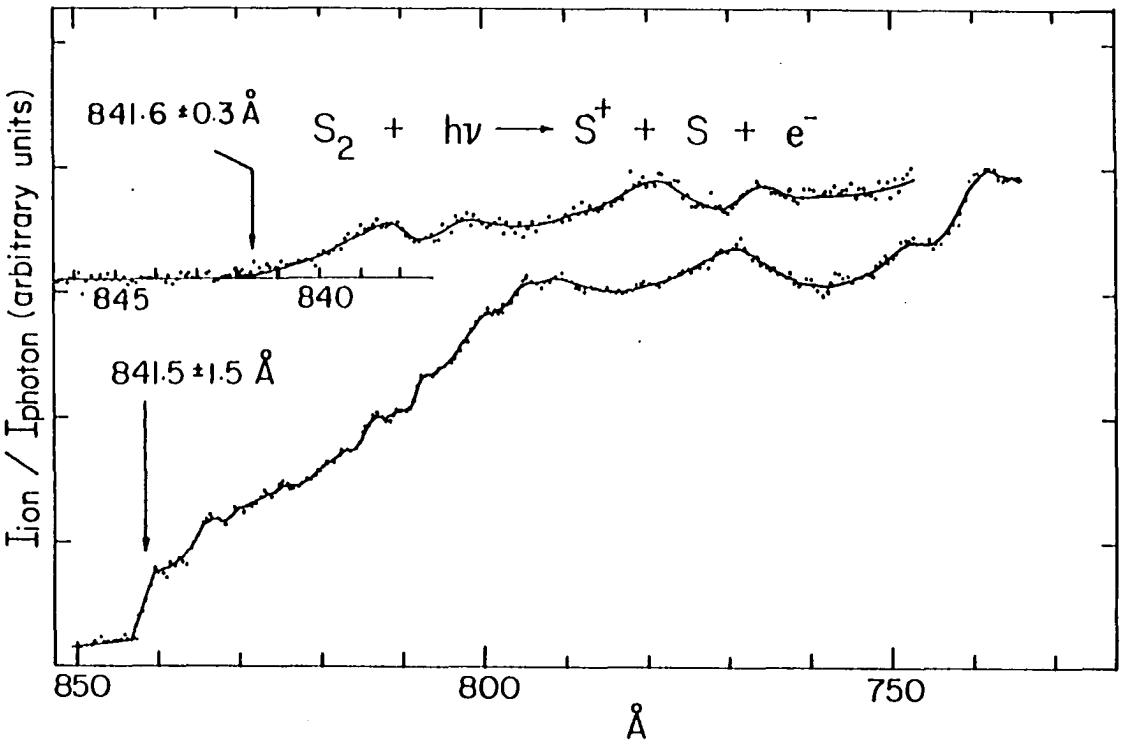

Figure 3(a). PIE curve for S^+ in the region of 730-850 Å [wavelength resolution = 1.4 Å (FWHM)]

Figure 3(b). PIE curve for S^+ in the region of 825-846.5 Å [wavelength resolution = 0.29 Å (FWHM)]

References

1. R. J. Donovan, D. Husain, C. D. Stevenson, Trans. Faraday Soc. 66, 1 (1970).

2. J. M. Dyke, L. Golob, N. Jonathan, and A. Morris, J. Chem. Soc. Faraday Trans. II 71, 1026 (1975).

3. J. Berkowitz, J. Chem. Phys. 62, 4074 (1975).

4. M. Wu and T. P. Fehlner, J. Am. Chem. Soc. 98, 7578 (1976).

5. J. Berkowitz and C. Lifshitz, J. Chem. Phys. 48, 4346 (1968).

6. J. Berkowitz and W. Chupka, J. Chem. Phys. 50, 4245 (1969).

7. S. H. Linn, J. M. Brom, Jr., W.-B. Tzeng, and C. Y. Ng, J. Chem. Phys. 78, 37 (1983).

8. S. H. Linn, W.-B. Tzeng, J. M. Brom, Jr., and C. Y. Ng, J. Chem. Phys. 78, 50 (1965).

9. J. Berkowitz, in "Elemental Sulphur," edited by B. Meyer (Interscience, New York, 1965).

10. K. E. Schubert and R. D. Hudson, Rep. No. ATN-64 (9233)-2 (Aerospace Corp., Los Angeles, 1963).

11. A. J. Capel, J. H. D. Eland, and R. F. Barrow, Chem. Phys. Lett. 82, 496 (1981).

12. W. C. Price and G. Collins, Phys. Rev. 48, 714 (1935).

13. P. M. Dehmer and W. A. Chupka, J. Chem. Phys. 62, 4525 (1975).

14. K. Yoshino and Y. Tanaka, J. Chem. Phys. 48, 4859 (1968).

15. T. Takamine and Y. Tanaka, Phys. Rev. 59, 771 (1941).

16. K. Codling and R. P. Madden, J. Chem. Phys. 42, 3935 (1965).

17. E. Lindholm, Ark. Fys. 40, 97 (1969).

18. The designation of the states at 18.10 and 18.66 eV is uncertain (see Ref. 2).

19. E. Lindholm Ark. Fys. 40, 117 (1969).

20. B. Narayana and W. C. Price. J. Phys. B 5, 1784 (1972).

21. C. E. Moore, Natl. Stand. Ref. Data Ser., Natl. Bur. Stand. NSRDS-NBS34 (1970).

22. J. M. Ricks and R. F. Barrow, Can. J. Phys. 47, 2423 (1969).

SECTION II. MOLECULAR BEAM PHOTOIONIZATION STUDY OF Hg_2

Abstract

Photoionization efficiency data for Hg_2^+ have been obtained in the region of 650-1400 Å. The ionization energy of Hg_2 was determined to be 9.103±0.010 eV. This value allows the calculation of the dissociation energy of Hg_2^+ to be 1.40±0.02 eV. By analyzing the differences in energy between corresponding autoionization peaks observed in the Hg^+ and the Hg_2^+ spectra and by assuming the charge induced-dipole interaction to be the dominant interaction between $Hg^+(^2D_{5/2,3/2})$ and Hg at the equilibrium bond distance of Hg_2, the equilibrium bond distance for Hg_2 was deduced to be 3.35 Å.

Introduction

In recent years, interest in the photoionization study of metal clusters has increased dramatically. The prime motivation for these studies is to understand the change in electronic states as a function of the degree of aggregation and to provide a foundation for understanding the physical and chemical basis for catalysis. Ionization energy (IE) measurements, in combination with theoretical investigations of metal clusters, will yield information about the structures and stabilities of these species.[1] However, due to difficulties in both preparing metal clusters in high concentration and in obtaining high photon intensity in the vacuum ultraviolet (VUV) region, the photoioniza-

tion study of metal clusters remains nearly an unexplored field. For metal clusters which have IEs below ∿ 2000 Å (6.2 eV), laser radiations can in principle be used as the light sources. The only systems which have been relatively well-characterized near the thresholds by one-photon ionization mass spectrometry are alkali metal clusters.[1-5] These measurements have mainly been made by using conventional high-pressure Hg-lamp.[1,4] The odd/even alternation in IEs was observed in alkali metal clusters, indicating that even-numbered clusters are more stable than odd-numbered clusters.[1,4] Accurate two-photon photoionization thresholds for Na_2 and K_2 have been obtained by Herrmann et al.[1,6] and Leutwyler et al.[7]. Recently, Smalley and co-workers have developed a pulsed laser evaporization metal cluster beam source.[8-10] Using resonance two-photon ionization with mass selective detection, they have also been able to determine the IEs of Cu_2[11] and Mo_2.[9] The IE of Mn_2 has been estimated indirectly from the collision-induced dissociation threshold of Mn_2^+ by Ervin et al.[12]

At the present stage, it is still difficult, if not impossible, to obtain single-photon ionization spectra of metal dimers and clusters in the whole energy range of 6-21 eV by the laser photoionization method. Because of the low duty factor of the pulsed metal cluster source developed by Smalley and co-workers, it is not suitable to use the pulsed metal cluster source together with laboratory discharge sources or synchrotron radiation for photoionization studies. Nevertheless, with the proper selection of oven materials, continuous oven-type supersonic nozzle sources can be operated successfully to provide high

concentrations of many metal dimers and small clusters. A hot-oven supersonic copper nozzle source has been demonstrated by Preuss et al.[13]

To our knowledge, no photoionization efficiency (PIE) spectra of metal dimers, with the exception of alkali metal dimers, has been reported previously. This paper presents the results of the first photoionization study of Hg_2 synthesized by the supersonic expansion of Hg vapor. The IEs of Hg_n ($n \leq 12$) have been measured previously by electron impact ionization.[14,15]

Experimental

The experimental procedures and arrangement are similar to those described previously.[16-18] Briefly, the apparatus consists of a windowless 3-m near normal incidence VUV monochromator (McPherson 2253 M), an oven-type supersonic beam production system, a capillary discharge light source, and a quadrupole mass filter for ion detection. The grating employed in this study was a Bausch and Lomb 1200 lines/mm MgF_2 coated aluminum grating blazed at 1360 Å. Either the hydrogen many-lined pseudocontinuum or the helium Hopfield continuum was used as the light source, depending on the wavelength region desired.

The oven beam source used is a two-stage stainless steel oven.[16] By maintaining the second stage (the nozzle) at a slightly higher temperature than that of the first stage (the main oven), a stable beam of Hg could be obtained. Most of the data presented in this work were taken with the main oven and nozzle at $\sim$ 610 and 640 K, respectively.

The vapor pressure of Hg in the main oven was estimated to be ∿ 500 Torr. In a typical run, the fluctuation in the oven and nozzle temperatures was less than ± 3 K, as monitored with thermocouples.

The Hg used in this study was obtained from Fisher Scientific Company. It is stated to have less than 5 ppm of foreign metals. Argon was used as the carrier gas. The carrier gas pressure, which was maintained in the range of ∿ 560-760 Torr, was higher than the vapor pressure of the sample at a given oven temperature.

The wavelength resolution used in this study is 1.4 Å (FWHM). Photoionization efficiency data were taken at intervals of 0.5 Å. Depending on the wavelength region, the counting time at each point varied from 12 to 30 sec. The counting rate for Hg_2^+ at 1276 Å was ∿6000 count/s. The standard deviations for PIE data obtained in this experiment are better than ±10%. The PIE spectra presented here are based on more than two scans. The wavelength scales were calibrated by using known atomic resonance lines or H_2 emission line[19] when the H_2 pseudocontinuum was used.

Results and Discussion

Figures 1(a) and (b) show the PIE curves for Hg^+ and Hg_2^+, respectively, in the region of 600-1400 Å. The peak heights of the autoionization features at 1127 Å observed in the PIE curves for Hg^+ and Hg_2^+ have been arbitrarily normalized to the same value.

The ionization threshold of Hg exhibits a sharp step-like structure at 1189 ± 1.5 Å. The IE of Hg (10.428 ± 0.013 eV) determined here

is in good agreement with values reported in the literature.[20] The PIE for Hg_2^+ was found to increase gradually near the threshold, indicating that the Franck-Condon factor is unfavorable for the photoionization process. Nevertheless, a small step-like feature is evident at 1362 ± 1.5 Å (9.103 ± 0.010 eV), which is identified to be the IE of Hg_2. This value is approximately 0.3 eV lower than those determined previously by electron-impact ionization studies.[14,15,21] The dissociation energy of Hg_2 (D_o) has been estimated by transport coefficient measurements and optical spectroscopy.[22] A value between 0.065 and 0.091 is recommended by Ref. 22. Recently, in a high-temperature mass spectrometric study with a Knudsen cell, the dissociation enthalpy at 0 K of Hg_2 was determined to be 0.074 ± 0.020 eV.[23] Using the latter value and the IEs of Hg and Hg_2, the dissociation energy for Hg_2^+ was calculated to be 1.40 ± 0.02 eV.

The PIE curve for Hg^+, shown in Figure 1(a), is in agreement with those obtained previously using similar wavelength resolutions.[24-26] Autoionization structures have been assigned to transition of the Rydberg series.[27-29]

$$(5d)^{10}(6s)^2\ {}^1S_o \rightarrow [(5d)^9(6s)^2\ {}^2D_{5/2,3/2}]\ n(p,f)\ {}^{1,3}P_1^o \text{ and}$$

$$(5d)^{10}(6s)^2\ {}^1S_o \rightarrow [(5d)^9(6s)^2\ {}^2D_{3/2}]np,\ {}^3D_1^o.$$

The $(5d)^{10}(6s)^2\ {}^1S_o \rightarrow [(5d)^9(6s)^2\ {}^2D_{5/2,3/2}]np$ are the dominant autoionizing series. The assignments of these Rydberg series are indi-

cated in Figure 1(a).

Autoionization structures resolved in the PIE curve for Hg_2^+ are broader than, but in general, similar to those found in the Hg^+ spectrum. With the exception of the autoionization peak at 1127 Å, which is essentially unchanged in peak position in comparison to that of the $[(5d)^9(6s)^2\ ^2D_{3/2}]6p,\ ^3P_1^\circ$ atomic Rydberg state, all the other autoionization features found in the PIE curve for Hg_2^+ appear to be red-shifted with respect to the corresponding atomic autoionization peaks. Similar observations have been reported previously in the photoionization of rare gas dimers.[30-32]

The correlations between autoionization peaks observed in the Hg^+ and Hg_2^+ spectra are summaried in Table 1. The two major Rydberg series found in the Hg_2^+ spectrum have been correlated with the $[(5d)^9(6s)^2\ ^2D_{5/2}]$ np, $^1P_1^\circ$ and the $[(5d)^9(6s)^2\ ^2D_{3/2}]$ np, $^3P_1^\circ$ series. The $[(5d)^9(6s)^2\ ^2D_{5/2,3/2}]$ nf series cannot be resolved in the PIE curve for Hg_2^+. Only two members (n = 6 and 7) of the $[(5d)^9(6s)^2\ ^2D_{3/2}]$ np, $^3D_1^\circ$ series are identifiable in Figure 1(b). The autoionization peak at 1276.5 Å in the Hg_2^+ spectrum is most likely to have originated from the atomic Rydberg state, $[(5d)^9(6s)^2\ ^2D_{5/2}]$ 6p, $^1P_1^\circ$. Since this state is below the IE of Hg, it cannot be seen in the Hg^+ spectrum. In an electron-impact study of mercury vapor, Skerbele et al.[33] have observed relatively intense peaks at 1301, 1260 and 1250 Å, which were attributed to Rydberg excitations, $(6s)^2\ ^1S_o \rightarrow 6snp,\ ^1P^\circ$, n = 8, 9, and 10, respectively. It is possible that the shoulders of the peak at 1276.5 Å partly arise from these transitions. The nature of the three

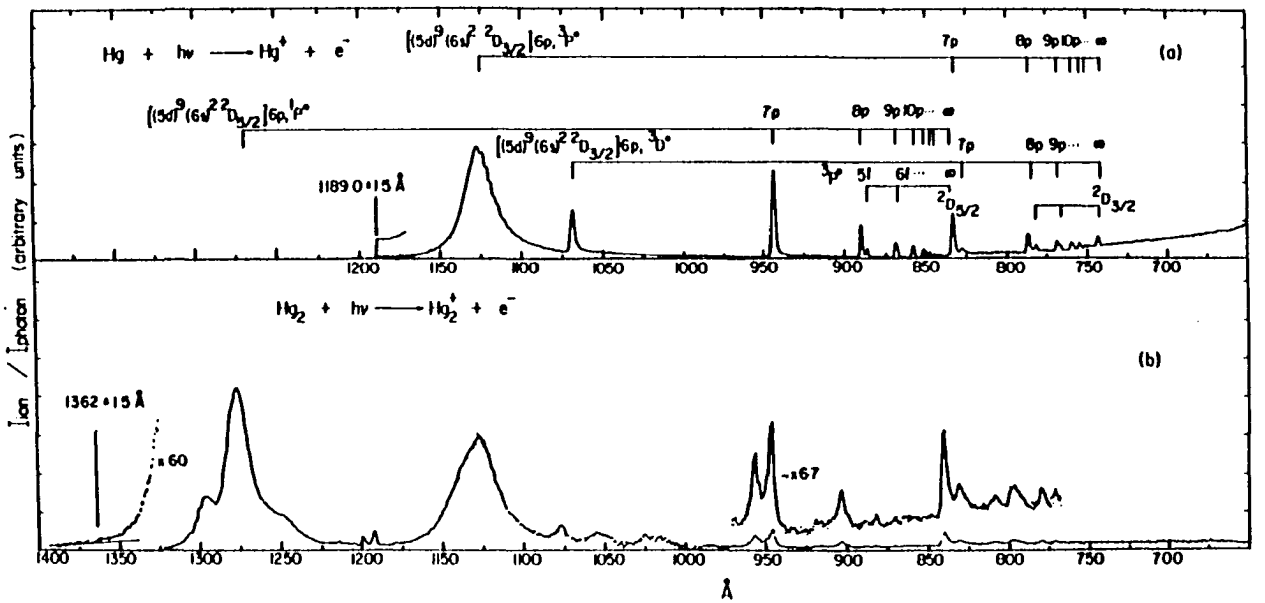

Figure 1(a). PIE curve for Hg^+ in the region of 650-1200 Å

Figure 1(b). PIE curve for Hg_2^+ in the region of 650-1400 Å

Table 1. Potential energy of $Hg^*([(5d)^9(6s)^2\ ^2D_{5/2}$ or $^2D_{3/2}]\ np] \cdot Hg$ at the equilibrium bond distance of Hg_2

Hg Rydberg Series[a] (eV)	n_1^*[b]	$E_1^*(n)$[c] (eV)	$E_2^*(n)$[d] (eV)	n_2^*[b]	$\Delta E(n)$[e] (eV)	$D^*(n)$[f] (eV)
$[(5d)^9(6s)^2\ ^2D_{5/2}]\ np,\ ^1P_1^\circ$						
n = 6 9.772 (1268.8Å)	1.637	...	9.713 (1276.5Å)	1.662	-0.059[g]	-0.133
7 13.128 (944.5Å)	2.819	13.134 (944Å)	12.969 (956Å)	2.854	-0.165	-0.239
			13.106 (946Å)	2.979	-0.028	-0.102
8 13.920 (890.7Å)	3.846	13.915 (891Å)	13.730 (903Å)	3.869	-0.185	-0.259
9 14.263 (869.3Å)	4.854	14.259 (869.5Å)	14.057 (882Å)	4.835	-0.202	-0.276
10 14.444 (858.4Å)	5.862	14.442 (858.2Å)	14.243 (870.5Å)	5.862	-0.199	-0.273
∞ 14.850 (835Å)			14.639		-0.211	-0.285

[a] References 27 and 29.

[b] n_1^* and n_2^* are the effective principal quantum numbers for the atomic and molecular Rydberg series, respectively.

[c] Autoionization peak observed in the PIE curve for Hg^+.

[d] Autoionization peak observed in the PIE curve for Hg_2^+.

[e] $\Delta E(n) = E_2^*(n) - E_1^*(n)$.

[f] The potential energy of $Hg^*(n) \cdot Hg$ at the equilibrium bond distance of Hg_2 calculated using Eq. (1).

[g] This value is calculated using $E_1^*(n=6) = 9.772$ eV.

Table 1. continued

Hg Rydberg Series (eV)		n_1^*	$E_1^*(n)$ (eV)	$E_2^*(n)$ (eV)	n_2^*	$\Delta E(n)$ (eV)	$D^*(n)$ (eV)
$[(5d)^9(6s)^2\ ^2D_{3/2}]$ np, $^3P_1^\circ$							
n = 6	11.005 (1126.6Å)	1.545	11.001 (1127Å)	11.001 (1127Å)	1.572	0.0	-0.074
7	14.872 (833.7Å)	2.725	14.875 (833.5Å)	14.760 (840Å)	2.792	-0.115	-0.189
8	15.743 (787.6Å)	3.765	15.744 (787.5Å)	15.566 (796.5Å)	3.806	-0.178	-0.252
9	16.108 (769.7Å)	4.776	16.112 (769.5Å)	15.906 (779.5Å)	4.766	-0.206	-0.280
10	16.297 (760.8Å)	5.777	16.303 (760.5Å)	16.092 (770.5Å)	5.739	-0.211	-0.285
∞	16.716			16.505		-0.211	-0.285
$[(5d)^9(6s)^2\ ^2D_{3/2}]$ np, $^3D_1^\circ$							
n = 6	11.622 (1066.8Å)		11.615 (1067.5Å)	11.512 (1077Å)		-0.103	-0.177
7	14.967 (828.4Å)		14.974 (828Å)	14.911 (831.5Å)		-0.063	-0.137

weak peaks at 1199, 1192, and 808 Å and the two broad features at $\sim$ 1054 and 1020 Å are not known.

The members, n = 6 and 7, of the Rydberg series $[(5d)^9(6s)^2\ ^2D_{5/2}]$ $\cdot np,\ ^1P_1^\circ$ seem to be split into doublets in the Hg_2^+ spectrum. The ground state for Hg_2 is a 0_g^+ state. Stemming from the consideration that the interaction of a mercury atom in an excited Rydberg state, $[(5d)^9(6s)^2\ ^2D_{5/2}]$ np, $^1P_1^\circ$, and $Hg(^1S_o)$ can give rise to the 0_u^+ and 1_u excited molecular states, the doublets probably arise from the allowed molecular transitions, $0_u^+ \leftarrow 0_g^+$ and $1_u \leftarrow 0_g^+$. In a high resolution experiment, these autoionization peaks will probably resolve into vibrational bands. This expectation has been illustrated in the high resolution photoionization study of rare gas dimers.[31,32,34-37]

When the vapor pressure of Hg was increased by raising the temperature of the main oven and/or when the stagnation pressure for the Ar carrier gas was increased, the ratio of the peak height of the autoionization peak at 1127 Å to that at 1276.5 Å in the Hg_2^+ spectrum was found to increase correspondingly. The two peaks at 946 and 956 Å become unresolved and emerge into a single broad feature as the Ar carrier gas pressure was raised to $\sim$ 2500 Torr. Under these nozzle expansion conditions, the concentrations of mercury trimers and higher clusters are expected to be higher than those obtainable by using the nozzle conditions described in the experimental section. These observations are probably due to efficient fragmentation of $Hg_n^+(n \geq 3)$ to form Hg_2^+ at higher energies.

As pointed out by Ng et al.[30] and Ono et al.[38] from the measured peak position of an autoionizing state in the Hg^+ spectrum ($E_1^*(n)$) and the corresponding peak position in the Hg_2^+ spectrum ($E_2^*(n)$), the interaction potential energy between an excited Rydberg mercury atom and a mercury atom in the ground state at the equilibrium bond distance of Hg_2 ($D^*(n)$) can be calculated by the relationship,

$$D^*(n) = E_2^*(n) - E_1^*(n) + D_o \qquad (1)$$

Using the value of -0.074 for D_o, values for $D^*(n)$ were calculated according to Eq. (1). These are listed in Table 1. Based on the discussion in the analyses of Rydberg series resolved in PIE curves for other dimer ions such as the rare gas dimer ions,[30] $(CS_2)_2^+$,[38] and $(OCS)_2^+$,[39] one expects that the absolute value for $D^*(n)$ increases as n increases and converges to a constant value when n becomes sufficiently large. This trend is observable for values of $D^*(n)$ derived from the analysis of the two major Rydberg series. The value for $D^*(n)$ seems to converge to -0.28 eV in both series. The uncertainty for $\Delta E^*(n)$ is estimated to be $\sim$ 1 Å, which corresponds to approximately 20 meV in the region of 900-750 Å. Within the uncertainty of this experiment, the convergence limits for the series, $[(5d)^9(6s)^2\ ^2D_{5/2}]$ np, $^1P_1^\circ$ and $[(5d)^9(6s)^2\ ^2D_{3/2}]$ np, $^3P_1^\circ$, found in the Hg_2^+ spectrum, are consistent with values of 14.639 and 16.505 eV, respectively. These values correspond to $D^*(\infty)$ = -0.285 eV. Here, $D^*(\infty)$ is the potential energy of $Hg^+(^2D_{5/2}$ or $^2D_{3/2}) \cdot Hg$ at the equilibrium bond distance of Hg_2. The

effective principal quantum numbers (n_2^*) calculated using these convergence limits are also listed in Table 1.

It has been shown previously in similar systems that the interaction potential for a dimer ion at the equilibrium bond distance of the neutral dimer (R_e) is consistent with the prediction from a charge induced-dipole interaction, $V = -e^2\alpha/2R_e^4$. The polarizability (α) for Hg is equal to 5.03-5.17 Å^3.[40] Assuming V to be equal to $D^*(\infty)$, the equilibrium bond distance for Hg_2 is predicted to be 3.35 Å. This value is found to be in excellent agreement with values determined by transport coefficient measurements.[41]

In summary, the PIE spectrum for Hg_2^+ in the region of 650-1400 Å has been measured by the molecular beam photoionization method. This study shows that when photoionization of van der Waals dimer consisting of two atoms is carried out with sufficiently high resolution and the differences in energy between corresponding Rydberg peaks resolved in the PIE spectra for the monomer and dimer ions are measured, accurate value for the equilibrium bond distance of the neutral dimer can be determined using the known value for the polarizability of the atom. In the case when the equilibrium bond distance of the neutral dimer is known, the polarizability of the atom can also be determined.

References

1. A. Herrmann, E. Schumacher, and Woste, J. Chem. Phys. 68, 2327 (1978).

2. E. J. Robbins, R. E. Leckenby, and P. Willis, Adv. Phys. 16, 739 (1967).

3. P. J. Foster, R. E. Leckenby, and E. J. Robbins, J. Phys. B2, 478 (1969).

4. A. Herrmann, S. Leutwyler, E. Schumacher, and L. Woste, Helv. Chim. Acta 61, 453 (1978).

5. E. Schumacher, W. H. Gerber, H. P. Harri, M. Hofmann, and E. Scholl, in J. Gole and W. C. Stwalley, Eds., "Metal Bonding and Interactions in High Temperature Systems," ACS Symp. Series No. 179, 83 (1982).

6. A. Herrmann, M. Hofmann, S. Leutwyler, E. Schumacher, and L. Woste, Chem. Phys. Lett. 62, 216 (1979).

7. S. Leutwyler, A. Herrmann, L. Woste, and E. Schumacher, Chem. Phys. 48, 253 (1980).

8. T. G. Dietz, M. A. Duncan, D. E. Powers, and R. E. Smalley, J. Chem. Phys. 74, 6511 (1981).

9. J. B. Hopkins, P. R. R. Langridge-Smith, M. D. Morse, and R. E. Smalley, J. Chem. Phys. 78, 1627 (1983).

10. D. E. Powers, S. G. Hansen, M. E. Geusic, A. C. Puiu, J. B. Hopkins, T. G. Dietz, M. A. Duncan, P. R. R. Langridge-Smith, and R. E. Smalley, J. Phys. Chem. 86, 2556 (1982).

11. D. E. Powers, S. G. Hansen, M. E. Geusic, D. L. Michalopoulos, and R. E. Smalley, J. Chem. Phys. 78, 2866 (1983).

12. K. Ervin, S. K. Loh, N. Aristov, and P. B. Armentrout, J. Phys. Chem. 87, 3593 (1983).

13. D. R. Preuss, S. A. Pace, and J. L. Gole, J. Chem. Phys. 71, 3553 (1978).

14. P. J. Harbour, J. Phys. B4, 528 (1971).

15. B. Cabaud, A. Hoareau, and P. Melinon, J. Phys. D13, 1831 (1980).

16. S. H. Linn, J. M. Brom, Jr., W. B. Tzeng, and C. Y. Ng, J. Chem. Phys. 78, 37 (1983).

17. Y. Ono, S. H. Linn, H. F. Prest, M. E. Gress, and C. Y. Ng, J. Chem. Phys. 73, 2523 (1980).

18. S. H. Linn, W. B. Tzeng, J. M. Brom, Jr., and C. Y. Ng, J. Chem. Phys. 78, 50 (1983).

19. K. E. Schubert and R. D. Hudson, "A Phtoelectric Atlas of the Intense Lines of the Hydrogen Molecular Emission Spectrum from 1025 to 1650 Å at a Resolution of 0.1 Å," (Report Number ATN-64(9233)-2, Aerospace Corp., Los Angeles, 1963).

20. H. M. Rosenstock, K. Draxl, B. W. Steiner, and J. T. Heron, J. Phys. Chem. Ref. Data 6, Suppl. 1 (1977).

21. F. L. Arnot and M. B. M'Ewen, Proc. Roy. Soc. (London) A165, 133 (1938).

22. K. P. Huber and G. Herzberg, "Molecular Spectra and Molecular Structure, IV Constants of Diatomic Molecules," (Van Nostrand Reinhold, New York, 1979), p. 312 and references therein.

23. K. Hilpert, J. Chem. Phys. 77, 1425 (1982).

24. J. Berkowitz and C. Lifshitz, J. Phys. B1, 438 (1968).

25. B. Brehm, Z. Naturforsch. A21, 196 (1966).

26. R. B. Cairns, H. Harrison, and R. I. Schoen, J. Chem. Phys. 53, 96 (1970).

27. J. Beutler, Z. Physik, 86, 710 (1933).

28. W. R. S. Garton and J. P. Connerade, Astrophys. J. 155, 667 (1968).

29. C. E. Moore, Natl. Bur. Std. (US) Circ. 467, Vol. 3 (1958).

30. C. Y. Ng, P. W. Tiedemann, B. H. Mahan, and Y. T. Lee, J. Chem. Phys. 66, 5737 (1977).

31. P. M. Dehmer and S. T. Pratt, J. Chem. Phys. 76, 3433 (1982).

32. P. M. Dehmer and S. T. Pratt, J. Chem. Phys. 77, 4804 (1982).

33. A. Skerbele, K. J. Ross, and E. N. Lassettre, J. Chem. Phys. 50, 4486 (1969).

34. P. M. Dehmer and E. D. Poliakoff, Chem. Phys. Lett. 77, 326 (1981).

35. P. M. Dehmer, J. Chem. Phys. 76, 1263 (1982).

36. S. T. Pratt and P. M. Dehmer, Chem. Phys. Lett. 87, 533 (1982).

37. P. M. Dehmer and S. T. Pratt, J. Chem. Phys. 75, 5265 (1981).

38. Y. Ono, S. H. Linn, H. F. Prest, M. E. Gress, and C. Y. Ng, J. Chem. Phys. 73, 2523 (1980).

39. Y. Ono, E. A. Osuch, and C. Y. Ng, J. Chem. Phys. 74, 1645 (1981).

40. R. R. Teachout and R. T. Pack, Atomic Data 3, 195 (1971).

41. L. F. Epstein and M. D. Powers, J. Phys. Chem. 57, 336 (1953) and references therein.

SECTION III. MOLECULAR BEAM PHOTOIONIZATION STUDY OF HgKr AND HgXe

Abstract

Photoionization efficiency data for $HgKr^+$ and $HgXe^+$ have been obtained in the region of 730-1290 Å. The ionization energies (IE) of HgKr and HgXe were determined to be 10.056 ± 0.012 eV (1233 ± 1.5 Å) and 9.709 ± 0.011 eV (1277 ± 1.5 Å), respectively. Using these values, the known dissociation energies of HgKr and HgXe and the IE of Hg, the binding energies for the ground state mercury-rare gas molecular ions were deduced to be 0.393 ± 0.013 eV for $HgKr^+$ and 0.748 ± 0.013 eV for $HgXe^+$. By analyzing the shifts in energy between corresponding autoionization peaks observed in the Kr^+, $HgKr^+$, Xe^+, and $HgXe^+$ spectra and by assuming the charge induced-dipole interaction to be the dominant interaction at the equilibrium bond distances for HgKr and HgXe, the equilibrium bond distances for HgKr and HgXe were deduced to be 3.98 and 4.23 Å, respectively. The latter values are in excellent agreement with values determined by previous spectroscopic studies.

Introduction

The mercury-rare gas van der Waals molecules have been the subject of numerous spectroscopic investigations.[1-12] The current interest of these molecules stems in part from their potential as mediums for high power excimer lasers.[13] The previous studies have provided accurate spectroscopic information for the neutral mercury-rare gas molecules.

On the contrary, only a few spectroscopic studies on $HgAr^+$ have been made.[13-18] Spectroscopic information for $HgKr^+$ and $HgXe^+$ is essentially unavailable. Recently, Linn et al.[18] have performed a photoionization study on HgAr using the supersonic oven beam method. Combining the ionization energy (IE) of HgAr determined in their study and the known dissociation energy (D_o) for HgAr, they have deduced an accurate value for $D_o(HgAr^+)$. In this report, we present the results of a similar photoionization study on HgKr and HgXe.

Experimental

The experimental arrangement and procedures are similar to those described previously.[18-21] Briefly, the apparatus consists of a windowless 3-m near normal incidence vacuum ultraviolet (VUV) monochromator (McPherson 2253 M), an oven-type supersonic beam production system, a capillary discharge light source, a VUV light detector, and a quadrupole mass filter for ion detection. The grating employed in this study was a Bausch and Lomb 1200 lines/mm MgF_2 coated aluminum grating blazed at 1360 Å. Either the hydrogen many-lined pseudocontinuum or the helium Hopfield continuum was used as the light source, depending on the wavelength region desired.

The oven beam source is a two-state quartz oven which has a design similar to the stainless steel oven reported previously.[18-21] The chemical inertness of quartz enables stable operation of the oven for a sufficiently long period of time such that accurate photoioniza-

tion efficiency (PIE) data can be recorded without interruption. By maintaining the second stage (the nozzle) at a slightly higher temperature than the first stage (the main oven), a stable beam of Hg can be obtained. In this experiment, the main oven and the nozzle were kept at $\sim$ 580 and 620 K, respectively. The vapor pressure of Hg in the main oven was estimated to be $\sim$ 200 Torr. The HgKr (HgXe) complexes were prepared by seeding Hg vapor in $\sim$ 1600 Torr of Kr (Xe) and then expanding the mixture through the nozzle.

The Hg used in this study was obtained from Fisher Scientific Company. It is stated to have less than 5 ppm foreign metals. The Kr and Xe were obtained from Air Products and have the purities of > 99.995%.

The wavelength resolution used in this study is 1.4 Å (FWHM). Photoionization efficiency data were taken at intervals of 0.5 Å. Depending on the wavelength region, the counting time at each point varied from 30 to 70 s. The counting rates for $HgKr^+$ and $HgXe^+$ at 1127 Å were $\sim$ 100 and 250 cts/s, respectively. The wavelength scales were calibrated by using known atomic resonance lines or H_2 emission lines[22] when the H_2 pseudocontinuum was used.

Results and Discussion

The PIE curves for $HgKr^+$ and $HgXe^+$ in the region of 730-1290 Å are compared to that for Hg^+ in Figures 1(a)-(c). The Hg^+ spectrum was obtained in a previous photoionization study.[20,21] The threshold

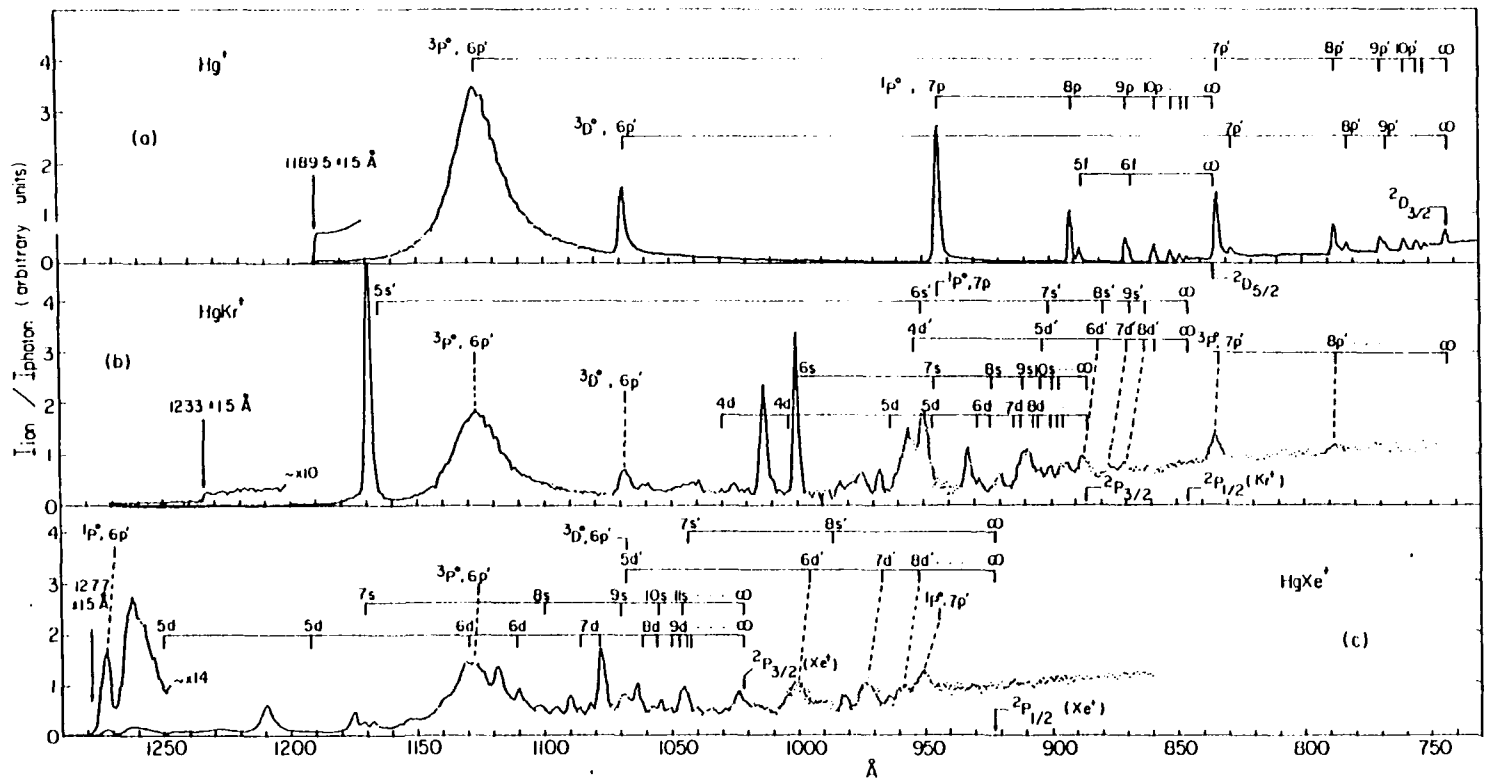

Figure 1(a). PIE curve for Hg^+ in the region of 730-1200 Å

Figure 1(b). PIE curve for $HgKr^+$ in the region of 750-1270 Å

Figure 1(c). PIE curve for $HgXe^+$ in the region of 860-1290 Å (wavelength resolution = 1.4 Å (FWHM))

behavior for $HgKr^+$ is similar to those observed for Hg^+, Hg_2^+, and $HgAr^+$. A distinct step-like feature is evident at 1233 ± 1.5 Å (10.056 ± 0.12 eV) which is identified to be the IE of HgKr. In contrast to HgKr, the PIE curve for $HgXe^+$ exhibits a tailing structure at the threshold. A sharp rise in PIE is observed at 1277 ± 1.5 Å (9.709 ± 0.011 eV). At wavelength longer than 1277 Å, the $HgXe^+$ ion signal is found to be within the noise level. Thus, the value of 9.709 ± 0.011 eV is assigned to be the IE of HgXe.

The values for $D_o(HgKr)$ and $D_o(HgXe)$ are well known from previous spectroscopic studies.[1-7] An accurate value of 168 cm^{-1} for $D_o(HgKr)$ has been obtained recently from the analysis of the fluorescence excitation spectrum for HgKr observed in a supersonic jet experiment by Fuke et al.[1] This value is in good agreement with those determined by Bousquet, Bras, and Majdi[2] and Grycuk and Czerwosz.[4] The values of 240 ± 10 and 220 ± 20 cm^{-1} for $D_o(HgXe)$ obtained by Grycuk and Findeisen[3] and Bousquet, Bras, and Majdi,[2] respectively, are within the experimental uncertainties of their experiments. Combining the IEs of Hg, HgKr, and HgXe and the known values for $D_o(HgKr)$ and $D_o(HgXe)$, we deduce values of 0.393 ± 0.013 and 0.748 ± 0.013 eV for $D_o(HgKr^+)$ and $D_o(HgXe^+)$, respectively. The values for $D_o(Hg_2^+)$,[19] $D_o(HgAr^+)$,[18] $D_o(HgKr^+)$, and $D_o(HgXe^+)$ are summarized in Table 1. The value for $D_o(Hg_2^+)$ is approximately twice that for $HgXe^+$. The bond dissociation energies for the ground state HgX^+, X = Ar, Kr, and Xe, ions are in the order $D_o(HgXe^+) > D_o(HgKr^+) > D_o(HgAr^+)$. This trend is similar to that

Table 1. Dissociation energy (D_o) for the mercury-rare gas molecular ions

Ions	D_o (eV)
Hg_2^+	1.42 ± 0.02[a]
$HgAr^+$	0.228 ± 0.017[b]
	$\sim 0.202 \pm 0.012$[c]
$HgKr^+$	0.393 ± 0.013[d]
$HgXe^+$	0.748 ± 0.013[d]

[a]Reference 19.

[b]Reference 18.

[c]Reference 17.

[d]This work.

observed in the ground state dissociation energies for the rare gas dimer ions.[23-31] This trend is expected from simple molecular orbital theory which has been used to rationalize the measured dissociation energies for heterogeneous rare gas dimer ions.[31]

Autoionization peaks resolved in the PIE spectrum for $HgAr^+$ [18] were found to correlate well with known optically allowed absorption lines of Hg and Ar indicating that transitions involved in the HgAr system are perturbed atom-like transitions. This observation is consistent with the small values observed for $D_o(HgAr^+)$ and $D_o(HgAr)$. Since $D_o(HgX)$ and $D_o(HgX^+)$, X = Kr and Xe are greater than $D_o(HgAr)$ and $D_o(HgAr^+)$, respectively, transitions associated with the HgKr

and HgXe system are expected to be more molecule-like as compared to those involved in the HgAr system. The positions of the optically allowed Rydberg transitions,[32-34] $[5d^9(^2D_{5/2,3/2})\ np,\ n \geq 6]$ and $[5d^9(^2D_{5/2})\ nf,\ n \geq 5]$ of Hg, $[4p^5(^2P_{3/2,1/2})\ ns,\ n \geq 5]$ and $[4p^5(^2P_{3/2,1/2})\ nd,\ n \geq 4]$ of Kr and $[5p^5(^2P_{3/2,1/2})\ ns,\ n \geq 7]$ and $[5p^5(^2P_{3/2,1/2})\ nd,\ n \geq 5]$ of Xe are marked in Figures 1(a)-(c). The correlations between optically allowed atomic lines and many autoionization peaks resolved in the $HgKr^+$ and $HgXe^+$ spectra are not apparent. Similar to the observation found in the photoionization of rare gas dimers,[23-31] most of the autoionization peaks appearing in the $HgKr^+$ and $HgXe^+$ spectra in Figures 1(b) and 1(c) should be resolved into vibrational fine structures when a sufficiently high wavelength resolution is used.

The autoionization features of HgKr at 1126.2, 835, and 789 Å obviously originate from the Rydberg states $5d^9(^2D_{3/2})\ np$, $^3P^o$, n = 6, 7 and 8, of Hg. The structure of the $HgKr^+$ spectrum in the region of ∿ 850-1100 Å has the resemblance of that found in the $XeKr^+$ spectrum obtained using a similar wavelength resolution. It is most likely that autoionization peaks in this wavelength region arise from transitions having strong Kr character. The autoionization peaks at 887.5, 876.4, and 870.0 Å can be correlated to the atomic Rydberg states of $4p^5(^2P_{1/2})\ nd$, $[\frac{3}{2}]_1^o$, n = 6, 7, and 8, of Kr. The strongest peak at 1168.5 Å may have the origin from the $4p^5(^2D_{1/2})\ 5s$, $[\frac{1}{2}]_1^o$ state of Kr. The correlations of autoionizing peaks to atomic Rydberg states are indicated by dash lines in the figures. Table 2

Table 2. Potential energies of $Hg^*[5d^9(^2D_{3/2})\ np] \cdot Kr$ and $Hg \cdot Kr^*[4P^5(^2P_{1/2})\ nd]$ at the equilibrium bond distance of HgKr

Rydberg series	n_1^* [a]	$E_1^*(n)$ [b] (eV)	n_2^* [a]	$E_2^*(n)$ [c] (eV)	$\Delta E(n)$ [d] (eV)	$D^*(n)$ [e] (eV)
$Kr(4p^5(^2P_{1/2})\ nd\ [\frac{3}{2}]_1^o)$						
n = 6	4.789	14.072 (881.06 Å)	4.886	13.970 (887.5 Å)	-0.102	-0.1239
n = 7	5.788	14.260 (869.49 Å)	5.885	14.147 (876.4 Å)	-0.112	-0.134
n = 8	6.797	14.371 (862.74 Å)	6.863	14.252 (870.0 Å	-0.120	-0.141
n = ∞		14.666 (845.42 Å		14.540 (852.7 Å)	-0.126	-0.147
$Hg(5d^9(^2D_{3/2})\ np\ ^3P^o)$						
n = 6	1.545	11.005 (1126.63 Å)		11.001 (1127.0 Å)	-0.004	-0.025
n = 7	2.725	14.872 (833.66 Å)		14.849 (835.0 Å)	-0.023	-0.044

[a] n_1^* and n_2^* are the effective principal quantum numbers for the atomic and molecular Rydberg series, respectively.

[b] References 32-34.

[c] Autoionization peak observed in the PIE curve for $HgKr^+$.

[d] $\Delta E(n) = E_2^*(n) - E_1^*(n)$.

[e] The potential energy of $Hg \cdot Kr^*(n)$ or $Hg^*(n) \cdot Kr$ at the equilibrium bond distance of HgKr calculated using Eq. (1).

Table 2. continued

Rydberg series	n_1^*	$E_1^*(n)$ (eV)	n_2^*	$E_2^*(n)$ (eV)	$\Delta E(n)$ (eV)	$D^*(n)$ (eV)
n = 8	3.761	15.743 (787.57 Å)	3.761	15.714 (789.0 Å)	-0.029	-0.050
n = ∞		16.705 (742.21 Å)				
$Hg(5d^9(^2D_{3/2})\ np\ ^3D^o)$						
n = 6		11.615 (1066.81 Å)		11.598 (1069 Å)	-0.017	-0.038

summarizes the assignments of autoionizing peaks appearing in the $HgKr^+$ spectrum.

The assignments of autoionizing features resolved in the $HgXe^+$ spectrum to optically allowed atomic Xe and Hg transitions are more difficult in comparison with those encountered in the analysis of the $HgAr^+$ and $HgKr^+$ spectra. Autoionizing states of HgXe, which can be unambiguously correlated to atomic Rydberg states of Hg and Xe are listed in Table 3.

The positions of autoionization peaks for $HgKr^+$ and $HgXe^+$ listed in Tables 2 and 3 are red-shifted with respect to the corresponding positions of the atomic autoionizing states. As pointed out previously by Linn et al.,[19] Ng et al.[23] and Ono et al.[35] from the measurements of the peak position of an autoionizing state in Kr^+ (Xe^+) spectrum

Table 3. Potential energies of $Hg^*[5d^9(^2D_{3/2})\ np] \cdot Xe$ and $Hg \cdot Xe^*[5p^5(^2P_{1/2})\ nd]$ at the equilibrium bond distance of HgXe

Rydberg series	n_1^* [a]	$E_1^*(n)$ [b] (eV)	n_2^* [a]	$E_2^*(n)$ [c] (eV)	$\Delta E(n)$ [d] (eV)	$D^*(n)$ [e] (eV)
$Xe(5p^5(^2P_{1/2})\ nd\ [\frac{3}{2}]_1^o)$						
n = 6	3.715	12.450 (995.84 Å)	3.781	12.399 (1000.0 Å)	-0.079	-0.106
n = 7	4.707	12.822 (966.94 Å)	4.785	12.756 (972.0 Å)	-0.067	-0.094
n = 8	5.730	13.022 (952.12 Å)	5.775	12.942 (958.0 Å)	-0.080	-0.107
n = ∞		13.436 (922.76 Å)		13.350 (928.73 Å)	-0.086	-0.114
$Hg(5d^9(^2D_{3/2})\ np\ ^3P^o)$						
n = 6	1.545	11.005 (1126.63 Å)		10.977 (1129.5 Å)	-0.0280	-0.055
$Hg(5d^9(^2D_{5/2})\ np\ ^1P^o)$						
n = 7	2.819	13.128 (944.46 Å)		13.051 (950.0 Å)	-0.077	-0.104

[a] n_1^* and n_2^* are the effective principal quantum numbers for the atomic and molecular Rydberg states, respectively.

[b] References 32-34.

[c] Autoionization peak observed in the PIE curve for $HgXe^+$.

[d] $\Delta E(n) = E_2^*(n) - E_1^*(n)$.

[e] The potential energy of $Hg \cdot Xe^*(n)$ or $Hg^*(n) \cdot Xe$ at the equilibrium bond distance of HgXe calculated using Eq. (1).

($E_1^*(n)$) and the corresponding peak position in the $HgKr^+$($HgXe^+$) spectrum ($E_2^*(n)$), the interaction potential energy ($D^*(n)$) between an excited Rydberg Kr(Xe) atom and a Hg atom at the equilibrium distance (Re) of HgKr (HgXe) can be calculated by the equation

$$D^*(n) = E_2^*(n) - E_1^*(n) + D_o(HgX) \qquad (1)$$

Here, X represents Kr or Xe. The calculated values for $D^*(n)$ using Eq. (1) are listed in Tables 2 and 3. The values for the series limits $E_2^*(n\rightarrow\infty)$ were determined by fitting the observed Rydberg states of HgKr and HgXe to the standard Rydberg equation. Using Eq. (1), the potential energy $D^*(n\rightarrow\infty)$ due to the interaction of Hg and Kr^+ (Xe^+) at Re(HgKr) (Re(HgXe)) is calculated to be 0.147 eV (0.114 eV). It has been shown previously in similar systems that the value for $D^*(n\rightarrow\infty)$ of a dimer ion is consistent with the prediction from a charge induced-dipole interaction, $V = -e^2\,\alpha/2\,Re^4$. The polarizability for Hg^{36} is equal to 5.03-5.17 Å.[3] Assuming V to be equal to $D^*(n\rightarrow\infty)$, we obtained a value of 3.96-3.99 Å for Re(HgKr) and 4.22-4.25 Å for Re(HgXe). These values are in excellent agreement with those determined by previous spectroscopic measurements.[1-6]

Since the converging limits $E_2^*(n\rightarrow\infty)$ for the Rydberg series $Hg^*[5d^9(^2D_{3/2})\ np]\cdot Kr$ and $Hg^*[5d^9(^2D_{5/2,3/2})\ np]\cdot Xe$ cannot be deduced accurately in this experiment, it is difficult to obtain reliable values for Re(HgKr) and Re(HgXe) using the above method. However, the smaller values observed for $D^*(n)$ of $Hg^*(n)\cdot Kr$ and $Hg^*(n)\cdot Xe$

in comparison with those of $Hg \cdot Kr^*(n)$ and $Hg \cdot Xe^*(n)$ are consistent with the fact that the polarizabilities for Kr and Xe are smaller than that for Hg.

References

1. K. Fuke, T. Saito, and K. Kaya, J. Chem. Phys. 81, 2591 (1984); 79, 2487 (1983).
2. C. Bousquet, N. Bras, and Y. Majdi, J. Phys. B 17, 1831 (1984).
3. T. Grycuk and M. Findeisen, J. Phys. B 16, 975 (1983).
4. T. Grycuk and E. Czerwosz, Physica C 106, 431 (1981).
5. N. Bras and C. Bousquet, J. Physique 40, 945 (1979).
6. L. K. Lam, A. Gallagher, and R. E. Drullinger, J. Chem. Phys. 68, 4411 (1978).
7. R. Heller, J. Chem. Phys. 9, 154 (1941).
8. W. Behmenberg, Z. Naturforsch. Teil A 27, 31 (1972).
9. H. C. Petzold and W. Behmenberg, Z. Naturforsch. Teil A 33, 1461 (1978).
10. D. Perrlin, Z. B. Lakhar, J. C. Jeannet, and R. Lennuier, J. Physique 43, 45 (1982).
11. O. P. Strausz, J. M. Campbell, S. DePaoli, H. S. Sandhu, and H. E. Gunning, J. Am. Chem. Soc. 95, 732 (1981).
12. J. R. Fuhr, W. L. Wiese and L. J. Roszman, "Bibliography on Atomic Line Shapes and Shifts," Natl. Bur. Stand. (U.S), Spec. Publ. (1972), Suppl. 1 (1974) and Suppl. 2 (1975).
13. R. Woodworth, J. Chem. Phys. 66, 754 (1977).
14. N. J. Bridge, J. Mol. Spectrosc. 42, 370 (1972).
15. J. T. Hougen, J. Mol. Spectrosc. 42, 381 (1972).
16. C. Santaram and J. G. Winans, Can. J. Phys. 44, 1516 (1966).

17. N. J. Bridge, Chem. Commun. 1970, 358 (1970).

18. S. H. Linn, J. M. Brom, Jr., W. B. Tzeng, and C. Y. Ng, J. Chem. Phys. 82, 648 (1985).

19. S. H. Linn, C. L. Liao, C. X. Liao, J. M. Brom, Jr., and C. Y. Ng, Chem. Phys. Lett. 105, 645 (1984).

20. S. H. Linn, J. M. Brom, Jr., W. B. Tzeng, and C. Y. Ng, J. Chem. Phys. 78, 37 (1983).

21. S. H. Linn, W. B. Tzeng, J. M. Brom, Jr., and C. Y. Ng, J. Chem. Phys. 78, 50 (1983).

22. K. E. Schubert and R. D. Hudson, "A Photoelectric Atlas of the Intense Lines of the Hydrogen Molecular Emission Spectrum from 1025 to 1650 Å at a Resolution of 0.1 Å," Report No. ATN-64(9233)-2, Aerospace Corp., Los Angeles (1963).

23. C. Y. Ng, P. W. Tiedemann, B. H. Mahan, and Y. T. Lee, J. Chem. Phys. 66, 5737 (1977).

24. C. Y. Ng, D. J. Trevor, B. H. Mahan, and Y. T. Lee, J. Chem. Phys. 65, 4327 (1976).

25. C. Y. Ng, D. J. Trevor, B. H. Mahan, and Y. T. Lee, J. Chem. Phys. 66, 446 (1977).

26. P. M. Dehmer and E. D. Poliakoff, Chem. Phys. Lett. 77, 326 (1981).

27. P. M. Dehmer, J. Chem. Phys. 76, 1263 (1982).

28. S. T. Pratt and P. M. Dehmer, Chem. Phys. Lett. 87, 533 (1982).

29. P. M. Dehmer and S. T. Pratt, J. Chem. Phys. 75, 5265 (1981).

30. S. T. Pratt and P. M. Dehmer, J. Chem. Phys. 76, 3433 (1981).

31. P. M. Dehmer and S. T. Pratt, J. Chem. Phys. 77, 4804 (1982).

32. C. E. Moore, Natl. Bur. Stand. (U.S.) Circ. 467, Vol. I-III (1949).

33. H. Beutler, Z. Physik, 86, 710 (1933).

34. H. Beutler, Z. Physik, 93, 177 (1935).

35. Y. Ono, S. H. Linn, H. F. Prest, M. E. Gress, and C. Y. Ng, J. Chem. Phys. 73, 2523 (1980).

36. R. R. Teachout and R. T. Pack, Atomic Data 3, 195 (1971).

PART 2. STATE-SELECTED AND STATE-TO-STATE STUDIES OF ELECTRON TRANSFER REACTIONS

SECTION IV. A STUDY OF THE SYMMETRIC CHARGE TRANSFER REACTION $H_2^+ + H_2$ USING THE HIGH RESOLUTION PHOTOIONIZATION AND CROSSED ION-NEUTRAL BEAM METHODS

Abstract

A new ion-molecule reaction apparatus, which combines the crossed ion-neutral beam method, high resolution photoionization mass spectrometry, and charge transfer detection, has been developed. Using this apparatus, we have examined the relative total charge transfer cross sections of $H_2^+ + H_2$ as a function of the vibrational state of H_2^+, $v_o' = 0$-4, at the center-of-mass collision energy ($E_{c.m.}$) range of 0.38-200 eV. The relative total charge transfer cross sections measured at $E_{c.m.} = 8$, 16, 22.5, and 200 eV are in general agreement with a recent theoretical calculation based on the semiclassical energy conserving trajectory formulation. The vibrational energy effects on the charge transfer and the $H_3^+ + H$ channels at low collision energies ($E_{c.m.} \leq 1$ eV) were directly observed. The rotational states, J = 0, 1, and 2, of $H_2^+(v_o' = 0)$ were also selected in this experiment. Within experimental uncertainties, the rotational excitations of $H_2^+(v_o' = 0)$ show no effect on the relative total charge transfer cross sections at $E_{c.m.} = 2$ and 4 eV. By calibrating the relative total charge transfer cross sections obtained with an ionizing photon energy of 18 eV (688 Å) to absolute total charge transfer cross sections determined previously using low energy electron impact ionization, absolute total charge transfer cross sections for $v_o' = 0$ and 1

in the kinetic energy range of $E_{c.m.}$ = 8-200 eV were estimated. The absolute total charge transfer cross sections thus obtained for $v'_o = 0$ and 1 are lower than the theoretical values by approximately a factor of 2. However, the kinetic energy dependence of the total charge transfer cross section is in agreement with the theoretical calculation. The final vibrational state distributions of the charge transfer products H_2^+ from the reaction $H_2^+(v'_o = 0) + H_2(v''_o = 0) \rightarrow H_2(v') + H_2^+(v'')$ at $E_{c.m.}$ = 4, 8, and 16 eV have been probed by charge transfer reactions $H_2^+(v'') + N_2$ and $H_2^+(v'') + CO$. The results are consistent with the theoretical prediction that approximately 92% and 85% of the product H_2^+ ions formed at $E_{c.m.}$ = 8 and 16 eV are in the $v'' = 0$ state, respectively.

Introduction

Charge transfer processes represent an important class of reactions in ion chemistry. When such a reaction is exothermic, it is usually a dominant product channel in the outcome of ion-neutral interactions. Because of their large cross-sections, charge transfer reactions play a significant role in relaxation processes and reaction kinetics in ionized gases. Therefore, the microscopic understanding of these phenomena is of particular interest to gas discharges, lasers, flames, and controlled thermonuclear fusion research. Although the concentrations of ions in flames are low, thermal charge exchange processes are possible pathways for the conversion of ions into free radical chain carriers.

At the present stage, the theory of charge exchange between

atomic gaseous ions and atoms is quite well-developed.[1-14] However, the detailed theoretical understanding of charge transfer processes involving molecular ions, in which energy can be transferred to or from internal motions of molecules and/or molecular ions, is still in a rudimentary state.

The symmetric charge transfer reaction

$$H_2^+(v_o') + H_2(v_o'' = 0) \rightarrow H_2(v') + H^+(v'') \qquad (1)$$

has been the subject of many theoretical studies.[6,15-21] The simplicity of this process makes it an important system for the detailed investigation of the dynamics of molecular charge transfer processes. Bates and Reid[16] pioneered the development of a semiclassical impact parameter model and applied it to charge transfer and vibrational excitations in H_2^++H_2 collisions. Based on the spherical interaction potential and the multistate impact parameter treatment of Bates and Reid, McCann et al.[18] and Moran et al.[19] have calculated state-to-state differential and total cross-sections for Reaction (1). The calculated total cross-sections at the center-of-mass energies ($E_{c.m.}$) of 8, 78, and 200 eV, from $v_0' = 0$ to 4, were found to vary significantly with v_o'. A similar calculation on the $D_2^+ + D_2$ charge transfer reaction, which show a weak dependence of the total cross section on the vibrational state of the reactant D_2^+, was carried out by Stocker and Neumann.[17]

For collisions between molecular ions and molecules, it is neces-

sary to take into account the molecular orientations. In the case of symmetric charge transfer reactions between molecular ions and their parent molecules, such as Reaction (1), the exact symmetry is broken by the molecular orientations with respect to the collision axis of the interacting species. Reliable interaction potentials for both ground and excited states for different interacting geometrics are essential for accurate cross sectional calculations. For the $H_2^+ + H_2$ system, considerable work[22-27] has been done in the development of such potential energy surfaces. The most recent ab initio CI potential energy curves for the $H_2^+ + H_2$ interaction have been reported by Cobb et al.[25] and Borkman and Cobb.[26] Their calculations, with the application to charge transfer dynamics in mind, have included several interaction geometrics.

Recently, Lee and DePristo[20] have performed a theoretical calculation on Reaction (1) using the semiclassical energy conserving trajectory formulation (SCECT). The interaction potentials used are derived from a simple one-active-electron model[27] and have been shown to agree with the ab initio CI calculation of Borkman and Cobb.[26] The accuracy of the SCECT formulation has also been demonstrated.[28-30] Since this latter calculation has incorporated the effects of molecular orientations in the charge exchange dynamics, it is expected to be more accurate than previous theoretical studies. Contrary to the results of Moran and co-workers,[18-19] smooth variations were found when the calculated total cross sections were plotted versus v_o' at

$E_{c.m.}$ = 8, 16, and 200 eV.

Previous experimental studies of Reaction (1) mostly involved total cross-section measurements as a function of kinetic energy with the reactant H_2^+ ions prepared by electron ionization.[31-43] The H_2^+ ions formed by electron ionization can usually be assumed to have a broad distribution of vibrational states. There is general agreement that the total charge transfer cross section in $H_2^+ + H_2$ collisions slowly falls off as a function of collision energy characteristic of symmetrical resonance charge transfer;[6,9] but it reaches a minimum at approximately $E_{c.m.}$ = 250 eV, then rises again toward higher collision energy. The rise in the total cross-section at $E_{c.m.}$ > 250 eV has been attributed to increasing cross-sections for nonresonant processes.[16,17] The investigations of Hayden and Amme[32] and Latimer et al.[31] indicate that the total cross section for Reaction (1) varies with the vibrational population of the reactant H_2^+ ions.

Photoionization is the cleanest method for the preparation of ions with well-characterized distributions of internal states. The relative total cross sections for charge transfer of H_2^+ with H_2 as a function of the vibrational energy distribution of H_2^+ reactant ions measured at $E_{c.m.}$ = 215 eV was reported by Chupka.[44] This work clearly demonstrated the vibrational energy effect on the total cross section of Reaction (1). Using the photoion-photoelectron coincidence (PIPECO) method, it is now possible to measure total cross sections for many simple ion-molecule reactions with the reactant atomic and molecular ions at specific vibrational and electronic states.[45-56].

The only reported vibrational-state-selected total cross-section measurements for Reaction (1) was performed by Campbell et al.[53] in a PIPECO study using effusive H_2 sources. Since a retarding grid system was used in the latter study to analyze the energy of photoelectrons, the state-specific cross-sectional data must necessarily be deduced from the differences of coincidence signals with characterized distributions of vibrational states. The experimental uncertainties of the relative total cross sections deduced from their experiments are quite large. The relative state-selected total cross sections were also found to vary abruptly with v_o' at $E_{c.m.}$ = 8, 78, 200, and 500 eV. However, the agreement between the experimental results of Campbell et al.[53] and the theoretical calculation of McCann et al.[18] and Moran et al.[19] is poor. As expected, the measured total charge transfer cross sections as a function of v_o' are in better agreement with the calculation of Lee and DePristo.[20]

Furthermore, in the study of Campbell et al.,[53] the H_2^+ product ions were identified by time-of-flight (TOF) analysis. Due to inelastic charge transfer channels, the slow H_2^+ product ions can be scattered more than 10° away from the initial neutral H_2 beam direction. The collection efficiency in the TOF analysis for product ions scattered at wide angles is poor. Depending on the experimental arrangement, inelastic charge transfer can also cause the arrival time of the H_2^+ product ions to spread out in a wider temporal interval. When charge transfer is the only open channel,[45,46] TOF analy-

sis usually allows the identification of the fast reactant and slow product ions. For the reaction of $H_2^+ + H_2$, at low collision energies, $E_{c.m.} \leq 8$ eV, where the cross sections for the formation of $H_3^+ + H$ by the reaction

$$H_2^+(v_o') + H_2(v_o'' = 0) \rightarrow H_3^+ + H \qquad (2)$$

become appreciable,[57] TOF method might not be able to distinguish the H_3^+ and charge transfer product H_2^+ ions. In view of the fact that the collection efficiency and the TOF resolution are governed by opposing factors, the TOF method is not appropriate for study of Reaction (1) at low collision energies.

We note that preliminary measurements on the relative total cross sections of Reaction (1) as a function of the vibrational state of the reactant H_2^+ ions have also been measured by Cole et al.[58] in a PIPECO experiment using the effusive beam and TOF methods. They have been able to extend the study to higher vibrational states. Their experiment has suffered from similar difficulties as discussed above.

The work of Chupka and Berkowitz,[59-60] Berkowitz and Chupka,[61] Dehmer and Chupka[62] shows that because of the dominance of autoionization with $\Delta v = -1$ over predissociation, H_2^+ at vibrational states $v_o' =$ 0-5 can be prepared with high purity by the simple photoionization method. This requires the photoionization of H_2 at higher resolution to select specific autoionization peaks and to minimize the contribution from direct photoionization processes. The fact that autoionization proc-

esses are much stronger than direct ionization in H_2 allows the preparation of $H_2^+(v_o')$ at higher intensity than can be prepared by the PIPECO method. Due to selection in autoionization and the energy constraint, the $H_2^+(v_o' = 0)$ ions can be produced in specific rotational states J = 0, 1, and 2 by using the high resolution photoionization method.

Anderson et al.[63,66] and Houle et al.[64,65] have performed several state-selected experiments involving H_2^+ by the photoionization and guided beam methods with a wavelength resolution of 4 Å. Although the guided beam technique makes possible the formation of the reactant H_2^+ beam at well-defined translational energies, the low sensitivity of the photoionization source has prevented the study of these reactions in a crossed ion-neutral beam arrangement. By using the very high resolution PIE spectrum for H_2^+ of Dehmer and Chupka[62] to estimate the ratio of direct to autoionization, along with Franck-Condon factors deduced by photoelectron spectroscopy[67] to estimate the vibrational state distributions from direct ionization, they have estimated the vibrational distributions of H_2^+ formed by low resolution photoionization in the wavelength region of $\sim$ 745-805 Å. However, the errors for cross-sectional data deduced by using the estimated vibrational distributions are expected to the accumulative through the whole data set.

We have successfully combined the high resolution photoionization mass spectrometric method and the crossed ion-neutral beam technique to examine the vibrational, rotation, and kinetic energy effects on the total cross sections for Reaction (1). By using the crossed ion-neutral supersonic beam technique, we have not only mini-

mized the secondary reactions of the charge transfer H_2^+ ions with background neutral H_2 molecules to form $H_3^+ + H$ at low kinetic energies, but also attained higher kinetic energy resolution as compared to using an ion beam-gas cell experimental arrangement. Direct observation in the competition between charge transfer and the formation of H_3^+ at $E_{c.m.} \leq 1$ eV was made for the first time. We have also developed a charge transfer detector which was used to probe the vibrational state distribution of the product H_2^+ ions. A preliminary report of this study has been published.[68] This paper presents a full account of the experimental results in the context of its comparison to theoretical predictions.

Experimental

A brief description of the experimental arrangement and procedures have been reported previously.[68] After the preliminary work, the experimental setup has been modified to incorporate a charge exchange detector which allows the examination for the vibrational state distribution of the H_2^+ product ions. The crossed ion-neutral beam apparatus is developed from a high-resolution photoionization mass spectrometer.[69] The apparatus essentially consists of a 3-m near normal incidence vacuum ultraviolet (VUV) monochomator (McPherson 2253 M), a discharge lamp, a VUV light detector, two supersonic beam production systems, two quadrupole mass spectrometers, and two reaction gas cells.

The basic pumping arrangement is similar to that described in

Ref. 69. Figure 1 shows the detailed cross-sectional view of the differential pumping arrangement, the supersonic beam production systems, quadrupole mass spectrometers, photoionization region, collision region, and reaction gas cells. The lower nozzle (1), which was positioned at a distance of $\sim$ 0.65 cm from the photoionization region, has a quartz nozzle tip (2) with a diameter (D_o) of 60 μm. Using a hydrogen stagnation pressure (P_o) of $\sim$ 200 Torr, the pressure in the photoionization chamber was $\sim 2 \times 10^{-5}$ Torr. By moving the nozzle close to the photoionization region, a reactant H_2^+ beam with higher intensity can be formed. A quartz nozzle tip is used in order to minimize the perturbation of the electric field by the nozzle in the photoionization region. The H_2^+ reactant ions formed by photoionization at the photoionization region were extracted perpendicular to the H_2 beam and focused onto another neutral H_2 supersonic beam at an intersecting angle of 90°. The neutral reactant H_2 beam was produced by a supersonic expansion through the upper stainless steel nozzle (6) with D_o = 120 μm at $P_o \approx 250$ Torr and then collimated into the scattering chamber by a 0.75 mm diameter conical skimmer (7). The intensity of the H_2^+ reactant ion beam was monitored with the vertical quadrupole mass spectrometer (13). The intensity of the slow product H_2^+ ions formed in the collisions were measured by the horizontal quadrupole mass spectrometer (14) positioned in the direction of the neutral H_2 reactant beam. The horizontal quadrupole mass spectrometer can be floated at a DC potential up to ± 400 V with respect to ground. Since the horizontal mass spectrometer allows the identification of H^+, H_2^+, and

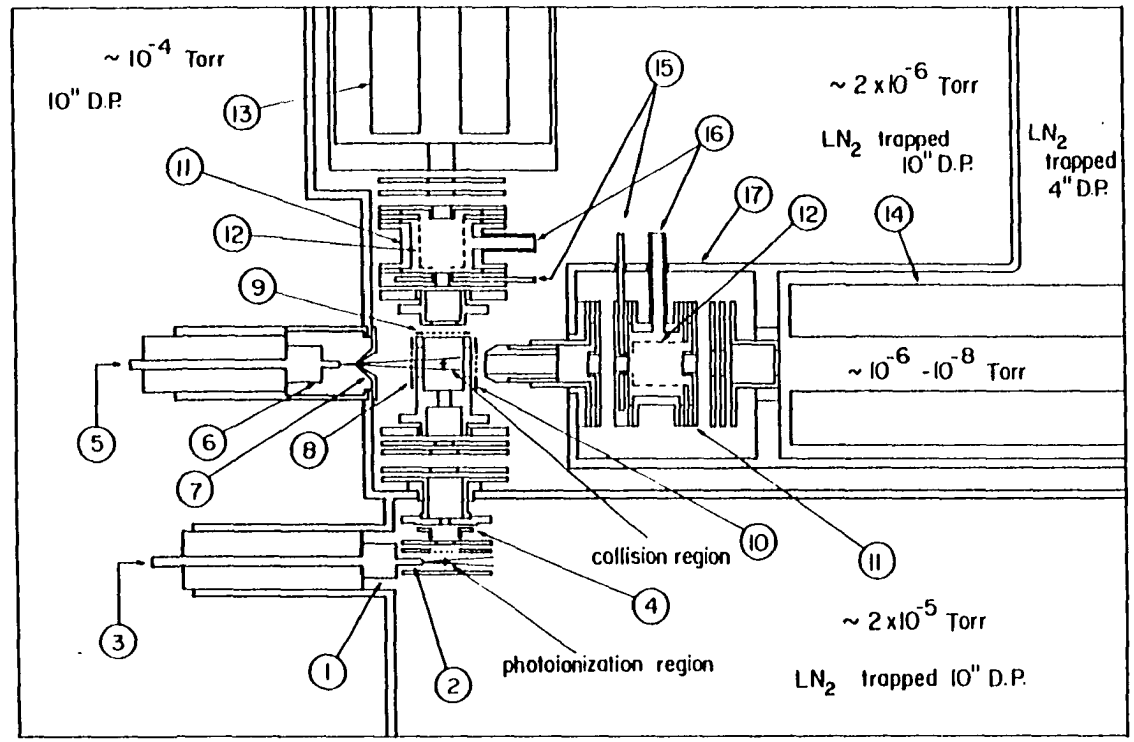

Figure 1. Cross sectional view of the crossed ion-neutral beam photoionization apparatus. (1) lower H_2 supersonic nozzle, (2) quartz nozzle tip, (3) H_2 inlet, (4) electrostatic deflector, (5) H_2 inlet, (6) upper H_2 supersonic nozzle, (7) skimmer, (8) grid 1, (9) grid 2, (10) grid 3, (11v) vertical gas cell, (11h) horizontal gas cell, (12) platinum grid, (13) vertical quadrupole mass spectrometer, (14) horizontal quadrupole mass spectrometer, (15) gas inlet, (16) to Baratron manometer, (17) horizontal gas cell chamber, (18) aperture

H_3^+ formed in the collisions, the study of Reaction (1) can be extended to low collision energies. The pressures maintained in the upper beam source chamber and the scattering chamber were $\sim 10^{-4}$ and $\sim 2 \times 10^{-6}$ Torr, respectively. The vertical and horizontal quadrupole mass spectrometer chambers were evacuated by a liquid-nitrogen (LN_2) trapped 4-in diffusion pump. With the upper H_2 beam off, the base pressure in the mass spectrometer chambers was $\sim 2 \times 10^{-8}$ Torr. During the crossed ion-neutral beam experiment, the detector chambers maintained a pressure of $\sim 8 \times 10^{-7}$ Torr.

The ion exit aperture of the repeller at the photoionization region was covered by a high (90%) transmission gold grid. This avoids the distortion of the electric field maintained at the photoionization region by field penetration due to adjacent focusing ion lenses. The collision region was also shielded by a small square ion lens and three 90%-transmission gold grids (8), (9) and (10) for a similar reason.

Previous studies [70,71] show that because of inelastic charge transfer channels, the slow product ions can be scattered more than $\pm 10°$ away from the initial neutral reactant beam direction. For accurate measurements of total charge transfer cross sections, it is important to have high collecting efficiency for inelastic charge transfer product ions scattered at wide angles. Based on the geometric angle sustained by grid 1 at the collision center, the ion lens system of the horizontal mass spectrometer is capable of accepting product H_2^+ ions scattered $\pm \leq 25°$ away from the neutral H_2

beam direction. The actual transmission through the horizontal mass spectrometer may depend on the scattering angle. A simple analysis based on the Newton diagram of the scattering involving a 2 eV H_2^+ ion beam and a supersonic H_2 beam at 90° predicts that charge transfer product H_2^+ ions formed with the change of one vibrational quantum can be scattered ± 23° away from the neutral H_2 beam direction. The scattering angles for inelastic charge transfer product H_2^+ ions will become smaller as the collisional energy increases. At lower collision energies, the scattering angles for inelastic charge transfer product H_2^+ ions are expected to be large. However, since resonance charge transfer is the dominant charge transfer channel at low collision energies, it should not be a problem here.

The laboratory collision energy (E_{lab}) is defined by the difference in potential between the photoionization and collision regions. In order to achieve high resolution in kinetic energy, it is necessary to minimize the repeller field strength at the photoionization region. For a given electrostatic field applied to the repellers, the resolution in kinetic energy of the reactant H_2^+ beam is governed by the height of the photon beam at the photoionization region. Using a 3-m monochromator in this experiment, the height of the photon beam is estimated to be < 1 mm. Typical repeller field used for E_{lab} = 16-400 eV was ∿ 10 V/cm. At lower collision energies, the focusing and ion transportation required low repeller fields. The repeller field used for E_{lab} = 0.75 eV was ∿ 1.5 V/cm. The actual kinetic energy resolution of the reactant H_2^+ ion beam can be measured by the

retarded field method. This involves measuring the reactant H_2^+ ion intensity by the vertical mass spectrometer as a function of retarding potential applied to the grid 2 at the collision region. The retarding potential analysis of the reactant H_2^+ ion beam having a nominal laboratory collision energy of 16 eV is shown in Figure 2. The retarding voltage is a measure of the potential of grid 2 with respect to that at the center of the repellers at the photoionization region. It can be seen from Figure 2 that the reactant H_2^+ beam intensity observed by the vertical mass spectrometer rises sharply at a retarding voltage of 15.7 V. The further increase in ion intensity for retarding voltages below $\sim$ 14 V is due to focusing effects. Similar observations[33,72] were reported previously in energy analysis of ion beams by the retarding field method. The half width of the sharp rise of 0.2 V was taken to be the laboratory kinetic energy resolution of the H_2^+ reactant beam. Knowing the repeller field and the energy spread, the height of the photon beam at the photoionization region is calculated as $\sim$ 0.5 mm, a value consistent with the estimation.

During the experiment, the square ion lens, grid 1 (8) and grid 2 (9) are at the same potential, while the potential of grid 3 (10) was varied to maximize the collecting efficiency of the product H_2^+ ions. Depending on the collision energy, the potential of grid 3 was set in the range of $\sim$ 0.1-14 V more negative with respect to the potential of grids 1 and 2 and the square ion lens. This range of extraction

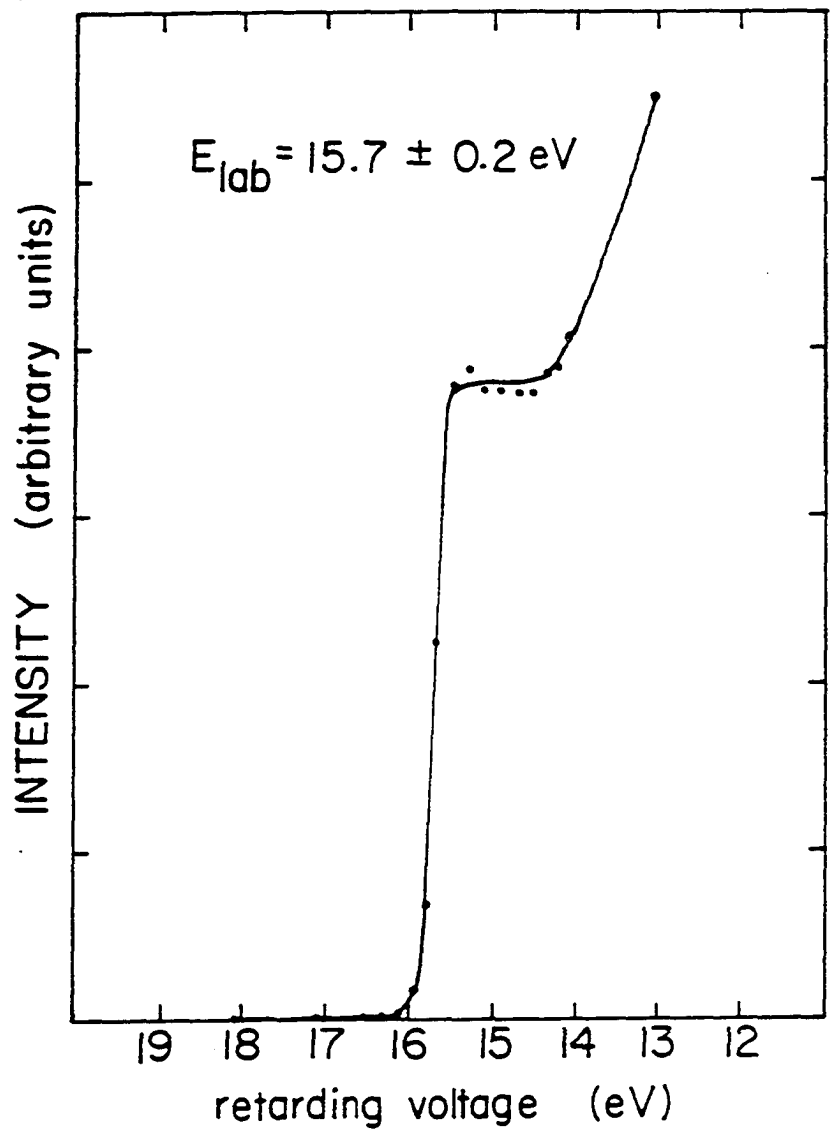

Figure 2. Retarding potential energy curve for a reactant H_2^+ ion beam with a nominal laboratory collisional energy of 16 eV

voltage corresponds to a range in electrostatic field strength of $\sim$ 0.4-6.2 V/cm. Since high extraction field can also degrade the resolution for E_{lab}, the lowest possible extraction field should be used after achieving the maximum collecting efficiency for the product H_2^+ ions at a given collision energy. The reason that a high collecting efficiency can be obtained with a weak extraction field is mainly due to the favorable accepting angle of the horizontal mass spectrometer for the product H_2^+ ions.

For the experiment at a nominal laboratory collisional energy of 16 eV, an extraction field of $\sim$ 2 V/cm was used. We estimated that the spread in collision energy caused by this extraction was less than 0.2 V. Because of translational cooling and narrow angular spread of the neutral reactant H_2 beam achieved by supersonic expansion, the collision energy spread due to the neutral reactant H_2 beam is expected to be negligible. Taking into account the kinetic energy of $\sim$ 0.1 eV associated with the neutral H_2 reactant beam, a nominal laboratory collision energy of 16 eV actually corresponded to $E_{c.m.} = 7.9 \pm 0.2$ eV. If an ion beam-static gas arrangement is used, the energy spread (ΔE) for a given value of $E_{c.m.}$ due to the target gas motion alone is predicted[73] to be

$$\Delta E = (11.1\ \gamma kT\ E_{c.m.})^{1/2} \qquad (3)$$

where γ is the ratio of the projectile ion mass to the total mass (projectile + target), k is the Boltzmann constant, and T is the tem-

perature of the gas cell. Assuming T = 300 K, for a equal mass system such as $H_2^+ + H_2$, ΔE = 1.2 eV when $E_{c.m.}$ = 8 eV. Therefore, the kinetic energy resolutions achieved in this experiment are significantly better than those attained in previous state-selected ion-molecule reaction studies[45-58,63,66,74-76] using the ion beam-gas cell or single gas cell methods.

At $E_{c.m.} \leq 1$ eV, by using a neutral He beam to replace the neutral reactant H_2 beam, we found that a small fraction of H_2^+ reactant ions could be scattered into the horizontal mass spectrometer even though the extraction field between the square ion lens and grid 3 was zero. This problem was partly alleviated by placing a gold-coated copper aperture (18) inside the square ion lens. The tube-like aperture extends the exit hole for the reactant H_2^+ ions in the square ion lens to $\sim$ 0.3 mm from the collision center. As a result of a better defined collision volume, the elastically scattered background H_2^+ reduced to $\sim$ 30% that of the total H_2^+ signal observed by the horizontal mass spectrometer at $E_{c.m.}$ = 0.38 eV. This difficulty improves dramatically as $E_{c.m.}$ increases. The elastically scattered H_2^+ background at $E_{c.m.}$ = 1 eV was found to be < 10% of the total H_2^+ intensity. For $E_{c.m.} \geq 2$ eV, H_2^+ background due to elastically scattered reactant H_2^+ ions observed with or without the aperture (8) was negligible as compared to the intensity of the charge transfer product H_2^+ ions.

The major impurity of the reactant H_2^+ ion beam in the wavelength region of interest in this experiment is H_3^+. The H_3^+ ions were formed by secondary reactions of H_2^+ with ambient H_2 at the photoionization

region. For the collision energy range $E_{c.m.}$ = 2-200 eV, H_3^+ constituted less than 5% of the total ion beam intensity. However, at $E_{c.m.}$ = 0.38 eV and 1 eV where small repeller fields of ∿ 1.5 and 4 V/cm were used to extract the reactant H_2^+ ions, the ratios of the intensity of H_3^+ to that of H_2^+ were ∿ 0.25 and 0.1, respectively. The ratios of the intensity of the elastically scattered H_3^+ background ions to that of H_3^+ formed by Reaction (2) observed by the horizontal mass spectrometer were ∿ 0.05 at $E_{c.m.}$ = 0.38 and 1 eV.

The intensity of the charge transfer product H_2^+ ions is directly proportional to that of the reactant H_2^+ ion beam at the collision region. The electrostatic deflector (4) shown in Figure 1 was helpful in optimizing the transportation of reactant H_2^+ ions from the photoionization region to the collision region. At $E_{c.m.} \leq 1$ eV, the obtainable intensity of the reactant H_2^+ ions at the collision region was lower by more than 20 times in comparison with that at $E_{c.m.} \geq$ 8 eV. Using a wavelength resolution of 1.4 Å (FWHM), the intensity observed at most autoionizing peaks in the photoionization efficiency (PIE) curve for H_2^+ at $E_{c.m.}$ = 16-400 eV was $\gtrsim 1 \times 10^5$ ct/s. At $E_{c.m.}$ = 0.38 eV, the obtainable reactant H_2^+ ion intensity at the strongest autoionization peak at ∿ 784 Å was only ∿ 5500 ct/s.

Depending on the value of $E_{c.m.}$, the ratio of the intensity for the product H_2^+ ions to that of the unattenuated reactant H_2^+ ions varied from ∿ 0.001 to ∿ 0.009. In order to obtain PIE data for the product H_2^+ and H_3^+ ions with standard deviations better than 10%, the counting time used at each point varied in the range of ∿ 20 to ∿ 300 sec.

A complete scan of the high resolution (0.14 Å or 0.28 Å FWHM) PIE spectra for the product H_2^+ ions and the low resolution (1.4 Å FWHM) PIE spectra for the product H_2^+ and H_3^+ ions at $E_{c.m.}$ = 0.38 and 1 eV required approximately 10-20 hours.

Many experimental methods such as translational energy measurements,[77-84] laser-induced fluorescence,[85-88] emission studies,[77,89] and fine structure angular distribution measurement[90] have been used previously to probe the internal energy distribution of product ions formed in charge exchange reactions. Since the charge transfer product ion intensity observed in a state-selected experiment such as this is usually less than 100 cts/s, it is difficult if not impossible to apply the above mentioned methods to measure the internal energy distributions of charge transfer product ions in this experiment or other state-selected experiments using a similar photoionization source. Previous state-selected charge transfer sutdies[45,46,49-56,63-66] have revealed dramatic variations in total cross-sections with ion internal and translational energy. As a result of the favorable kinematics in crossed ion-neutral beam studies of charge transfer processes, it is possible to use the charge transfer detection method to measure the internal energy distributions of product ions in many simple charge transfer reactions. Preliminary results on the state-to-state total charge transfer cross-section measurements for the reactions, $Ar^+(^2P_{3/2,1/2}) + Ar$ and $Ar^+(^2P_{3/2,1/2}) + H_2$, have been obtained in our laboratory using this method.[91]

The calculated state-to-state cross-section for Reaction (1) at $E_{c.m.}$ = 8 and 16 eV indicate that when the reactant H_2^+ ions are in the $v'_o = 0$ state, product $H_2^+(v'' = 0)$ ions constitute 92% and 85% of the product H_2^+ ions, respectively. For $H_2^+(v'' = 1)$, the percentages are $\sim$ 7% at $E_{c.m.}$ = 8 eV and $\sim$ 13% at $E_{c.m.}$ = 16 eV. We have used the charge transfer detection method to probe the vibrational distributions of the product $H_2^+(v'')$ ions formed by Reaction (1) with $v'_o = 0$ and 1 at $E_{c.m.}$ = 4, 8, and 16 eV. To illustrate the principle of the charge transfer detection method, we assume that the $H_2^+(v'')$ ions formed by Reaction (1), with $v'_o = 0$ at $E_{c.m.}$ = 8 and 16 eV only consist of H_2^+ in the $v'' = 0$ and 1 states. A more thorough description of the experimental details and considerations for the charge transfer detection method will be reported in a future publication.[88]

The reaction gas cells (11) associated with the ion lens systems of the vertical and horizontal mass spectrometer will be referred to here as the vertical and horizontal reaction gas cells, (11v) and (11h), respectively. After the formation of $H_2^+(v'')$ in the collisions, all the $H_2^+(v'')$ ions were collected and guided through the horizontal reaction gas cell in which the $H_2^+(v'')$ ions further reacted with other probing gases. The charge transfer reactions

$$H_2^+(v'') + N_2 \rightarrow N_2^+ + H_2 \qquad (4)$$

$$H_2^+(v'') + CO \rightarrow CO^+ + H_2 \qquad (5)$$

were used as the probing reactions. Reactions (3) and (4) were selected because of the substantial differences in total cross-sections for v" = 0($\sigma_{v"=0}$) and v' = 1($\sigma_{v"=1}$). For thin target conditions, the measured ion intensities of $N_2^+[i(N_2^+)]$ and $CO^+[i(CO^+)]$ formed via Reaction (3) and (4) at a given kinetic energy in the horizontal gas cell are related to the intensities of $H_2^+(v" = 0)$ (I_o) and $H_2^+(v" = 1)$ (I_1), the densities (n) of N_2 and CO, the effective length of the reaction gas cell (ℓ), and the values for $\sigma_{v"=0}(N_2^+)$, $\sigma_{v"=1}(N_2^+)$, $\sigma_{v"=0}(CO^+)$ and $\sigma_{v"=1}(CO^+)$ measured at the same kinetic energy by the equations

$$I_0\ n\ell\sigma_{v"=0}(N_2^+) + I_1\ n\ell\sigma_{v"=1}(N_2^+) = i(N_2^+) \tag{6}$$

$$I_0\ n\ell\sigma_{v"=0}(CO^+) + I_1\ n\ell\sigma_{v"=1}(CO^+) = i(CO^+) \tag{7}$$

Furthermore, we have the relations

$$I_0 + I_1 = I_T \tag{8}$$

$$i(N_2^+) = I_T\ n\ell\sigma_m(N_2^+) \tag{9}$$

$$i(CO^+) = I_T\ n\ell\sigma_m(CO^+) \tag{10}$$

where I_T is the total intensity for the $H_2^+(v")$ ions measured when the reaction gas cell was empty; $\sigma_m(N_2^+)$ and $\sigma_m(CO^+)$ represent the total

cross sections for Reactions (4) and (5) characteristic of the $H_2^+(v'')$ ions formed by Reaction (1) with $v_o' = 0$. Combining Eqs. (6)-(10), it can be shown that

$$X_0\ n\ell\sigma_{v''=0}(N_2^+) + X_1\ n\ell\sigma_{v''=1}(N_2^+) = n\ell\sigma_m(N_2^+) \tag{11}$$

$$X_0\ n\ell\sigma_{v''=0}(CO^+) + X_1\ n\ell\sigma_{v''=1}(CO^+) = n\ell\sigma_m(CO^+) \tag{12}$$

Here, X_0 and X_1 are the fractions of H_2^+ in the $v'' = 0$ and 1 states, respectively. Since $n\ell\sigma_{v''=0}(N_2^+)$, $n\ell\sigma_{v''=1}(N_2^+)$, $n\ell\sigma_{v''=0}(CO^+)$, and $n\ell\sigma_{v''=1}(CO^+)$ can be measured, the 2x2 linear Eqs. (10) and (11) allow the calculation of X_0 and X_1. If the $H_2^+(v'')$ ions only consist of H_2^+ in the $v' = 0$ and 1 state, the sum of the calculated values for X_0 and X_1 should be unity.

$$X_0 + X_1 = 1 \tag{13}$$

The calculation of X_0 and X_1 need not involve the determination of the absolute values for $\sigma_{v''=0}$, $\sigma_{v''=1}$, and σ_m provided that they are measured at the same collision energy using the same or identical gas cell and a constant value of n.

The vertical and horizontal reaction gas cells have an identical design. Each cell consists of a front and a back ion lens, a cylindrical platinum grid (12) and a cylindrical wall. The probing gas N_2 or CO entered through the gas inlet (15) connected to the front ion lens and emerged into the gas cell from a circular opening on the front

ion lens. This feature restricted the gas to flow in nearly the same direction of the H_2^+ ions such that reactions between H_2^+ and N_2 or CO should mainly take place in a merged beam fashion. The gas inlet was regulated by Granville-Phillip variable leak valve and the pressure in the gas cell was monitored with a MKS Baratron manometer (Model 370 HS-1). The reaction volume of the gas cell was defined by the platinum grid. During the experiment, product N_2^+ or CO^+ ions formed in the cell were trapped inside the platinum grid by applying a high positive potential to the cylindrical wall of the cell. The front lens and the platinum grid were at the same potential, whereas the potential of the back ion lens was slightly lower than the grid so that the product ions could be extracted and sampled by the mass spectrometer.

The horizontal reaction gas cell and the ion lens system of the horizontal mass spectrometer were enclosed by the horizontal gas cell chamber (17). In this experiment, the gas cell chamber was connected with the horizontal mass spectrometer chamber and evacuated by the same LN_2-trapped 4-in diffusion pump. For a pressure of $\sim 1 \times 10^{-3}$ Torr in the horizontal gas cell, the pressure in the mass spectrometer chamber was maintained at $\sim 3 \times 10^{-6}$ Torr. By combining the gas inlet design and differential pumping, the N_2^+ or CO^+ background ions formed at the collision region were found to be negligible in comparison to product N_2^+ or CO^+ ions formed in the horizontal gas cell.

The vertical reaction gas cell can be used to measure the values

for $n\ell\sigma_{v''=0}(N_2^+)$, $n\ell\sigma_{v''=1}(N_2^+)$, $n\ell\sigma_{v''=0}(CO^+)$, and $n\ell\sigma_{v''=1}(CO^+)$. We found that the reactant H_2^+ ions formed at the photoionization region can be bent and sent through the horizontal gas cell by adjusting the voltages of grid (1), (2), and (3) with only moderate loss in intensity. Therefore, the parameters $n\ell\sigma_{v''=0}$, $n\ell\sigma_{v''=1}$ and $n\ell\sigma_m$ were all measured using the horizontal gas cell.

Results and Discussion

Figure 3 compares the PIE curves for the product H_2^+ ions observed by the horizontal mass spectrometer at several collision energies using a wavelength resolution of 1.4 Å (FWHM) and the PIE curve for the reactant H^+ ions recorded with the same wavelength resolution. The latter spectrum was obtained with the neutral H_2 reactant beam off. As expected, the spectrum for the reactant H_2^+ ions was found to be independent of the kinetic energy for the reactant H_2^+ which was defined to be the difference in potential between the photoionization and collision regions. Since the standard deviations for these low resolution PIE data were better than 2%, the PIE data were connected by solid or dashed lines. The PIEs of the product and reactant H_2^+ ion spectra in the region of 790-805 Å, which corresponds to the formation of H_2^+ in the ground vibrational state, were arbitrarily normalized to have the same values. From the comparison of these low resolution spectra, it is obvious that the total charge transfer cross section for Reaction (1) ($\sigma_{v_o'}(H_2^+)$) depends on both the vibra-

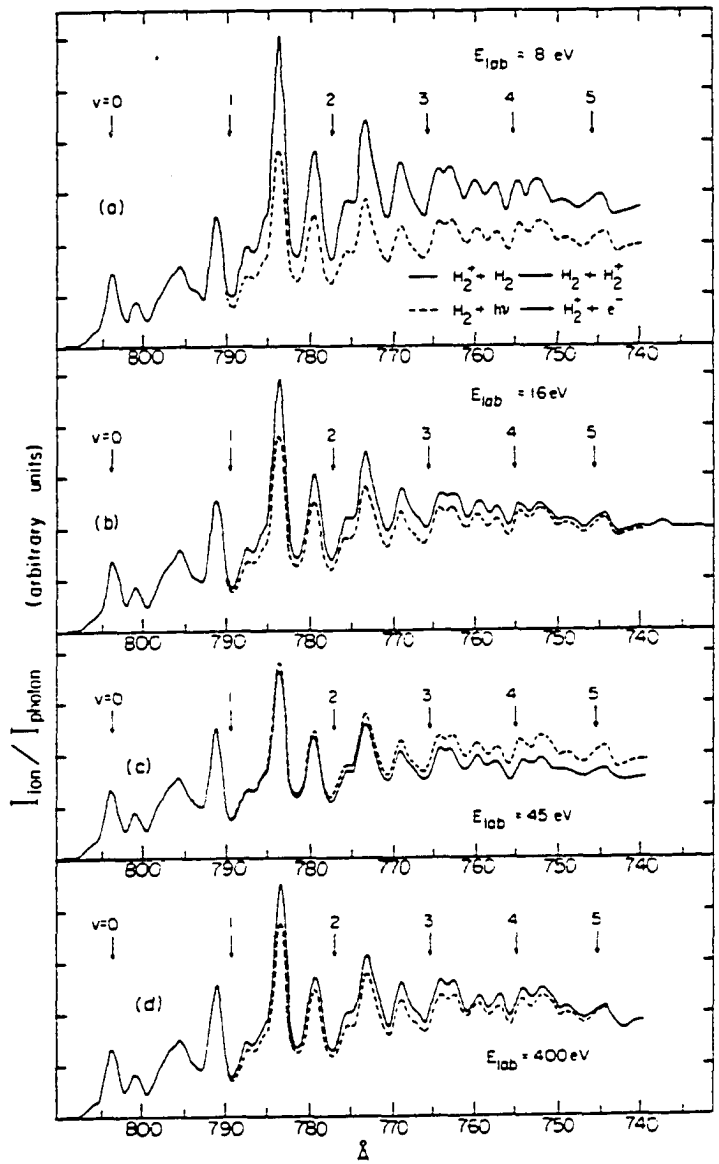

Figure 3. The comparisons of PIE curves for the H_2^+ product ions (——) formed at E_{lab} equals to (a) 8 eV, (b) 16 eV, (c) 45 eV, and (d) 400 eV with that for the H_2^+ reactant ions (---) in the region of 730-810 Å. The PIEs for the product and reactant ions in the region of 790-810 Å, which corresponds to the formation of $H_2^+(v_o' = 0)$, are normalized to the same values (wavelength resolution = 1.4 Å (FWHM))

tional and kinetic energies of the reactant H_2^+ ions. At E_{lab} = 8 eV (Figure 3(a)), the PIEs for the product H_2^+ ions in vibrational states $v_o' \geq 1$ are approximately $\sim$ 50% higher than those for the reactant H_2^+ ions, an observation consistent with the conclusion that $\sigma_{v_o'}(H_2^+)$ increases with vibrational excitations of the reactant H_2^+ ions. The vibrational enhancement for $\sigma_{v_o'}(H_2^+)$ manifested by the spectra at E_{lab} = 16 eV (Figure 3(b)) has reduced considerably. As E_{lab} increases to 45 eV, Figure 3(c) shows that $\sigma_{v_o'}(H_2^+)$ is inhibited by vibrational excitations of the reactant H_2^+ ions. At E_{lab} = 400 eV, the vibrational enhancement for $\sigma_{v_o'}(H_2^+)$ is again evident from the comparison depicted in Figure 3(d). The vibrational effect on the total cross section for charge transfer between H_2^+ with H_2 at E_{lab} = 400 eV revealed in the comparison in Figure 3(d) is consistent with that observed at E_{lab} = 430 eV by Chupka.[44] The difference in PIE between the product and reactant H_2^+ ion spectra at E_{lab} = 16 and 400 eV was found to diminish gradually toward higher photon energies in the wavelength region of $\sim$ 740-755 Å, indicating that $\sigma_{v_o'=4}(H_2^+)$ and $\sigma_{v_o'=5}(H_2^+)$ are probably lower than $\sigma_{v_o'=1}(H_2^+)$, $\sigma_{v_o'=2}(H_2^+)$, and $\sigma_{v_o'=3}(H_2^+)$ at E_{lab} = 16 and 400 eV.

The PIE data for the product H_2^+ ions in the region of $\sim$ 743-809 Å observed at $E_{c.m.}$ = 2, 4, 8, 16, 22.5 and 200 eV using a wavelength resolution of 0.3 Å (FWHM) are plotted in Figure 4(b), Figures 5(a), 5(b), 5(c), 5(d), and 5(e), respectively. Similar to the procedures used by Chupka and co-workers, relative values for $\sigma_{v_o'}(H_2^+)$ were deduced

by comparing the intensities of corresponding autoionization peaks resolved in the spectra for the product and reactant H_2^+ ions. However, instead of using the relative heights of autoionization peaks above the apparent continuum, the relative areas of autoionization peaks above the apparent continuum are used here. Because of the low signal level for the product H_2^+ ions obtainable in a high resolution experiment, using the peak areas is necessary to reduce the uncertainties for the derived relative values of $\sigma_{v_o'}(H_2^+)$ due to counting statistics.

Figure 4(a) displays the PIE spectrum for the reactant H_2^+ ions measured by the vertical mass spectrometer using an optical resolution of 0.3 Å (FWHM). Most of the autoionization features found in this spectrum still consist of more than one autoionization states. Nevertheless, the resolution used is sufficiently high to allow for the correction of photoionization yields arisen from direct photoionization. In the wavelength range of $\sim$ 791-807 Å, H_2^+ can only be formed in the $v_o' = 0$ state. The positions of the base lines, which account for photoionization yields from direct photoionization in wavelength intervals corresponding to the formation of H_2^+ in the $v_o' =$ 1, 2, 3, and 4 states, were defined by the lowest value in PIE measured in each wavelength interval. In arriving at the base lines shown in Figure 4(a), we have also assumed that direct photoionization gives rise to uniform PIE within a vibrational interval. Since the positions of the base lines thus determined necessarily represent the upper limits in photoionization yield due to direct photo-

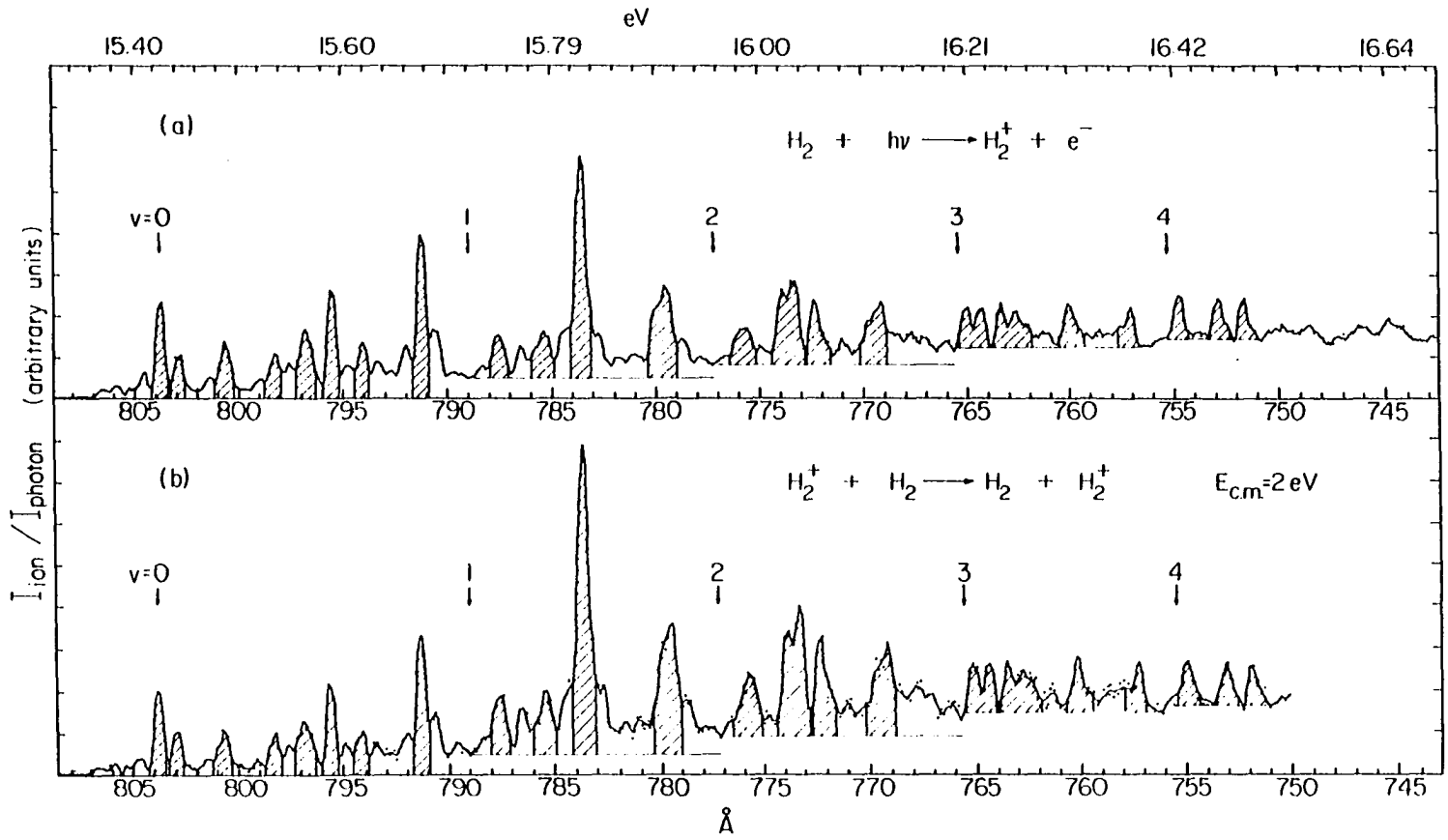

Figure 4(a). PIE curve for the H_2^+ reactant ions in the region of 743-809 Å (wavelength resolution = 0.3 Å (FWHM))

Figure 4(b). PIE curve for the H_2^+ product ions in the region of 750-809 Å observed at $E_{c.m.}$ = 2 eV (wavelength resolution = 0.3 Å (FWHM))

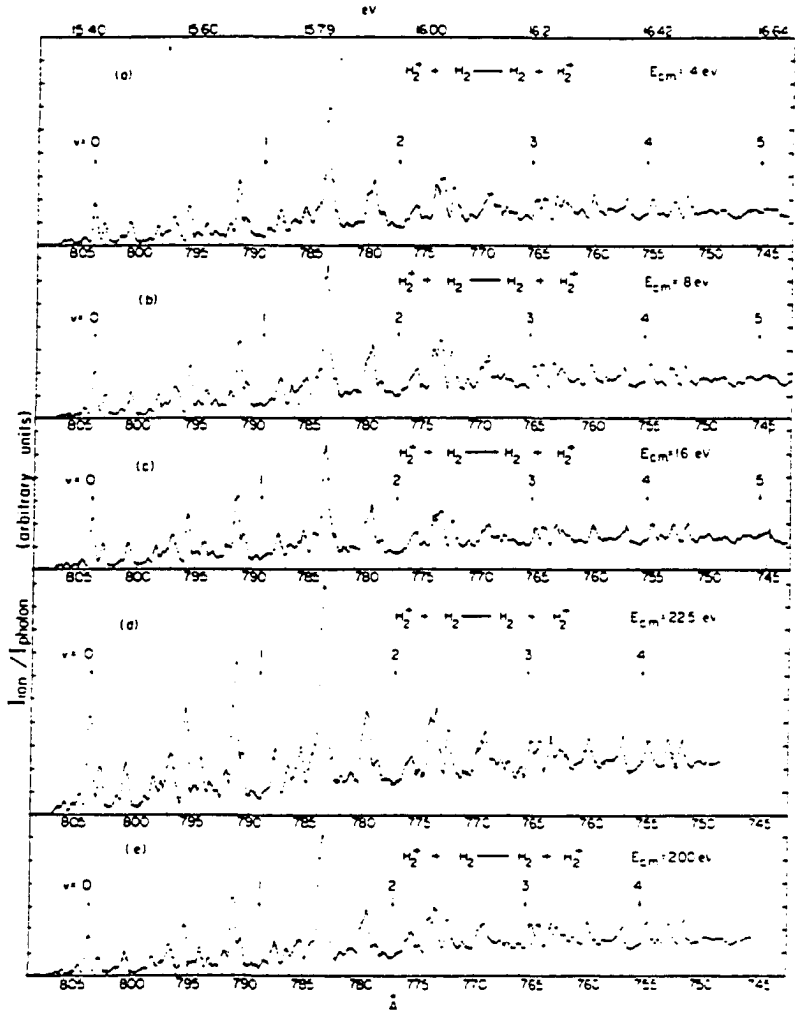

Figure 5. PIE curves for the H_2^+ product ions in the region of ∿ 743-809 Å observed at (a) $E_{c.m.}$ = 4 eV, (b) $E_{c.m.}$ = 8 eV, (c) $E_{c.m.}$ = 16 eV, (d) $E_{c.m.}$ = 22.5 eV, and (e) $E_{c.m.}$ = 200 eV using a wavelength resolution of 0.3 Å (FWHM)

ionization, photoionization yields above these base lines can be solely ascribed to autoionization. According to the above discussion, the shaded areas of autoionization peaks above the base line in a photon energy region higher than the threshold for the formation of $H_2^+(v_o')$ and below that of $H_2^+(v_o'+1)$ can be taken as a measure for the intensity of reactant H_2^+ ions formed in the v_o' state. Similar procedures to correct for photoionization yields due to direct photoionization can be applied to a PIE curve for the product H_2^+ ions such as that shown in Figure 4(b). The fact that the PIE curve for H_2^+ is highly structured makes the location of these base lines relatively straightforward. As a result of the weak autoionization structure found in the product and reactant ion spectra in the wavelength region above the threshhold for the formation of $H_2^+(v_o'=5)$, it is difficult to use this method for the determination $\sigma_{v_o'=5}(H_2^+)$ with high accuracy. Therefore, the relative values for $\sigma_{v_o'}(H_2^+)$ presented here are limited to $v_o' = 0$-4.

Relative values for $\sigma_{v_o'}(H_2^+)$, $v_o' = 0$-4, at $E_{c.m.} = 2$ eV were determined by calculating the ratios of the shaded areas for corresponding autoionization peaks resolved in the PIE curves for the product and reactant H_2^+ ions shown in Figures 4(b) and 4(a), respectively. The shaded areas of autoionization peaks were arbitrarily chosen for comparison. Relative total charge transfer cross sections for other collision energies $E_{c.m.} = 4$, 8, 16, 22.5, and 200 eV were obtained by the same procedures.

The derived values for $\sigma_{v_o'}(H_2^+)/\sigma_{v_o'=0}(H_2^+)$ at $E_{c.m.} = 2$, 4, 8, 16,

22.5, and 200 eV are listed in Table 1 and plotted as a function of v_o' in Figure 6 to compare with the theoretical calculations of Lee and DePristo.[20] The uncertainties of the experimental values given in Table 1 represent the weighed deviations in ratios of the areas for corresponding autoionization peaks used within a vibrational interval. The uncertainties due to counting statistics are in general smaller than the weighed deviation. The major errors for the derived relative cross sections are caused by finite uncertainties in locating the positions of the base lines which account for errors of $\sim$ 3-5% for $\sigma_{v_o'}(H_2^+)/\sigma_{v_o'=0}(H_2^+)$, v_o' = 1 and 2, and $\sim$ 5-10% for those with v_o' = 3 and 4. The normalized values for $\sigma_{\underline{<}v_o'}(H_2^+)/\sigma_{v_o'}(H_2^+)$ deduced from the ratios of the areas for corresponding autoionization peaks without corrections for direct photoionization are also included in Table 1 and Figure 6. Here, $\sigma_{\underline{<}v_o}(H_2^+)$ represents the total charge transfer cross sections for the reaction $H_2^+ + H_2$ characteristic of reactant H_2^+ ions formed under the selected autoionization peaks. The relative values for $\sigma_{v_o'}(H_2^+)/\sigma_{v_o'=0}(H_2^+)$ at $E_{c.m.}$ = 4, 8, and 200 eV reported by Campbell et al. are also included in Table 1 and Figure 6. The latter values were obtained by scaling the plots shown in Figure 1 of Ref. 53. The values for $\sigma_{\underline{<}v_o'}(H_2^+)/\sigma_{v_o'=0}(H_2^+)$ are found to be close to those for $\sigma_{v_o'}(H_2^+)/\sigma_{v_o'=0}(H_2^+)$ indicating that H_2^+ ions produced under the selected autoionization peaks are dominated by H_2^+ ions in a particular vibrational state even before corrections for photoionization yields from direct photoionization. Furthermore, since no baseline corrections are involved in the derivation of $\sigma_{\underline{<}v_o'}(H_2^+)/\sigma_{v_o'}(H_2^+)$, the similar

Table 1. Relative total cross sections $\sigma_{v_o'}(H_2^+)/\sigma_{v_o'=0}(H_2^+)$ for the charge transfer reaction $H_2^+(v_o')$ with $H_2(v_o''=0)$ at $E_{c.m.}$ = 2, 4, 8, 16, 22.5 and 200 eV as a function of the vibrational quantum number v_o' of H_2^+

			$\sigma_{v_o'}(H_2^+)/\sigma_{v_o'=0}(H_2^+)$		
			Experimental		
$E_{c.m.}$ (eV)	v_o'	$\sigma_{\leq v_o'}(H_2^+)/\sigma_{v_o'=0}(H_2^+)$[a]	This work[b]	Ref. 53[c]	Theoretical[d]
2	0	1.00	1.00±0.02	...	...
	1	1.55	1.64±0.04	...	...
	2	1.62	1.75±0.07	...	...
	3	1.50	1.54±0.04	...	...
	4	1.39	1.36±0.02	...	...
4	0	1.00	1.00±0.03	1.00	...
	1	1.39	1.47±0.04	1.52	...
	2	1.43	1.52±0.06	1.61	...
	3	1.36	1.38±0.04	1.38	...
	4	1.25	1.22±0.11	1.33	...

[a] $\sigma_{\leq v_o'}(H_2^+)$ represents the total charge transfer cross section for the H_2^+-H_2 system characteristic of reactant H_2^+ ions formed under selected autoionization peaks. The values for $\sigma_{\leq v_o}(H_2^+)/\sigma_{v_o'=0}(H_2^+)$ are deduced from the ratios of the corresponding areas of autoionization peaks resolved in the product and reactant H_2^+ spectra without the corrections for direct photoionization.

[b] The uncertainties represent the variations in the ratios of the corresponding areas of the autoionization peaks in the PIE curves for the product and reactant H_2^+ ions.

[c] Values obtained by scaling the plot shown in Figure (1) of Ref. (53).

[d] References (20) and (68).

Table 1. continued

$E_{c.m.}$ (eV)	v'_o	$\sigma_{\leq v'_o}(H_2^+)/\sigma_{v'_o=0}(H_2^+)$	$\sigma_{v'_o}(H_2^+)/\sigma_{v'_o=0}(H_2^+)$ Experimental: This work	Experimental: Ref. 53	Theoretical
8	0	1.00	1.00±0.03	1.00	1.00
	1	1.28	1.32±0.03	1.40	1.24
	2	1.35	1.41±0.04	1.38	1.32
	3	1.24	1.28±0.06	1.37	1.26
	4	1.14	1.07±0.04	1.20	1.13
16	0	1.00	1.00±0.03	...	1.00
	1	1.04	1.04±0.02	...	0.98
	2	0.98	0.95±0.03	...	0.90
	3	0.94	0.88±0.04	...	0.82
	4	0.88	0.76±0.05	...	0.68
22.5	0	1.00	1.00±0.04	...	1.00
	1	0.95	0.94±0.05	...	0.95
	2	0.86	0.83±0.05	...	0.86
	3	0.82	0.75±0.05	...	0.77
	4	0.78	0.62±0.07	...	0.61
200	0	1.00	1.00±0.03	1.00	1.00
	1	1.24	1.27±0.02	1.19	1.25
	2	1.26	1.32±0.04	1.15	1.35
	3	1.22	1.27±0.05	1.10	1.26
	4	1.18	1.22±0.04	1.10	1.03

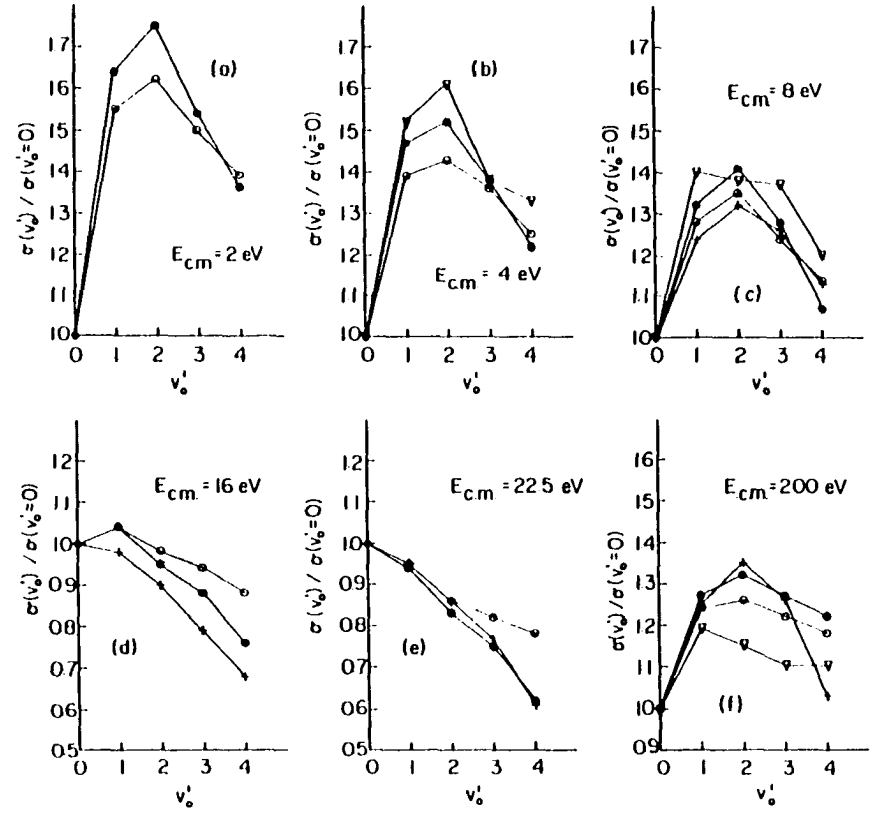

Figure 6. Relative total charge transfer cross sections $\sigma(v_o')/\sigma(v_o' = 0)$ for the reaction $H_2^+(v_o') + H_2(v_o'' = 0)$ plotted as a function of vibrational quantum number v_o'. (a) $E_{c.m.}$ = 2 eV, (b) $E_{c.m.}$ = 4 eV, (c) $E_{c.m.}$ = 8 eV, (d) $E_{c.m.}$ = 16 eV, (e) $E_{c.m.}$ = 22.5 eV, (f) $E_{c.m.}$ = 200 eV. (•) This work; (o) this work, obtained without corrections of direct photoionization; (∇) Ref. 53; (+) Theoretical, Ref. 20

trends observed for $\sigma_{v_o'}(H_2^+)/\sigma_{v_o'=0}(H_2^+)$ and $\sigma_{\leq v_o'}(H_2^+)/\sigma_{v_o'=0}(H_2^+)$ at all energies can be taken as a support that the general trends for $\sigma_{v_o'}(H_2^+)/\sigma_{v_o'=0}(H_2^+)$ on v_o' determined here are reliable.

The best agreement between the experimental results and theoretical calculations of Lee and DePristo was observed at $E_{c.m.}$ = 22.5 eV as shown in Figure 6(e). The value for $\sigma_{v_o'}(H_2^+)/\sigma_{v_o'=0}(H_2^+)$ was found to decrease monotonically with v_o', consistent with the comparison of the low resolution spectra depicted in Figure 3(c). The experimental values for $\sigma_{v_o'}(H_2^+)/\sigma_{v_o'=0}(H_2^+)$, v_o' = 1-4, at $E_{c.m.}$ = 16 eV are higher than the corresponding calculated values by $\sim$ 5-10%. The careful analysis of repetitive scans at $E_{c.m.}$ = 16 eV indicates unambiguously that the value for $\sigma_{v_o'=1}(H_2^+)$ is higher than that for $\sigma_{v_o'=0}(H_2^+)$. At $E_{c.m.}$ = 8 eV (Figure 6(c)), the value for $\sigma_{v_o'=0}(H_2^+)$ is the lowest in comparison with those for v_o' = 1-4. The profile for the vibrational dependence of $\sigma_{v_o'}(H_2^+)$ determined here was again found to be consistent with the theoretical prediction. Within experimental uncertainties, the relative values for $\sigma_{v_o'}(H_2^+)$, v_o' = 0, 3, and 4 are in agreement with the calculated values. However, the theoretical calculation seems to underestimate the values for $\sigma_{v_o'}(H_2^+)$, v_o' = 1 and 2, with respect to that for $\sigma_{v_o'=0}(H_2^+)$ by approximately 10%. Unlike the experimental results of Campbell et al.,[53] which show a maximum for $\sigma_{v_{o=1}'}(H_2^+)$, both theory of Lee and DePristo and experimental results of this study indicate that the value for $\sigma_{v_o'}(H_2^+)$ is peaked at v_o' = 2 at $E_{c.m.}$ = 8 eV. The trend observed for

$\sigma_{v'_o}(H_2^+)/\sigma_{v'_o=0}(H^+_2)$, v'_o = 1-4, at $E_{c.m.}$ = 4 eV, is similar to that found at $E_{c.m.}$ = 8 eV except that the difference between $\sigma_{v'_o=1}(H_2^+)$ and $\sigma_{v'_o=0}(H_2^+)$ at $E_{c.m.}$ = 4 eV is greater than that at $E_{c.m.}$ = 8 eV. Taking into account the error limits of both experiments, the results of Campbell et al. are in agreement with those determined here at $E_{c.m.}$ = 4 eV (see Figure 6(b)). Of all the collision energies investigated in this study, the greatest vibrational enhancement for Reaction (1) was observed at $E_{c.m.}$ = 2 eV. As will be shown in a latter section, there is evidence that the vibrational effect actually starts to diminish as the collision energy further decreases from $E_{c.m.}$ = 2 eV. No theoretical results are available for comparison at $E_{c.m.}$ = 2 and 4 eV. Due to the semiclassical nature of the SCECT formulation and the fact that the calculation has not included the H_3^+ + H channel, which is a dominant product channel at low collision energies, the theoretical calculation of Lee and DePristo is not expected to be accurate at low collision energies ($E_{c.m.}$ < 8 eV).

Previous studies [22,92] of the H_4^+ potential energy surface by the diatomics-in-molecules method have provided insight into the charge transfer process for the $H_2^+ + H_2$ system. Resonance charge transfer essentially involves the crossing of a barrier of the ground state adiabatic surface which divides the two charge transfer states. The barrier, which arises from an avoided intersection between the ground and the first excited electronic surfaces of H_4^+, has a height dependent on the H_2^+-H_2 distance. At a H_2^+-H_2 distance of $\geq$ 4.2 Å, the calcula-

tions show that the reactant pair $H_2^+(v_o'=0) + H_2(v_o''=0)$ at zero collision energy cannot cross the barrier. For shorter H_2^+-H_2 distances, the barrier is reduced as a result of a larger splitting between the ground and the first excited surfaces; and the reactants, even in their ground vibrational states, can traverse the barrier. At low collision energies, the interaction between H_2^+ and H_2 is mainly governed by long-range forces, and large impact parameter collisions will contribute more to the charge transfer cross sections. Furthermore, one also anticipates that resonance charge transfer will become more important as the collision energy is lowered. Since vibrational excitations of the reactants will afford the crossing of the barrier, the calculations predict vibrational enhancements for Reaction (1) at low collision energies. Stemming from the expectation that the barrier is higher for a larger impact parameter, these calculations also imply a greater inhabitation for Reaction (1) with $v_o' = 0$ as the collision energy decreases. The experimental observations, that the relative values for $\sigma_{v_o'}(H_2^+)/\sigma_{v_o'=o}(H_2^+)$, $v_o' = 1\text{-}4$, remain relatively unchanged, while the difference between $\sigma_{v_o'=0}(H_2^+)$ and $\sigma_{v_o'=1}(H_2^+)$ increases as $E_{c.m.}$ decreases in the range of $E_{c.m.} = 2\text{-}8$ eV, are in complete accord with this picture.

According to the above discussion, one might expect that the Franck-Condon factors for the ionization transitions between the vibrational ground state of $H_2(\tilde{X}\ ^1\Sigma_g^+)$ and vibrational states of $H_2^+(\tilde{X}\ ^2\Sigma_g^+)$ will play a role in the vibrational dependence of $\sigma_{v_o'}(H_2^+)$ at low col-

lision energies. The Franck-Condon factors for the transitions from the ground vibrational state of $H_2(\tilde{X}\ ^1\Sigma_g^+,\ v''=0)$ to $H_2^+(\tilde{X}\ ^2\Sigma_g^+,$ $v_o'=0,1,2,3$, and 4 are 0.0925, 0.1754, 01960, 0.1700, and 0.1274, respectively.[93] If the Franck-Condon factors were the sole parameter, which determines $\sigma_{v_o'}(H_2^+)$, $\sigma_{v_o'}(_2^+)$ should be proportional to the square of the corresponding Franck-Condon factor. This predicts the values for $\sigma_{v_o'}(H_2^+)/\sigma_{v_o'=0}(H_2^+)$, v_o' = 0-4 to be 1, 3.60, 4.49, 3.38, and 1.90, respectively. The fact that rigorous theoretical treatments of the dynamics for symmetric charge transfer do not reveal a simple Franck-Condon factor dependence for $\sigma_{v_o'}(H_2^+)$, it is thus of no surprise to find that the vibrational enhancements observed at $E_{c.m.}$ = 2, 4, and 8 eV are less pronounced than that predicted by the Franck-Condon factor alone. Nevertheless, it is interesting to note that the vibrational dependences of $\sigma_{v_o'}(H_2^+)$ measured at $E_{c.m.}$ = 2, 4, and 8 eV are in qualitative agreement with the Franck-Condon factor prediction.

The magnitude of the vibrational enhancements observed at $E_{c.m.}$ = 200 eV (Figure 6(f)) is comparable to that found at $E_{c.m.}$ = 8 eV with the exception that the fall off of $\sigma_{v_o'}(H_2^+)$, v_o' = 3 and 4, with respect to $\sigma_{v_o'=2}(H_2^+)$ is less dramatic than that at $E_{c.m.}$ = 8 eV. The measured values for $\sigma_{v_o'}(H_2^+)/\sigma_{v_o'=0}(H_2^+)$, v_o' = 0-3, are in excellent agreement with the theoretical values. However, the theoretical value for $\sigma_{v_o'=4}(H_2^+)/\sigma_{v_o'=0}(H_2^+)$ was found to be lower than the experimental value. At high collision energies, such as $E_{c.m.}$ = 200 eV, the short range interactions between H_2^+ and H_2, which are responsible for inelastic

charge transfer processes, are expected to play a more important role in charge transfer collisions. Since the number of near resonance product channels becomes greater as the vibrational energy for the reactant H_2^+ ion increases, the slow drop off of $\sigma_{v_o'}(H_2^+)$, $v_o' = 3$ and 4 with respect to $\sigma_{v_o'=2}(H_2^+)$ observed at $E_{c.m.} = 200$ eV is probably due to higher cross sections for nonresonant charge transfer channels. The calculation indeed shows that the cross sections of many off-resonant product channels at $E_{c.m.} = 200$ eV are as large as those of the resonant channels.[20] We note that the interaction potential based on the one-active-electron model, which was used in the dynamical calculation, shows the least agreement with the ab initio CI calculation at short H_2^+-H_2 distances. Therefore, the discrepancy observed between the experimental and theoretical values for $\sigma_{v_o'=4}(H_2^+)/\sigma_{v_o'=0}(H_2^+)$ can be partly ascribed to the inaccuracy of the one-active-electron model at short H_2^+-H_2 distances. In order to test this speculation, it would be helpful to extend the comparison between experimental measurements and theoretical calculations for $v_o' > 4$. The lower values for $\sigma_{v_o'}(H_2^+)/\sigma_{v_o'=0}(H_2^+)$, $v_o' = 1$-4, obtained by Campbell et al., might be due to lower collecting efficiencies for inelastic charge transfer product H_2^+ ions by the TOF method.

The relative theoretical cross sections used in the above comparison are based on the average values of the cross sections calculated at three different initial molecular orientations. Since the strengths of the interaction potentials for different molecular orientations are different, the calculated cross sections for different molecular orien-

tations can vary by as much as 20%. To a lesser extent, the vibrational dependence for $\sigma_{v_o'}(H_2^+)$ also depends on the initial molecular orientation. In view of the fact that the differences found between the experimental and theoretical results are in most cases within 10%, a more thorough calculation to sample more initial molecular orientations may reduce the discrepancies.

The variations of $\sigma_{v_o'}(H_2^+)/\sigma_{v_o'=0}(H_2^+)$ as a function of v_o' at different collisional energies depicted in Figure 6(a)-(f) suggest that the kinetic energy dependence of $\sigma_{v_o'}(H_2^+)$ may exhibit structure in the energy range $E_{c.m.}$ = 2-200 eV. Because of the necessities to change the kinetic energy of the reactant H_2^+ ion beam and to maximize the reactant H_2^+ ion intensity at the collision region, the voltage arrangement of the ion lenses between the photoionization and collision regions cannot be kept constant. Considering the fact that the collision volume in the crossed ion-neutral beam arrangement depends on the focusing property of the ion lenses, the collision volume, which is defined by the intersection volume of the H_2^+ and H_2 beams, may also vary with $E_{c.m.}$. In principle, if the collision volume could be held constant in the energy range of interest, under thin target conditions, relative total cross section for Reaction (1) as a function of $E_{c.m.}$ can be determined by measuring the ratio $i(H_2^+)/I(H_2^+)$ at different collision energies. Here, $i(H_2^+)$ is the product H_2^+ ion intensity measured by the horizontal mass spectrometer and $I(H_2^+)$ is the reactant H_2^+ ion intensity measured by the vertical mass spectrometer with the neutral reactant H_2 beam off. In order to determine

$\sigma_{v_o'}(H_2^+)$ as a function of $E_{c.m.}$, a correction function, which accounts for the changes in the collision volume and the spacial distributions of H_2^+ and H_2 within the collision volume, in the collision energy range of interest must be known.

The previous measurements on the absolute total charge transfer cross sections for the $H_2^+ + H_2$ system, which used low energy electron ionization to prepare the reactant H_2^+ ions, have been reviewed recently by Barnett et al.[43] Within the range E_{lab} = 8-400 eV, essentially all these measurements are in good agreement that the total charge transfer cross section decreases monotically as E_{lab} increases. However, the absolute magnitudes of these measurements were found to differ substantially. The recommended values for the absolute total charge transfer cross sections for the $H_2^+ + H_2$ reactions in the range E_{lab} = 8-400 eV are shown as the dashed line in Figure 7. The uncertainty in absolute magnitude of the recommended values was estimated to be ± 40%. Most of the previous electron ionization studies used electron energies greater than 18 eV. The vibrational distribution of the reactant H_2^+ ions produced by electron ionization in the previous experiments can be characterized by the Franck-Condon factors of the transitions from the ground vibrational state of $H_2(\tilde{X}\ ^1\Sigma_g^+)$ to vibrational states of $H_2^+(\tilde{X}\ ^2\Sigma_g^+)$. It is possible to produce reactant H_2^+ ions with a vibrational distribution similar to those obtained in previous electron ionization studies by using a photon energy of $\gtrsim$ 18 eV provided that the selected photon energy does not coincicde with excitation energies of autoionizing states.

In order to obtain the kinetic energy dependence for $\sigma_{v_o'=0}(H_2^+)$, the relative values for the ratios $i(H_2^+)/I(H_2^+)$ (i.e., the relative total charge transfer cross sections) with the reactant H_2^+ ions formed by photoionization at wavelengths 792 Å and 688 Å were first measured by the crossed ion-neutral beam arrangement at fixed values of E_{lab}. Since at a given value of E_{lab} the same voltage arrangement for the ion optics are used to measure the ratios $i(H_2^+)/I(H_2^+)$ at 792 Å and 688 Å, the relative total cross sections thus determined should be reliable. At 792 Å, all reactant H_2^+ ions were formed in $v_o' = 0$ state, while at 688 Å, H_2^+ ions should have a broad vibrational distribution characteristic of the Franck-Condon transition probabilities between the ground vibrational state of $H_2(\tilde{X}\ ^1\Sigma_g^+)$ and $H_2^+(\tilde{X}\ ^2\Sigma_g^+, v_o')$ with the highest value of v_o' up to 18. The photon energy corresponding to 688 Å (18 eV) is slightly lower than the dissociative ionization threshold (18.077 eV) of H_2.[94] The selection of this wavelength is to minimize the contamination of the H_2^+ reactant beam by H^+ which can be formed by the dissociative ionization process at higher photon energies. The intensity of H^+ formed by the ion-pair process at 688 Å is less than 0.1% that of H_2^+. Assuming the vibrational distribution for H_2^+ prepared at 688 Å to be identical to that for H_2^+ formed by electron ionization, the values for $i(H_2^+)/I(H_2^+)$ measured at 688 Å in the range E_{lab} = 8-400 eV were scaled to fit the dashed line determined by previous electron ionization studies. The values for $\sigma(v_o'=0)$ depicted in Figure 7 were obtained by multiplying the values for $i(H_2^+)/I(H_2^+)$ measured at 792 Å with the same scaling factors at cor-

responding collision energies. These procedures in effect allow the corrections for the change in collision volume as a function of E_{lab} due to focusing effects of the reactant H_2^+ beam and the variations in spatial distributions of H_2^+ and H_2 within the collision volume.

The experimental values for $\sigma_{v_o'=0}(H_2^+)$ thus determined reveal a broad peak centered at $E_{lab} \approx 35$ eV. Since the state-selected experiment of Campbell et al.[53] only measured $\sigma_{v_o'=0}(H_2^+)$ at E_{lab} = 8, 16, 156, and 400 eV, the broad maximum was not observed previously. Once the kinetic energy dependence of $\sigma_{v_o'=0}(H_2^+)$ is known, $\sigma_{v_o'}(H_2^+)$, v_o' = 1–4, can be determined from the known vibrational dependences of $\sigma_{v_o'}(H_2^+)$ at fixed collision energies such as those listed in Table 1. The values for $\sigma_{v_o'=1}(H_2^+)$ at E_{lab} = 8, 16, 32, 45, and 400 eV deduced by this method are shown in Figure 7. It seems obvious that $\sigma_{v_o'=1}(H_2^+)$ crosses below $\sigma_{v_o'=0}(H_2^+)$ at a value of E_{lab} between 32 and 45 eV and $\sigma_{v_o'=1}(H_2^+)$ recrosses above $\sigma_{v_o'=0}(H_2^+)$ at a higher value of E_{lab} between 45 and 400 eV. The precise positions of these intersections should be sensitive to the dynamics and the potential energy surfaces of the $H_2^+ + H_2$ system. In order to locate the positions of the crossings and obtain a better estimate of the profile for $\sigma_{v_o'=1}(H_2^+)$, we have measured the ratio of the height of the autoionization peak at 784 Å (I(784 Å)) to that at 792 Å (I(792 Å)) resolved in the PIE curve for the product H_2^+ ion as a function of E_{lab} using a wavelength resolution of 1.4 Å (FWHM). In these measurements, a 2 V/cm extraction field was maintained at the collision region and no effort was made to maximize the product H_2^+ ion intensity at specific collision energies. At

792 Å, all reactant H_2^+ ions were produced in the $v_o' = 0$ state, while those formed under the strongest autoionization feature at 784 Å were predominately in the $v_o' = 1$ state. The measured values for I(784 Å)/I(792 Å) in the range E_{lab} = 2-400 eV were plotted in Figure 8. The observation that the value for I(784 Å)/(792 Å) at E_{lab} = 2 eV is lower than that at E_{lab} = 4 eV can be taken as evidence that the difference between $\sigma_{v_o'=0}(H_2^+)$ and $\sigma_{v_o'=1}(H_2^+)$ reaches the maximum at $\sim E_{lab}$ = 4. The measured ratio of the autoionization peak intensities at 784 Å and 792 Å in the PIE spectrum for the reactant H_2^+ ions is 1.48 which is shown as a straight line in Figure 8. It can be seen that at E_{lab} < 30 eV and > 120 eV, $\sigma_{v_o'=1}(H_2^+)$ is greater than $\sigma_{v_o'=0}(H_2^+)$ and in the range E_{lab} = 35-100 eV, $\sigma_{v_o'=1}(H_2^+)$ is lower than $\sigma_{v_o'=0}(H_2^+)$. Therefore, we conclude that the total charge transfer cross sections for $v_o' = 0$ and 1 intersect at $E_{lab} \approx 33$ and 115 eV. The functional form for $\sigma_{v_o'}(H_2^+)$ depicted in Figure 7, which is estimated by the measurements summarized in Figure 8, is similar to that for $\sigma_{v_o'=0}(H_2^+)$. The maximum for $\sigma_{v_o'=1}(H_2^+)$ was observed at $E_{lab} \approx 16$ eV.

The nature of the broad beak observed in the collision energy dependence of $\sigma_{v_o'=0}(H_2^+)$ shown in Figure 7 has been explored by Lee et al.[95] The theoretical cross sections for $v_o'=0$ calculated by Lee et al. were plotted in Figure 7 to compare with the experimental values. In the SCECT calculation, the molecular orientation was fixed with H_2^+ parallel to and H_2 perpendicular to the initial velocity. This configuration has been shown to provide "average orientation" results.[20] Sufficient numbers of vibrational states and impact parameters were

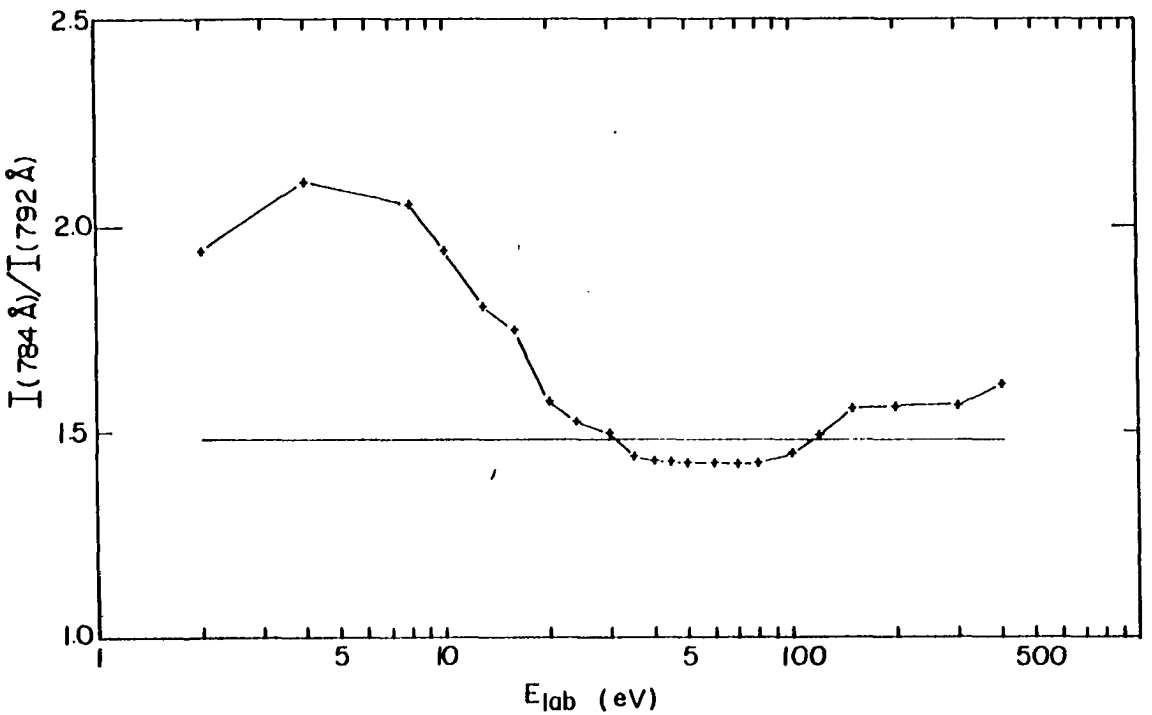

Figure 8. (+——+) The ratio of the intensities for the product H_2^+ ions measured at 784 Å and 792 Å [I(784 Å)/I(792 Å)] plotted as a function of the laboratory collision energy (E_{lab}). (——) The ratio of I(784 Å)/I(792 Å) for the reactant ions

included in the calculation to ensure convergence of $\sigma_{v'_o=0}(H^+)$ to within $\sim$ 5-10%. As shown in Figure 7, the SCECT calculation predicts a broad peak centered at $E_{lab} \approx 40$ eV, in agreement with the experimental observation. The absolute theoretical values are approximately a factor of two higher than the experimental values. In addition to the numerical uncertainty, the SCECT results also contain intrinsic inaccuracies due to the neglect of $H_3^+ + H$ and $H^+ + H$ channels. The measurements of Vance and Bailey[33] indicate that in the range E_{lab} = 10-100 eV the cross sections for the dissociative ionization channel to form $H^+ + H$ are nearly half those for the charge transfer channel. The fact that H_2^+ ions were formed by electron ionization with an electron energy of 80 eV the high cross sections observed for the $H^+ + H$ channel are certainly due to greater probabilities for collisional dissociations of H_2^+ ions in high vibrational states characteristic of electron ionization. Judging from the state-selected experiment of Anderson et al.,[63] the cross sections for collisional dissociation of $H_2^+(v'_o = 0)$ are likely to be less than 1 $\mathring{A}^2$. The cross sections for the $H_3^+ + H$ channel only become important at $E_{lab} < 16$ eV. In the range of E_{lab} = 8-16 eV, previous measurements indicate that the cross sections for the H_3^+ formation are less than 4 $\mathring{A}^2$. The inclusion of these processes should definitely reduce the SCECT values (via conservation of probability restrictions). Taking into account the error in the absolute magnitude of the electron impact data of $\sim \pm$ 40% and the uncertainty of the theoretical values of $\sim \pm$ 30% due to numerical, intrinsic, and orientation influences, the magnitudes of the

experimental and theoretical results are actually in reasonable agreement.

For atomic systems such as $He^+ + He$, the kinetic energy dependence of the total charge transfer cross section at high collision energies reveals regular oscillations.[96] These oscillations have been interpreted as measurements of the number of times of electron jump between the nuclei of the colliding pairs. It is also known that for symmetric electron transfer in atomic systems, a resonant two-state cross section when plotted versus E_{lab} exhibits small oscillations if the coupling has a maximum[12,97,98]. Using the spherical interaction of Bates and Reid,[16] which has a maximum at an intermolecular distance of $\sim$ 1 Å, the calculation of Moran et al.[19] also predicts such oscillations in the collision energy dependence for $\sigma(v_o')$. Since the collision energies involved in this study are relatively low and the couplings for the $H_2^+ + H_2$ system used the SCECT calculation does not have a maximum, these are not the nature of the broad peaks observed in the kinetic energy dependences for $\sigma_{v_o'}(H_2^+)$ $v_o' = 0$ and 1.

The collisional energy dependence for $\sigma_{v_o'=0}(H_2^+)$ based on the calculations for a recti-linear trajectory is also shown in Figure 7.[95] The predicted profile for $\sigma_{v_o'=0}(H_2^+)$ is similar to that obtained using the SCECT method. This indicates that the uses of Ehrenfest's theorem and the direct-direct and exchange-exchange interactions in the SCECT formulation to generate curved trajectories are not significant factors in the energy dependence of $\sigma_{v_o'=0}(H_2^+)$. Interestingly, when the

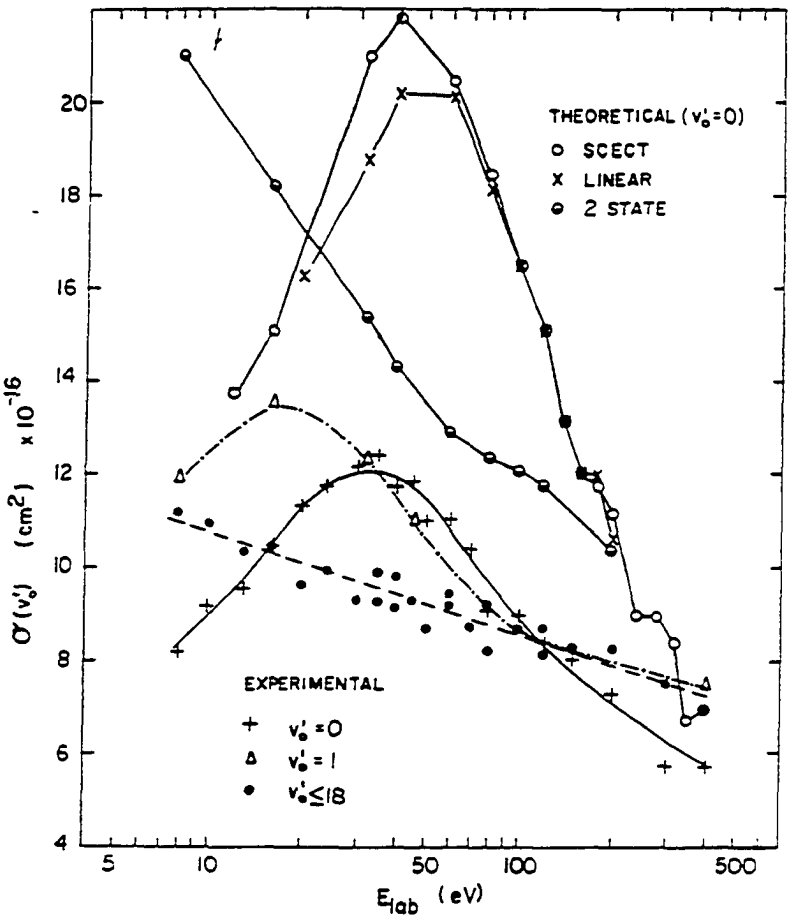

Figure 7. Comparisons of the experimental and theoretical state-selected total charge transfer cross sections $\sigma(v_o')$ for the reaction $H_2^+(v_o') + H_2(v_o'' = 0)$. Experimental values: (---) electron impact values recommended by Barnett et al. (Ref. 43); (+) $\sigma(v_o' = 0)$ measured at 792 Å; (Δ) $\sigma(v_o' = 1)$; (•) $\sigma(v_o' \leq 18)$ measured at 688 Å. Theoretical values: (o) $\sigma(v_o' = 0)$ SCECT; (x) $\sigma(v_o' = 0)$ linear trajectory; (⊖) $\sigma(v_o' = 0)$ 2-state

calculations are restricted to the two channels, resonant direct ($v'_o = 0$, $v''_o = 0$) and exchange ($v' = 0$, $v'' = 0$), the calculated total charge transfer cross section[95] simply decreases monotonically as a function of E_{lab} (Figure 7). The analysis of Lee et al. shows that the collisional energy dependence of the SCECT resonant cross section also has a broad maximum centered at $E_{lab} \simeq 40$ eV, whereas the sum of the SCECT nonresonant cross sections increases smoothly through the peak region. Thus, they concluded that the initial rise $\sigma_{v'_o=0}(H_2^+)$ is due to the increase of both the resonant and nonresonant cross sections, while the decrease of $\sigma_{v'_o=0}(H_2^+)$ at higher collision energy ($E_{lab} > 40$ eV) is a result of the fall-off of the resonant channel. Stemming from the consideration that the $H_3^+ + H$ channel is the dominant product channel at low collision energies, it is logical to believe that the decreases of $\sigma_{v'_o}(H_2^+)$, $v'_o = 0$ and 1, toward lower energies are partly due to the competition of Reaction (2).

The theoretical analysis clearly shows that the broad peak of the $\sigma_{v'_o=0}(H_2^+)$ versus E_{lab} curve arose from the strongly coupled multistate nature in the dynamics of Reaction (1). A complementary interpretation could be made in terms of the transition from diabatic to adiabatic vibrational dynamics as the kinetic energy decreases. Since previous calculations for the $H_2^+ + H_2$ system only indicate a potential energy barrier of less than 0.5 eV,[22,92] it is intriguing to find the peak at $E_{c.m.} \simeq 20$ eV.

In order to have a full understanding of the reaction dynamics of the $H_2^+ + H_2$ system at low energies, it is important to investigate

the competition between the $H_3^+ + H$ and charge transfer channels. The formation of $H_3^+ + H$ by Reaction (2) is among the most studied ion-molecule reactions.[57] The vibrational energy dependence for the total cross section of Reaction (2) ($\sigma_{v_o'}(H_3^+)$) has been investigated by Chupka et al.[75] and Koyano and Tanaka[47] at $E_{c.m.} < 1$ eV using the single gas cell method. The charge transfer and the $D_2H^+ + H$ channels were examined recently in a state-selected study of the reactions $H_2^+ + D_2$ and $D_2^+ + H_2$ by Anderson et al.[63] Because of the difficulty in distinguishing the reactant and product ions, the vibrational energy effects on Reactions (1) and (2) have not been examined simultaneously.

There is general agreement from previous emerged beam,[57,99] beam collision cell,[100] and crossed-beam[92] experiments that the angular distribution of H_3^+ resulted from Reaction (2) appears to exhibit the forward and backward symmetry at $E_{c.m.} \lesssim 10$ eV. The observation has been attributed to adiabatic charge equilibrium between H_2^+ and H_2 prior to proton transfer. Thus, it is meaningless to interpret the forward and backward product H_3^+ peaks as arised from proton and atom transfer mechanism. The isotopic substitution studies[57,63] were found to be consistent with this picture. At $E_{c.m.} \lesssim 1$ eV, the merged-beam experiment of Douglas et al.[57] indicates that a small fraction of the reaction exothermicity and the excitation energy is converted into translational energies of $H_3^+ + H$. The kinematics of the present experiment does not allow for favorable collection of the forward scattered product H_3^+ ions. Nevertheless, the backward scattered H_3^+ ions can be

sampled with good efficiency. Figures 9(a) and (b) show the mass spectra observed by the horizontal mass spectrometer at E_{lab} = 2 and 0.75 eV, respectively, using a photon energy of 15.81 eV (784 Å). These spectra also illustrate the typical resolution used in this experiment.[101] Taking into consideration that approximately 10% and 30% of the observed total H_2^+ intensities in Figure 9(a) and (b), respectively, are due to elastically scattered H_2^+ background, the lower bounds of the branching ratios for the formations of H_3^+ and charge transfer H_2^+ at E_{lab} = 2 and 0.75 eV are estimates to be $\sim$ 0.7 and 3.8, respectively. Stemming from the fact that the reactant H_2^+ ions produced at 15.81 eV (784 Å), which corresponds to the strongest autoionizing peak in the v_o' = 1-2 vibrational interval, are predominately in the v_o' = 1 state, the estimated lower limits for the branching ratio can be considered as state specific values for v_o' = 1.

Figures 10(a) and (c) compare the PIE curves for the product H_2^+ ions and the reactant H_2^+ ions measured at E_{lab} = 2 eV and 0.75 eV, respectively. The PIEs for the product and reactant H_2^+ ions in the region of 790–805 Å have been normalized to the same values. Although high resolution PIE spectra for the product H_2^+ ions at E_{lab} = 2 eV and 0.75 eV cannot be obtained because of low H_2^+ signal intensities, it is clear from the comparison of Figures 3(a), 4(b), 5(a), 10(a), and 10(c) that the vibrational enhancement becomes less pronounced as E_{lab} decreases in the range of 4 to 0.75 eV. This observation is contrary to the prediction of the "trajectory surface hopping" (TSH) calculation by Stine and Muckerman[21] which shows that the

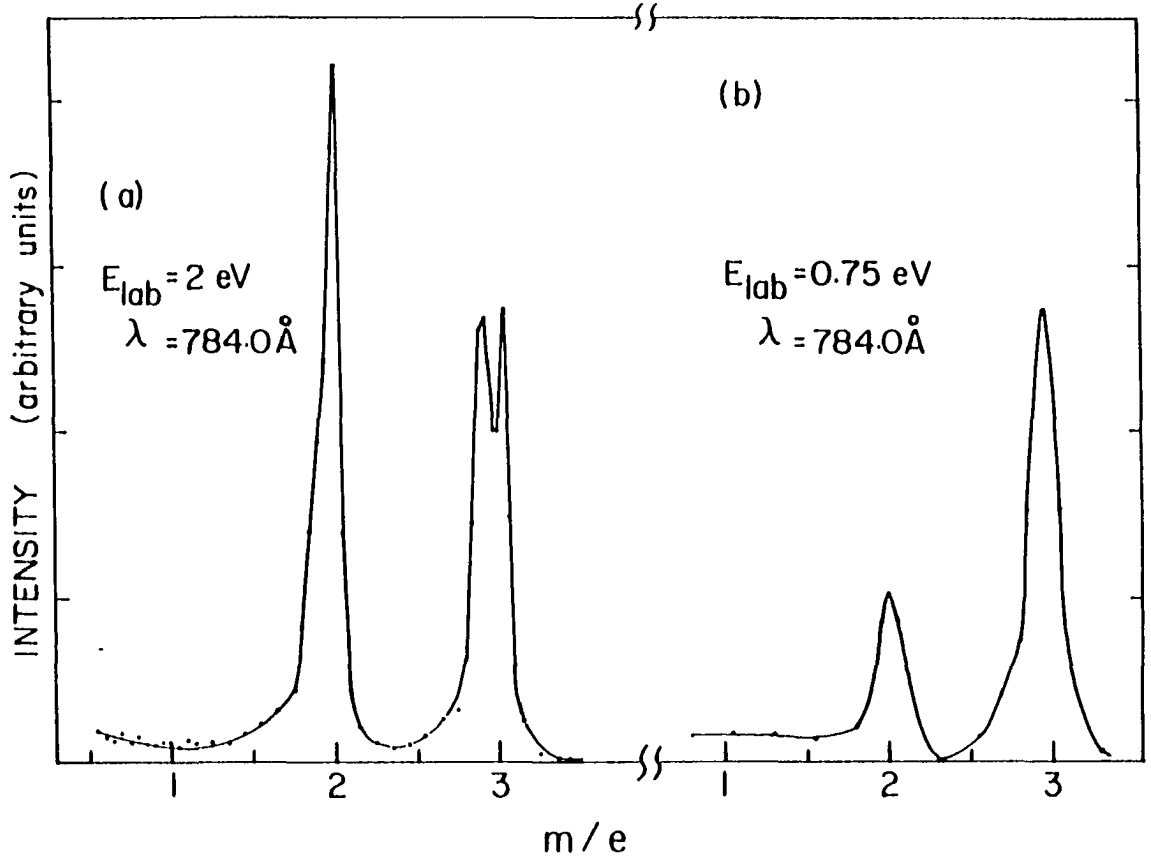

Figure 9. Mass spectra observed by the horizontal mass spectrometer using a photon wavelength of 784 Å at (a) E_{lab} = 2 eV and (b) E_{lab} = 0.75 eV

Figure 10. The comparisons of the PIE curves for the product (a) H_2^+ ions at E_{lab} = 2 eV, (b) H_3^+ ions at E_{lab} = 2 eV, (c) H_2^+ ions at E_{lab} = 0.75 eV, and (d) H_3^+ ions at E_{lab} = 0.75 eV. The PIEs for the product and reactant ions in the region of 740-810 Å, which corresponds to the formation of $H_2^+(v_o' = 0)$, are normalized to the same values (wavelength resolution = 1.4 Å FWHM)

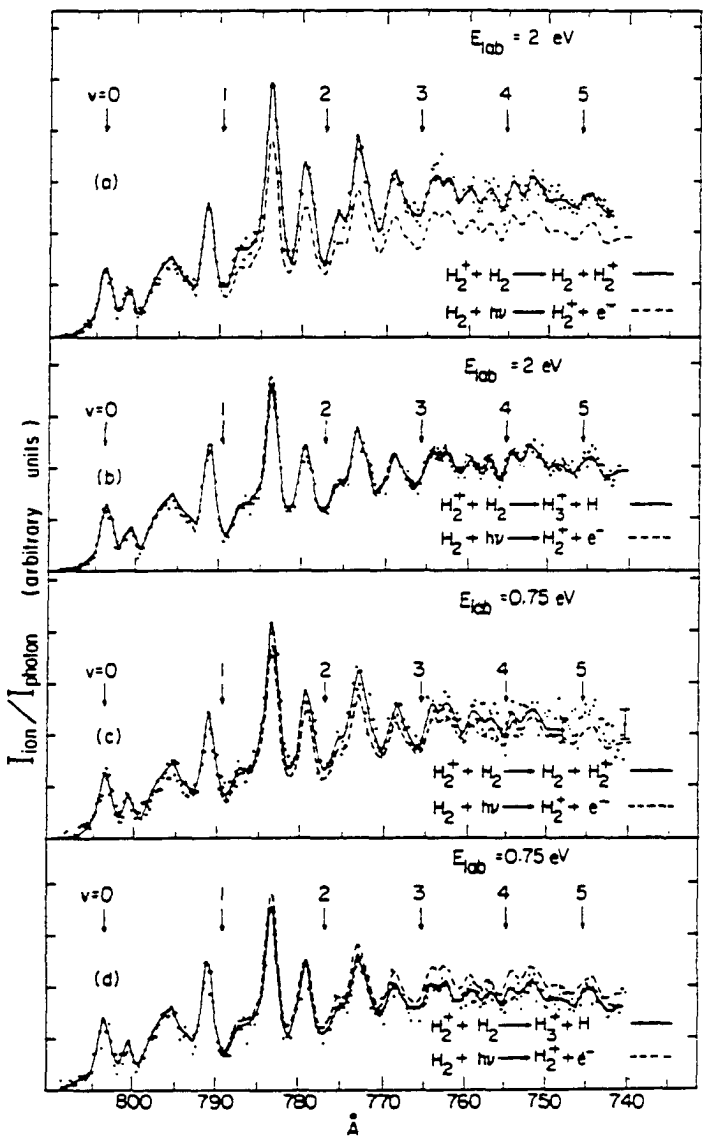
E_lab = 2 eV
v=0
1
2
3
4
5
(a)
H2+ + H2 — H2 + H2+
H2 + hν — H2+ + e−
E_lab = 2 eV
(b)
H2+ + H2 — H3+ + H
H2 + hν — H2+ + e−
E_lab =0.75 eV
(c)
H2+ + H2 — H2 + H2+
H2 + hν — H2+ + e−
E_lab =0.75 eV
(d)
H2+ + H2 — H3+ + H
H2 + hν — H2+ + e−
I_ion / I_photon (arbitrary units)
800
790
780
770
760
750
740
Å

ratio $\sigma_{v'_o=3}(H_2^+)/\sigma_{v'_o=0}(H_2^+)$ continues to increase as $E_{c.m.}$ decreases in the range of 3.0 to 0.25 eV.

The comparison of the PIE curve for H_3^+ observed at $E_{c.m.}$ = 0.38 eV (E_{lab} = 0.75 eV) with that for the reactant H_2^+ ion in Figure 10(d) indicates that the formation of H_3^+ is inhabited by vibrational excitations of the reactant H_2^+ ions. Since the close resemblance of the comparisons shown in Figures 10(d) and 3(c), the vibrational energy dependence of the total cross section for the formation of $H_3^+(\sigma_{v'_o}(H_3^+))$ should be similar to that found for $\sigma_{v'_o}(H_2^+)$ at $E_{c.m.}$ = 22.5 eV. The monotonically decreasing trend as a function of vibrational energy observed here for $\sigma_{v'_o}(H_3^+)$ at $E_{c.m.}$ = 0.38 eV is in agreement with the results obtained by Chupka et al.,[75] Koyano and Tanaka[47] at $E_{c.m.}$ = 0.5 eV. The PIE spectrum for H_3^+ recorded at $E_{c.m.}$ = 1 eV was found to be superimpossible with that for the reactant H_2^+ ion indicating that $\sigma_{v'_o}(H_3^+)$ is independent of v'_o. A similar observation for $\sigma_{v'_o}(H_3^+)$ at $E_{c.m.}$ = 0.93 eV was reported by Koyano and Tanaka.[47] In the state-selected study of the reaction $H_2^+(v'_o) + D_2 \rightarrow D_2H^+ + H$, Anderson et al.[63] found that $\sigma_{v'_o}(D_2H^+)$ decreases as v'_o increases at $E_{c.m.} \leq 0.77$ eV, while $\sigma_{v'_o}(D_2H^+)$ is enhanced by vibrational excitations of H_2^+ at $E_{c.m.} \geq 1.1$ eV. The decrease in $\sigma_{v'_o}(H_3^+)$ as a function of v'_o has been suggested by Krenos et al.[92] as due to vibrational energy induced hopping of the system from the ground surface $[H_2^+(^2\Sigma_g^+) + H_2]$ to the first excited surface $[H_2^+(^2\Sigma_u^+) + H_2]$ which has an energy barrier to reaction. The argument of hopping to the excited surface has also been used to rationalize the vibrational enhancement in the intermediate collision energy range

($E_{c.m.}$ $\sim$ 1-3 eV). Anderson et al.[63] argue that the vibrational enhancement in the intermediate collision energy range may arise from a more efficient reaction mechanism on the excited potential energy surface than that on the ground state. This interpretation implies that the potential energy barrier on the excited surface is $\sim$ 1 eV. Applying the same rationalization here, this study also yields a value of $\sim$ 1 eV for the energy barrier for Reaction (2) on the excited surface.

The TSH calculation of Stine and Muckerman[21] is the only theoretical study at low collision energies which takes into account both Reactions (1) and (2). They have reported state-selected total cross sections on the reactions of the $H_2^+(v_o' = 0,3,6;\ J' = 2) + H_2(v_o'' = 0;\ J'' = 1)$ at $E_{c.m.}$ = 0.25, 0.5, 1.0, 3.0, and 5.0 eV.[21] Here, J' and J'' represent the rotational quantum numbers for H_2^+ and H_2, respectively. At $E_{c.m.}$ = 0.25 and 0.5 eV, the calculated value for $\sigma_{v_o'=3}(H_2^+)$ is lower than $\sigma_{v_o'=0}(H_3^+)$, while $\sigma_{v_o'=3}(H_3^+)$ is greater than $\sigma_{v_o'=0}(H_3^+)$ at $E_{c.m.} \geq 1$ eV. The values for $\sigma_{v_o'}(H_2^+)$, v_o' = 0 and 3 are predicted to increase with increasing $E_{c.m.}$. The study also indicates that the critical impact parameter for charge exchange is larger than that for proton transfer, and is relatively independent of collision energy so that, as the latter decreases with increasing $E_{c.m.}$, more and more collisions lead to charge transfer without surmounting the centrifugal barrier for proton transfer. Moreover, vibrational excitation in the H_2^+ reactant is found to greatly enhance the charge transfer

process at low collision energies, in accord with the qualitative predictions based on the accessibility of the avoided crossing seam on the ground state potential energy surface. With the exception found in the calculated kinetic energy dependence for $\sigma_{v_o'=3}(H_2^+)/\sigma_{v_o'=0}(H_2^+)$ and that observed here, the calculations of Stine and Muckerman are in conformity to experimental observations.

The rotational energy effect on the ion-molecule reaction $H_2^+(v_o = 0,J) + H_2 \rightarrow H_3 + H$ has been examined previously by Chupka[44] in a single chamber photoionization experiment using a wavelength resolution of 0.12 Å (FWHM). They found that by changing the rotational quantum number of $H_2^+(v_o' = 0)$ from J = 0 to J = 2 changes the relative cross sections for the formation of H_3^+ by < 10%. In order for the rotational energy of $H_2^+(v_o' = 0)$ to play a role in the symmetric charge transfer reaction $H_2^+(v_o', J) + H_2$, one expects that the time for molecular interaction between H_2^+ and H_2 in the collision should be of the same order of magnitude as the rotational period of $H_2^+(\sim 5\times10^{-13}$ sec). Assuming that an effective length for charge exchange interaction of ~ 7 Å,[20] a collision time of $\sim 5\times10^{-13}$ sec would correspond to a collision energy $E_{c.m.} \ll 1$ eV. Because of the low signal intensity at low collision energies, it is impracticable to perform high resolution experiments at $E_{c.m.} \leq 1$ eV. We have obtained the high resolution (0.14 Å (FWHM)) PIE curves for the product H_2^+ ions in the region ~ 800-808 Å at $E_{c.m.}$ = 2 and 4 eV. Figure 11 compares the PIE curve for the product H_2^+ ions at $E_{c.m.}$ = 2 with that for the reactant

H_2^+ ions. The PIE curve for the reactant H_2^+ ions is similar to that recorded previously by Chupka.[44] using a similar wavelength resolution. The assignments of the autoionization peaks are based on the very high resolution photoionization study of Chupka and Berkowitz,[59-60] Berkowitz and Chupka,[61] Dehmer and Chupka,[62] and spectroscopic studies of Takezawa,[102] Namioka,[103] Monfils,[104] Herzberg,[105] and Herzberg and Jungen.[106]. The rotational states of the reaction H_2^+ ions formed have been inferred by autoionization selection rules[107,108] and energy constraint.[109] As a result of the preference for ionization to occur with no change in rotational quantum number, H_2^+ ions resulted from autoionization of the autoionization Rydberg states Q(1) $8p\pi(v=1)$ and R(1) and P(1) $8p\sigma(v=1)$ should be in the $J = 1$ rotational state. After normalizing the heights of the autoionization peaks at 804.12 Å for the reactant and the product ions to the same value, the PIE spectra for the reactant and product H_2^+ ions were found to be superimpossible (Figure 11). Therefore, we conclude that within the experimental uncertainty of $\sim$ 10%, changing the rotational quantum number of $H_2^+(v_o' = 0)$ from $J = 0$ to $J = 2$ has no observable effect on the symmetric charge transfer reaction $H_2^+(v_o' = 0,J) + H_2$ at $E_{c.m.} = 2$ eV. A similar observation was found at $E_{c.m.} = 4$ eV. The differences of the 0-0 vibrational overlap integral for several rotational transitions as computed by Moran et al.[19] are less than 3%. If resonance charge transfer channels are dominant at $E_{c.m.} = 2$ and 4 eV, one expects the effect on the charge transfer cross-section due to rotational excitation of $H_2^+(v_o' = 0)$ to be small.

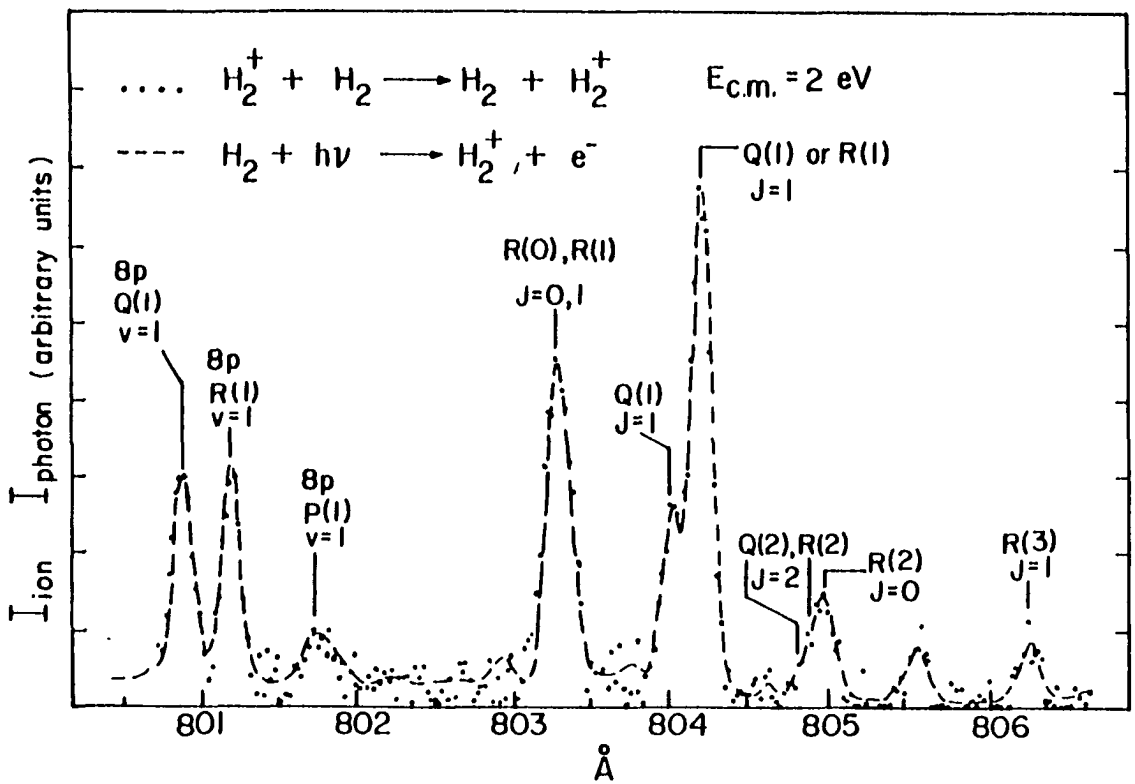

Figure 11. The comparison of the PIE curve for the product H_2^+ ions formed at $E_{c.m.}$ = 2 eV with that for the reactant H_2^+ ions in the region of 800.5-806.5 Å (wavelength resolution = 0.14 Å (FWHM))

The high resolution (0.3 Å (FWHM)) PIE data for N_2^+ and CO^+ in the region 798-770 Å formed by Reactions (4) and (5) measured by the horizontal mass spectrometer were plotted in Figure 12(a) and (b), respectively. The $H_2^+(v_o')$ ions were formed at the photoionization region and were bent at the collision region to pass through the horizontal reaction gas cell. Both reactions were measured at E_{lab} = 24 eV which is defined to be the difference in potential between the horizontal gas cell and the photoionization region. Using the same procedures as described above, the relative values for $\sigma_{v_o'=0}(N_2^+)$: $\sigma_{v_o'=1}(N_2^+)$: $\sigma_{v_o'=2}(N_2^+)$ are 1.00 : 1.63 : 1.34 and those for $\sigma_{v_o'=0}(CO^+)$: $\sigma_{v_o'=1}(CO^+)$: $\sigma_{v_o'=2}(CO^+)$ are 1.00 : 0.85 : 0.79. The values for $n\ell\sigma_{v_o'=0}(N_2^+)$ [$n\ell\sigma_{v_o'=0}(CO^+)$] can be determined by measuring the ratio of the intensity of $N_2^+(CO^+)$ to that of $H_2^+(v_o' = 0)$ with the horizontal gas cell evacuated. By calibrating the relative cross sections with $n\ell\sigma_{v_o'=0}(N_2^+)$ and $n\ell\sigma_{v_o'=0}(CO^+)$, the values for $n\ell\sigma_{v_o'}(N_2^+)$ and $n\ell\sigma_{v_o'}(CO^+)$, v_o' = 1 and 2 were calculated. The values for $n\ell\sigma_{v_o'}(N_2^+)$ and $n\ell\sigma_{v_o'}(CO^+)$, v_o' = 0-2, which are needed for the detection of the final states of product $H_2^+(v'')$ ions, are listed in Table 2. In order to maximize the signal intensity of $N_2^+(CO^+)$ in the final state detection experiment, it is necessary to lower the resolution of the horizontal quadrupole spectrometer to increase the transmission of $N_2^+(CO^+)$. The masses of $N_2^+(CO^+)$ and $N_2H^+(COH^+)$ cannot be resolved in these measurements. However, it should not affect the results of the final state detection experiment.[110]

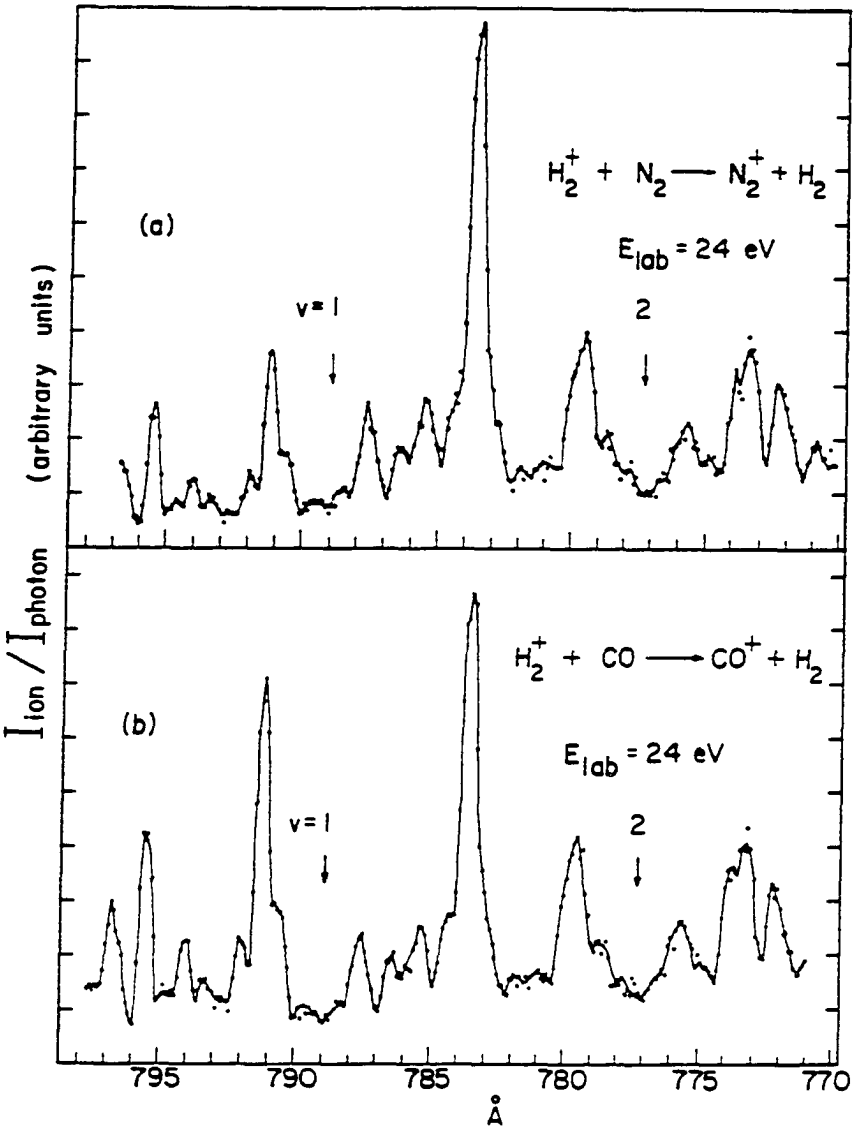

Figure 12(a). PIE curve in the region of 770-798 Å for the product N_2^+ ions formed by the reaction H_2^+ + N_2 at E_{lab} = 24 eV using the ion beam-gas cell arrangement

Figure 12(b). PIE curve in the region of 770-798 Å for the product CO^+ ions formed by the reaction H_2^+ + CO at E_{lab} = 24 eV using the ion beam-gas cell arrangement. Wavelength resolution = 1.4 Å (FWHM)

Table 2. Values for $n\ell\sigma_{v_o'}(N_2^+)^{a,b}$ and $n\ell\sigma_{v_o'}(CO^+)^{a,b}$ $v_o' = 0$-2, determined at E_{lab} = 24 eV

v_o'	$n\ell\sigma_{v_o'}(N_2^+)^c$	$n\ell\sigma_{v_o'}(CO^+)^c$
0	0.035±0.001	0.092±0.002
1	0.057±0.004	0.078±0.002
2	0.047±0.003	0.073±0.001

[a] $\sigma_{v_o'}(N_2^+)$ and $\sigma_{v_o'}(CO^+)$ represent the total cross sections for the reactions, $H_2^+(v_o') + N_2 \rightarrow H_2 + N_2^+$ and $H_2^+(v_o') + CO \rightarrow H_2 + CO^+$, respectively. n is the density of N_2 or CO and ℓ is the effective length of the gas cell.

[b] The resolution of the horizontal quadrupole mass spectrometer used in these measurements cannot distinguish the masses of $N_2^+(CO^+)$ and $N_2H^+(COH^+)$.

[c] The uncertainties represent the standard deviations due to counting statistics.

The measured values for $n\ell\sigma_m(N_2^+)$ and $n\ell\sigma_m(CO^+)$ for Reactions (4) and (5) at E_{lab} = 24 eV characteristic of product $H_2^+(v'')$ ions resulted from Reaction (1) at $E_{c.m.}$ = 4, 8, and 16 eV are listed in Table 3. Two photoionization wavelengths were used to prepare the reactant $H_2^+(v_o')$ ions. At 792 Å, all reactant H_2^+ ions should be in the v_o' = 0 state. If resonance charge exchange is the dominant channel, i.e., the product H_2^+ ions are mostly in the v" = 0 state, the values for $n\ell\sigma_m(N_2^+)$ and $n\ell\sigma_m(CO^+)$ are expected to be close to those for $n\ell\sigma_{v_o'=0}(N_2^+)$ and $n\ell\sigma_{v_o'=0}(CO^+)$, respectively. As shown in Table 3, this is the case here. Although the differences between the values for $n\ell\sigma_m(N_2^+)$ meas-

Table 3. Values for $n\ell\sigma_m(N_2^+)^{a,b}$ and $n\ell\sigma_m(CO^+)^{a,b}$ determined at E_{lab} = 24 eV[c]

(Å)[d]	$E_{c.m.}$ (eV)[e]	$n\ell\sigma_m(N_2^+)$[f]	$n\ell\sigma_m(CO^+)$[f]
792	4	0.031±0.003	0.097 0.004
	8	0.035±0.001	0.091 0.002
	16	0.037±0.001	0.088 0.002
784	4	0.055±0.003	0.073 0.003
	8	0.055±0.001	0.074 0.002
	16	0.050±0.001	0.083 0.002

[a] $\sigma_m(N_2^+)$ and $\sigma_m(CO^+)$ are the total cross sections for the reactions, $H_2^+(v'') + N_2 \rightarrow H_2 + N_2^+$ and $H_2^+(v'') + CO \rightarrow CO^+$, respectively. n is the density of N_2 or CO and ℓ is the effective length of the gas cell.

[b] The resolution of the horizontal quadrupole mass spectrometer used in these measurements cannot distinguish the masses of $N_2^+(CO^+)$ and $N_2H^+(COH^+)$.

[c] E_{lab} is defined to be the difference in potential between the collision region and the horizontal gas cell.

[d] Photoionization wavelength. At 792 Å, all reactant H_2^+ ions formed were in the v_o'=0 state, while at 784 Å, reactant H_2^+ ions were produced mainly in the v_o' = 1 state. The intensity of $H_2^+(v_o'=0)$ formed at 784 Å should be $\leq$ 10% of the total H_2^+ beam intensity.

[e] Center-of-mass energies of the reaction $H_2^+(v_o') + H_2 \rightarrow H_2(v') + H_2^+(v'')$.

[f] The uncertainties represent the standard deviations due to counting statistics.

ured at $E_{c.m.}$ = 4, 8, and 16 eV are small, the observed trend should be reliable. Since the value for $n\ell\sigma_{v_o'=0}(N_2^+)$ is lower than $n\ell\sigma_{v_o'}(N_2^+)$, $v_o' \geq 1$, the gradual increasing trend for $n\ell\sigma_m(N_2^+)$ as $E_{c.m.}$ increases in the range from 4 to 16 eV is consistent with the interpretation that inelastic charge transfer channels become more important as the collision energy increases. The same conclusion can be drawn from the measured values for $n\ell\sigma_m(CO^+)$. The observed decreasing trend as a function of $E_{c.m.}$ for $n\ell\sigma_m(CO^+)$ in the range of 4 to 16 eV is in accord with the fact that the value for $n\ell\sigma_{v_o'=0}(CO^+)$ is greater than $n\ell\sigma_{v_o'}(CO^+)$, v_o' = 1 or 2.

Assuming the product $H_2^+(v'')$ formed by Reaction (1) with v_o' = 0 at $E_{c.m.}$ = 16 eV only consists of H_2^+ in the v" = 0 and 1 states, the two linear equations, which are needed to solve for X_0 and X_1 are

$$0.035\ X_0 + 0.057\ X_1 = 0.037 \tag{14}$$

$$0.092\ X_0 + 0.078\ X_1 = 0.088 \tag{15}$$

The solution for these equations are X_0 = 0.86, X_1 = 0.12. The sum of X_0 and X_1 is slightly less than one; but the difference is well within experimental uncertainties. The value of 0.12 for X_1 is found to be in excellent agreement with the theoretical prediction of $\sim$ 0.13.[20] In fact, Eqs. (14) or (15) can be combined with Eq. (13) to obtain a set of values for X_0 and X_1. Combining Eqs. (13) and (14) gives a value of 0.09 for X_1, while a value of 0.29 is predicted by Eqs. (13) and (15). The information content for the determination of

X_1 in Eq. (14) is greater than that in Eq. (15) because $n\ell\sigma_{v_o'=1}(N_2^+)$ is higher than $n\ell\sigma_{v_o'=0}(N_2^+)$ whereas $n\ell\sigma_{v_o'=1}(CO^+)$ is lower than $n\ell\sigma_{v_o'=0}(CO^+)$. Thus, we expect that the value of 0.09 for X_1 deduced by using Eqs. (13) and (14) is more reliable than that calculated by combining Eqs. (13) and (15). In any case, the average value of 0.17±0.08 is probably a better estimate for X_1. The theoretical calculation of Lee and DePristo shows that ∿ 92% of the $H_2^+(v'')$ ions product by Reaction (1) at $E_{c.m.}$ = 8 eV with v_o' = 0 are in the v'' = 0 state. The comparison of the values for $n\ell\sigma_m(N_2^+)$ and $[n\ell\sigma_m(CO^+)]$ measured at $E_{c.m.}$ = 8 eV with those for $n\ell\sigma_{v_o'=0}(N_2^+)$ and $n\ell\sigma_{v_o'=0}(CO^+)$ indicates that $H_2^+(v'')$ ions formed at $E_{c.m.}$ = 8 eV are almost completely in the v'' = 0 state. Taking into account the experimental uncertainties for $n\ell\sigma_m(N_2^+)$ and $n\ell\sigma_m(CO^+)$ at $E_{c.m.}$ = 4 eV, a similar conclusion can be made for $H_2^+(v'')$ produced at $E_{c.m.}$ = 4 eV.

The photoionization wavelength used to prepare $H_2^+(v_o' = 1)$ coincides with the strongest autoionization peak at ∿ 784 Å. The intensity of $H_2^+(v_o' = 0)$ formed at this wavelength should be ≤ 10% of the total H_2^+ beam intensity.[63] The measured values for $n\ell\sigma_m(N_2^+)$ and $n\ell\sigma_m(CO^+)$ (Table 3) at 784 Å are found to be close to those for $n\ell\sigma_{v_o'=1}(N_2^+)$ and $n\ell\sigma_{v_o'=1}(CO^+)$, respectively. Furthermore, the value for $n\ell\sigma_m(N_2^+)$ decreases as a function of $E_{c.m.}$, while that for $n\ell\sigma_m(CO^+)$ shows an opposite trend. These observations again indicate that the majority of the $H_2^+(v'')$ ions formed by Reaction (1) with v_o' = 1 at $E_{c.m.}$ = 4, 8, 16 eV are mainly in the v'' = 1 state and that as E increases, inelastic

charge transfer will produce more H_2^+ in other vibrational states. The fact that the value for $n\ell\sigma_m(CO^+)$ is higher at $E_{c.m.}$ = 16 eV than those at $E_{c.m.}$ = 4 and 8 eV supports the conclusion that the fraction of $H_2^+(v'' = 0)$ increases as $E_{c.m.}$ increases. The calculated state-to-state cross sections for Reaction (1) with $v_o' = 1$ reveal that $H_2^+(v'' = 1)$ ions formed at $E_{c.m.}$ = 8 and 16 eV constitute $\sim$ 72% and $\sim$ 50% of the total $H_2^+(v'')$ intensity, respectively.[20] The $H_2^+(v'' = 0)$ intensity increase from $\sim$ 19% at $E_{c.m.}$ = 8 eV to $\sim$ 37% at $E_{c.m.}$ = 16 eV. Therefore, we conclude that the theoretical calculations of Lee and DePristo are in qualitative agreement with our experimental observations.

Conclusions and Summary

We have developed a new ion-molecule reaction apparatus which combines the high resolution photoionization mass spectrometry, crossed ion-neutral beam method, and charge transfer detection technique. This apparatus is most appropriate for state-selected total cross-section measurements of simple charge transfer and proton transfer reactions. Under specific experimental conditions, the final vibrational and electronic states of charge transfer product ions can be probed with the charge transfer detector. Using this apparatus, we have examined the vibrational, rotational, and kinetic energies effects on the total symmetric charge transfer cross section for the reaction of $H_2^+ + H_2$. The crossed ion-neutral beam arrangement has allowed the measurements of $\sigma_{v_o'}(H_2^+)$, $v_o' = 0$-4, at high kinetic energy resolutions. The

vibrational energy dependences for $\sigma_{v'_o}(H_2^+)$ in the kinetic energy range of $E_{c.m.}$ = 8-200 eV observed in this experiment were found to be in good agreement with the recent calculation based on the semi-classical energy conserving trajectory formulation. The kinetic energy dependences for $\sigma_{v'_o=0}(H_2^+)$, v'_o = 0 and 1, which were obtained indirectly by calibrating the relative total charge transfer cross-sections measured at 688 Å (18 eV) with absolute total charge transfer cross sections determined previously using electron ionization, reveals broad peaks at $E_{c.m.} \approx$ 35 and 16 eV, respectively. These broad features were attributed to the strongly coupled multistate nature in the dynamics of Reaction (1). No observable effect on $\sigma_{v'_o=0}(H_2^+)$ at $E_{c.m.}$ = 2 and 4 eV when the rotational quantum number of the reactant H_2^+ ions were varied from J = 0 to 2. The vibrational energy effects on Reactions (1) and (2) were directly observed. The observations are in accord with the qualitative predictions based on the accessibility of the avoided crossing seam on the ground state potential energy surface and the TSH calculation. The vibrational enhancement for Reaction (1) was found to reach the maximum at $E_{c.m.} \approx$ 2 eV and become less pronounced as $E_{c.m.}$ decreases from 2 to 0.38 eV, an observation in variance with the TSH calculation. The final vibrational state distributions of H_2^+ ions formed by Reaction (1) with v'_o = 0 and 1 at $E_{c.m.}$ = 8 and 16 eV as probed by the charge transfer detection method were found to be consistent with the SCECT state-to-state cross sections.

A logical development of the crossed ion-neutral beam apparatus is to incorporate the photoion photoelectron coincidence method such that state-selected experiments can be extended to more complicated systems. In the case of the reaction $H_2^+(v_o') + H_2$, higher vibrational state of H_2^+ can be selected by using the coincidence method. The charge transfer detection technique is a highly sensitive method and can in principle be used to measure product vibrational state distributions involving more than two states.

References

1. F. S. W. Massey and R. A. Smith, Proc. Roy. Soc. (London) A142, 142 (1933).
2. O. B. Firsov, J. Exptl. Theoret. Phys. (U.S.S.R.) 21, 1001 (1951).
3. H. S. W. Massey and E. H. S. Burhop, "Electronic and Ionic Impact Phenomena" (Oxford University Press, Oxford, 1952).
4. A. Dalgarno and H. N. Yadav, Proc. Phys. Soc. (London) A66, 173 (1953).
5. D. R. Bates, H. S. W. Massey and A. L. Stewart, Proc. Roy. Soc. (London) A216, 436 (1953).
6. E. F. Gurnee and J. L. Magee, J. Chem. Phys. 26, 1237 (1957).
7. D. R. Bates and R. McCarroll, Proc. Roy. Soc. (London) A245, 175 (1958).
8. I. Popescu-Iovitsu and N. Ionescu-Pallas, Soviet Phys.-Techn. Phys. 4, 781 (1960).
9. D. Rapp and W. E. Francis, J. Chem. Phys. 37, 2631 (1962).
10. D. R. Bates and R. McCarroll, Phil. Mag. Suppl. 11, 39 (1962).
11. D. R. Bates, in D. R. Bates, Ed., "Atomic and Molecular Processes" (Academic Press, New York, 1962).
12. F. J. Smith, Phys. Lett. 20, 271 (1966).

13. F. J. Smith, Plan. Space Sci. 14, 929 (1966).

14. R. A. Mapleton, "Theory of Charge Exchange" (Wiley-Interscience, New York, 1972).

15. J. J. Leventhal, T. F. Moran, and L. Friedman, J. Chem. Phys. 46, 4666 (1967).

16. D. R. Bates and R. H. G. Reid, Proc. Roy. Soc. (London) A310, 1 (1969).

17. R. N. Stocker and H. Neumann, J. Chem. Phys. 61, 3852 (1974).

18. K. J. McCann, M. R. Flannery, J. V. Hornstein and T. F. Moran, J. Chem. Phys. 63, 4998 (1975).

19. T. F. Moran, M. R. Flannery and D. L. Albritton, J. Chem. Phys. 62, 2869 (1975).

20. C. Y. Lee and A. E. DePristo, J. Chem. Phys. 80, 1116 (1984).

21. Data of Stine and Muckerman (1980). See J. T. Muckerman, in D. Henderson, Ed., "Theoretical Chemistry," Vol. 6A (Academic Press, New York, 1981) p. 1.

22. J. R. Stine and J. T. Muckerman, J. Chem. Phys. 68, 185 (1978).

23. R. D. Poshusta and D. F. Zetik, J. Chem. Phys. 58, 118 (1973).

24. R. Polák, Chem. Phys. 16, 353 (1976).

25. M. Cobb, T. F. Moran, R. F. Borkman, and R. Childs, Chem. Phys. Lett. 57, 326 (1978).

26. R. F. Borkman and M. Cobb, J. Chem. Phys. 74, 2920 (1981).

27. C. Y. Lee and A. E. DePristo, J. Am. Chem. Soc. 105, 6775 (1983).

28. A. E. DePristo, J. Chem. Phys. 78, 1237 (1983).

29. A. E. DePristo, J. Chem. Phys. 79, 1741 (1983).

30. C. Becker, J. Chem. Phys. 76, 5928 (1982).

31. C. J. Latimer, R. Browning, and H. B. Gilbody, J. Phys. B2, 1055 (1969).

32. H. C. Hayden and R. C. Amme, Phys. Rev. 172, 104 (1968).

33. D. W. Vance and T. L. Bailey, J. Chem. Phys. 44, 486 (1966).

34. W. H. Cramer, J. Chem. Phys. 35, 836 (1961).

35. H. L. Rothwell, B. V. Zyl, and R. C. Ame, J. Chem. Phys. 61, 3851 (1974).

36. F. Wolf, Ann. Physik 29, 33 (1937).

37. J. H. Simons, C. M. Fontana, E. E. Muschlitz, Jr. and S. R. Jackson, J. Chem. Phys. 11, 312 (1943).

38. T. F. Moran and J. R. Roberts, J. Chem. Phys. 49, 3411 (1968).

39. J. B. H. Stedeford and J. B. Hasted, Proc. Roy. Soc. (London) A227, 466 (1955).

40. W. H. Cramer and A. B. Marcus, J. Chem. Phys. 32, 186 (1960).

41. O. Hollricher, Z. Phys. 187 41 (1965).

42. D. W. Koopman, Phys. Rev. 154, 79 (1967).

43. C. F. Barnett, J. A. Ray, E. Ricci, M. I. Wilker, E. W. McDaniel, E. W. Thomas, and H. B. Gilbody, "Atomic Data for Controlled Fusion Research," Oak Ridge National Laboratory Report 5206 (1977).

44. W. A. Chupka, in J. L. Franklin, Ed., "Ion-Molecule Reactions," Vol. 1 (Plenum Press, New York, 1972) p. 33.

45. L. Squires and T. Baer, J. Chem. Phys. 65, 4001 (1976).

46. T. Baer, P. T. Murray and L. Squires, J. Chem. Phys. 68, 4901 (1978).

47. I. Koyano and K. Tanaka, J. Chem. Phys. 72, 4858 (1980).

48. K. Tanaka, J. Durup, T. Kato and I. Koyano, J. Chem. Phys. 74, 5561 (1981).

49. K. Tanaka, T. Kato and I. Koyano, J. Chem. Phys. 75, 4941 (1981).

50. T. Kato, K. Tanaka and I. Koyano, J. Chem. Phys. 77, 837 (1982).

51. K. Tanaka, T. Kato, P.-M. Guyon and I. Koyano, J. Chem. Phys. 77, 4441 (1982).

52. T. Kato, K. Tanaka and I. Koyano, J. Chem. Phys. 79, 5969 (1983).

53. F. M. Campbell, R. Browning and C. J. Latimer, J. Phys. B14, 3493 (1981).

54. F. M. Campbell, R. Browning and C. J. Latimer, J. Phys. B14, 1183 (1981).

55. C. J. Latimer and F. M. Campbell, J. Phys. B15, 1765 (1982).

56. F. M. Campbell, R. Browning and C. J. Latimer, J. Phys. B13, 4257 (1980).

57. C. H. Douglas, D. J. McClure and W. R. Gentry, J. Chem. Phys. 67, 4931 (1977) and references therein.

58. S. K. Cole, T. Baer, P.-M. Guyon and T. R. Govers, Chem. Phys. Lett. 109, 285 (1984).

59. W. A. Chupka and J. Berkowitz, J. Chem. Phys. 48, 5226 (1968).

60. W. A. Chupka and J. Berkowitz, J. Chem. Phys. 51, 4244 (1969).

61. J. Berkowitz and W. A. Chupka, J. Chem. Phys. 51, 2341 (1969).

62. P. M. Dehmer and W. A. Chupka, J. Chem. Phys. 65, 2243 (1976).

63. S. L. Anderson, F. A. Houle, D. Gerlich and Y. T. Lee, J. Chem. Phys. 75, 2153 (1981).

64. F. A. Houle, S. L. Anderson, D. Gerlich, T. Turner and Y. T. Lee, Chem. Phys. Lett. 82, 392 (1981).

65. F. A. Houle, S. L. Anderson, D. Gerlich, T. Turner and Y. T. Lee, J. Chem. Phys. 77, 748 (1982).

66. S. L. Anderson, T. Turner, B. H. Mahan and Y. T. Lee, J. Chem. Phys. 77, 1842 (1982).

67. J. A. R. Samson, J. Electron. Spectrosc. Relat. Phenom. 8, 123 (1976).

68. C. L. Liao, C. X. Liao and C. Y. Ng, Chem. Phys. Lett. 103, 418 (1984).

69. Y. Ono, S. H. Linn, H. F. Prest, M. E. Gress and C. Y. Ng, J. Chem. Phys. 73, 2523 (1980).

70. K. B. McAfee, Jr., W. E. Falconer, R. S. Hozack and D. J. McClure, Phys. Rev. A21, 827 (1980).

71. K. B. McAfee, Jr., C. R. Szmanda, R. S. Hozack and R. E. Johnson, J. Chem. Phys. 77, 2399 (1982).

72. C. F. Giese and W. B. Maier II, J. Chem. Phys. 39, 739 (1963).

73. P. J. Chantry, Bull. Am. Phys. Soc. 16, 212 (1971).

74. W. A. Chupka and M. E. Russell, J. Chem. Phys. 49, 5426 (1968).

75. W. A. Chupka, M. E. Russell and K. Refaey, J. Chem. Phys. 48, 1518 (1968).

76. W. A. Chupka and M. E. Russell, J. Chem. Phys. 48, 1528 (1968).

77. R. Derai, S. Fenistein, M. Gerard-Ain, T. R. Govers, R. Marx, G. Mauclaire, C. Z. Profous and C. Sourisseau, Chem. Phys. 44, 65 (1979).

78. G. Mauclaire, R. Derai, S. Fenistein, R. Marx and R. Johnsen, J. Chem. Phys. 70, 4017 (1979).

79. R. Derai, G. Mauclaire and R. Marx, Chem. Phys. Lett. 86, 275 (1982).

80. B. Friedrich, W. Trafton, A. Rockwood, S. Howard and J. H. Futrell, J. Chem. Phys. 80, 2537 (1984).

81. P. M. Hierl, V. Pacak and Z. Herman, J. Chem. Phys. 67, 2678 (1977).

82. Z. Herman, V. Pacek, A. J. Yencha and J. H. Futrell, Chem. Phys. Lett. 37, 329 (1976).

83. J. Golsik, B. Friedrich and Z. Herman, Chem. Phys. 60, 369 (1981).

84. T. Matsuo, N. Kobayashi and Y. Kaneko, J. Phys. Soc. (Japan) 51, 1558 (1982).

85. D. J. Dagigan and J. P. Doering, Chem. Phys. Lett. 64, 200 (1979).

86. J. Danon and R. Marx, Chem. Phys. 68, 255 (1982).

87. D. R. Guyer, L. Hüwel and S. R. Leone, J. Chem. Phys. 79, 1259 (1983).

88. B. H. Mahan, C. Martner and A. O'Keefe, J. Chem. Phys. 76, 4433 (1982).

89. T. R. Govers, M. Gerad and R. Marx, Chem. Phys. 15, 185 (1976).

90. K. B. McAfee, Jr., W. E. Falconer, R. S. Hozack and D. J. McClure, Phys. Rev. A21, 827 (1980).

91. C. L. Liao, C. X. Liao and C. Y. Ng, to be published.

92. J. K. Krenos, K. K. Lehmann, and J. C. Tully, P. M. Hierl and G. P. Smith, Chem. Phys. 16, 109 (1976).

93. R. W. Nicholls, J. Phys. B1, 1192 (1968).

94. R. Browning and J. Fryar, J. Phys. B6, 364 (1973).

95. C. Y. Lee, A. E. DePristo, C.-L. Liao, C. X. Liao and C. Y. Ng, submitted to Chem. Phys. Lett.

96. F. P. Ziemba and E. Everhart, Phys. Rev. Lett. 2, 299 (1959).

97. J. Perel, H. L. Daley, J. M. Peek, T. A. Green, Phys. Rev. Lett. 23, 677 (1969).

98. J. Perel, Phys. Rev. A1, 369 (1970).

99. R. H. Neynaber and S. M. Trujillo, Phys. Rev. 167, 63 (1968); 171E, 282 (1968).

100. L. D. Doverspike and R. L. Champion, J. Chem. Phys. 46, 4718 (1967).

101. The mass 3 peak in Figure 9(a), which was measured using smaller mass increments, was found to be split. This is believed to be the result of minor misalignments of the homemade quadrupole mass filter.

102. S. Takezawa, J. Chem. Phys. 52, 2575, 5793 (1970).

103. T. Namioka, J. Chem. Phys. 40, 3154 (1964); 41, 2141 (1964); 43, 1636 (1965).

104. A. Monfils, J. Mol. Spectrosc. 15, 265 (1965).

105. G. Herzberg, Phys. Rev. Lett. 23, 1081 (1969).

106. G. Herzberg and Ch. Jungen, J. Mol. Spectrosc. 1, 425 (1972).

107. R. de L. Dronig, Z. Phys. 50, 347 (1928).

108. H. Beutler and H. O. Jünger, Z. Phys. 100, 80 (1936); 101, 285, 304 (1936).

109. For details of assignments, see Refs. (60) and (62). The assignment of the strong autoionization peak at 804.12 Å is still in question. In the earlier work of Chupka and Berkowitz (Ref. (60)), it was assigned as R(1)3pπ, v=6. The later study of Dehmer and Chupka prefers the assignment of Q(1) 7pπ, v=1.

110. The difference between $n\ell\sigma_{v'_o=0}(N_2^+)$ and $n\ell\sigma_{v'_o=1}(N_2^+)$ was found to be greater when a higher resolution of the horizontal quadrupole mass spectrometer was used to reject the contribution of N_2H^+.

SECTION V. VIBRATIONAL STATE DISTRIBUTIONS OF $H_2^+(v'')$ RESULTING FROM THE ELECTRON TRANSFER REACTIONS $H_2^+(v_o' = 0,1) + H_2(v_o'' = 0) \rightarrow H_2(v') + H_2^+(v'')$ IN THE COLLISIONAL ENERGY RANGE OF $E_{c.m.}$ = 2-16 eV

Abstract

The vibrational state distributions of product $H_2^+(v'')$ resulting from the symmetric charge transfer reactions $H_2^+(v_o' = 0 \text{ or } 1) + H_2(v_o'' = 0) \rightarrow H_2(v') + H_2^+(v'')$ in the center-of-mass collisional energy ($E_{c.m.}$) range of 2-16 eV have been measured by the charge exchange method. When reactant H_2^+ ions are prepared in $v_o' = 0$, the majority (> 80%) of product H_2^+ ions are formed in $v'' = 0$. The vibrational relaxation channel for forming $H_2^+(v'' = 0)$ is found to be much more efficient than the vibrational excitation process for producing $H_2^+(v'' = 1)$ in the $H_2^+(v_o' = 1) + H_2(v_o'' = 0)$ charge transfer collisions. The experiment also reveals that inelastic charge transfer channels become more important as $E_{c.m.}$ is increased. The vibrational state distributions of product $H_2^+(v'')$ determined at $E_{c.m.}$ = 8 and 16 eV are compared with results of the semiclassical energy conserving trajectory calculations of Lee and DePristo. A better agreement between experimental and theoretical results is observed at $E_{c.m.}$ = 16 eV, a collisional energy at which charge transfer is the overwhelming channel.

Introduction

Recently, Liao, Liao and Ng[1] performed an experiment using the charge exchange detection method to probe the vibrational state distribution of $H_2^+(v'')$ formed in the charge transfer reaction

$$H_2^+(v_o' = 0 \text{ or } 1) + H_2(v_o'' = 0) \rightarrow H_2(v') + H_2^+(v''). \qquad (1)$$

The experimental observations were found to be in qualitative agreement with the theoretical calculations of Lee and DePristo[2] based on the semiclassical energy conserving trajectory (SECT) formulation. In the case when the reactant H_2^+ ions were prepared in $v_o' = 0$, the experimental and theoretical results were in quantitative agreement.

We have remeasured the vibrational state distributions of $H_2^+(v'')$ resulting from reaction (1) in the center-of-mass collision energy ($E_{c.m.}$) range of 2-16 eV using an improved apparatus. The analysis of the experimental data gives quantitative results for the vibrational state distributions of $H_2^+(v'')$ when the reactant H_2^+ are in the $v_o' =$ 0 and 1 states. This experiment reveals that vibrational energy relaxation of molecular ions via the charge transfer mechanism is highly efficient.

Experimental

The experimental arrangement and procedures are similar to those described recently.[1,3] The sensitivity of the charge exchange detector in the crossed ion-neutral beam photoionization apparatus has been im-

proved by inserting a quadrupole mass filter between the collision region and the horizontal charge exchange detection gas cell. This modification completely suppresses the noise arising from reaction of the reactant $H_2^+(v_o')$ ions with probing gas molecules effusing from the detection gas cell into the collision region. In order to illustrate the essential modification of the crossed ion-neutral beam photoionization apparatus, the cross-sectional view of the apparatus is shown in Figure 1. Briefly, the apparatus consists of a 3-m near normal incidence vacuum ultraviolet (VUV) monochromator (McPherson 2253 M), a discharge lamp, a VUV light detector, two supersonic H_2 beam production systems, three quadrupole mass filters and two reaction gas cells.

The $H_2^+(v_o')$ reactant ions were prepared by photoionization of a H_2 supersonic jet at the photoionization region. The neutral reactant H_2 beam was produced by supersonic expansion through the upper nozzle (3) (nozzle diameter of 120 μm, stagnation pressure of $\sim$ 250 Torr) and collimated into the scattering chamber by a conical skimmer (5). The reactant $H_2^+(v_o')$ and $H_2(v_o'' = 0)$ beams intersected at 90° at the collision center. The laboratory collision energy (E_{lab}) is defined by the difference in potential between the photoionization and collision regions. The intensity of reactant $H_2^+(v_o')$ was measured by the vertical quadrupole mass spectrometer (10). Slow product $H_2^+(v'')$ ions produced by reaction (1) were collected and measured by the front quadrupole mass filter (11). During the measurement of the product

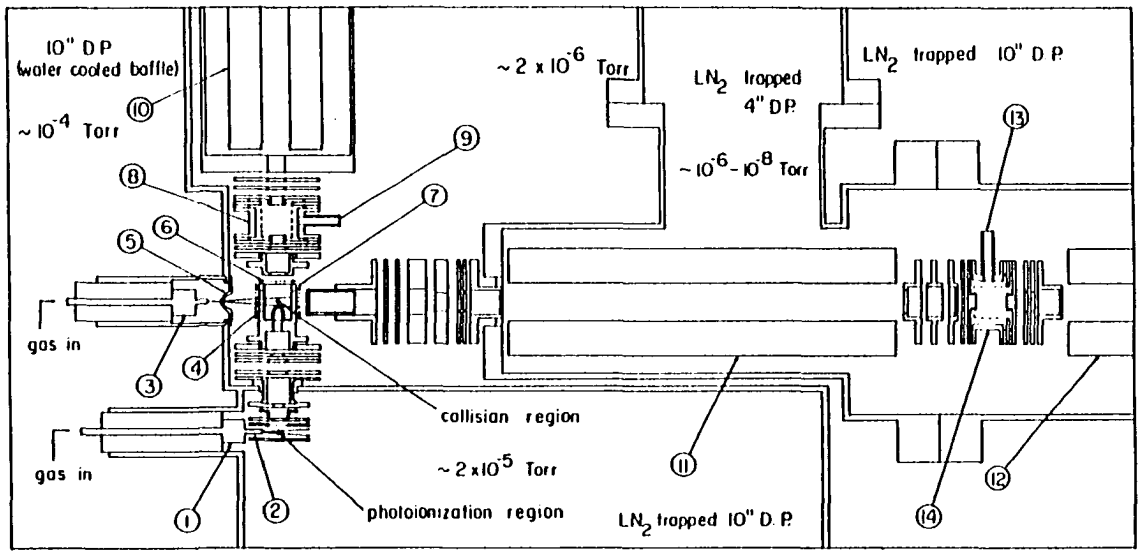

Figure 1. Cross-sectional view of the crossed ion-neutral beam photoionization apparatus.

(1) lower H_2 supersonic nozzle, (2) quartz nozzle tip, (3) upper H_2 supersonic nozzle, (4) grid 1, (5) skimmer, (6) grid 2, (7) grid 3, (8) vertical gas cell, (9) gas inlet of the vertical gas cell, (10) vertical quadrupole mass spectrometer, (11) front horizontal quadrupole mass spectrometer, (12) back horizontal quadrupole mass spectrometer, (13) gas inlet of the horizontal gas cell, (14) horizontal gas cell

$H_2^+(v'')$ ion intensity, the back quadrupole mass filter (12) was operated as an ion guide and the horizontal gas cell (14) was empty.

In this experiment, the charge exchange reactions

$$H_2^+(v'') + H_2 \rightarrow H_2 + N_2^+ \tag{2}$$

$$H_2^+(v'') + Ar \rightarrow H_2 + Ar^+ \tag{3}$$

at E_{lab} = 20 eV have been used as the probing reactions to deduce the vibrational state distribution of product $H_2^+(v'')$. The SECT theoretical calculation predicts that at $E_{c.m.} \leq 16$ eV, an overwhelming majority of the product H_2^+ formed by reaction (1) are in the v'' = 0, 1, and 2 states. The preliminary experimental study of Liao, Liao, and Ng[1] supports this prediction. Assuming the $H_2^+(v'')$ ions consist only of H_2^+ in the v'' = 0, 1, and 2 states, and using arguments presented previously, we arrive at the relations

$$X_0 + X_1 + X_2 = 1 \tag{4}$$

$$X_0 n\ell\sigma_0(N_2^+) + X_1 n\ell\sigma_1(N_2^+) + X_2 n\ell\sigma_2(N_2^+) = n\ell\sigma_m(N_2^+) \tag{5}$$

$$X_0 n\ell\sigma_0(Ar^+) + X_2 n\ell\sigma_1(Ar^+) + X_2 n\ell\sigma_2(Ar^+) = n\ell\sigma_m(Ar^+). \tag{6}$$

Here, X_0, X_1, and X_2 are the fractions of product H_2^+ ions formed in the v'' = 0, 1, and 2 states, respectively; σ_0, σ_1 and σ_2 are the state-selected total cross sections for reactions (2) and (3) when

H_2^+ ions are prepared in the 0, 1, and 2 vibrational states, respectively; $\sigma_m(N_2^+)$ and $\sigma_m(Ar^+)$ represent the total cross sections for reactions (2) and (3) characteristic of the $H_2^+(v'')$ ions formed by reaction (1), n is the density of N_2 (or Ar); and ℓ is the effective length of the gas cell. As mentioned in the previous studies,[1,3] the calculations of X_0, X_1, and X_2 need not involve the determination of absolute total cross sections provided $n\ell\sigma_0(N_2^+)$, $n\ell\sigma_1(N_2^+)$, $n\ell\sigma_2(N_2^+)$, $n\ell\sigma_0(Ar^+)$, $n\ell\sigma_1(Ar^+)$, $n\ell\sigma_2(Ar^+)$, $n\ell\sigma_m(N_2^+)$, and $n\ell\sigma_m(Ar^+)$ are measured in the same gas cell with the same value of n.

The main difficulty of the previous experimental arrangement[1,3] used in determining the vibrational distribution of $H_2^+(v'')$ is that probing gas molecules such as N_2 effuse from the charge transfer detection cell to the collision region and react with the reactant $H_2^+(v_o')$ ions giving rise to N_2^+. These N_2^+ are collected and appear as noise in the charge transfer detection experiment. Although the N_2^+ noise thus formed can be subtracted from the total N_2^+ signal, it affects the signal-to-noise ratio of the measurement. In this experiment, the N_2^+ (or Ar^+) noise can be completely suppressed by using the front quadrupole mass spectrometer to filter the N_2^+ (or Ar^+) noise. The front mass spectrometer can also prevent minor H_3^+ formed in the $H_2^+ + H_2$ collision from entering the charge transfer cell. The interactions of H_3^+ with probing gas molecules may affect the experiment in an unknown way. During the measurement of $n\ell\sigma_m(N_2^+)$ (or $n\ell\sigma_m(Ar^+)$) the front quadrupole mass filter was tuned to the mass of

H_2^+(m/e = 2) while the back quadrupole mass spectrometer was tuned to the mass of N_2^+ (or Ar^+).

Results and Discussion

In order to determine values for $n\ell\sigma_0(N_2^+)$, $n\ell\sigma_1(N_2^+)$, $n\ell\sigma_2(N_2^+)$, $n\ell\sigma_0(Ar^+)$, $n\ell\sigma_1(Ar^+)$, and $n\ell\sigma_2(Ar^+)$, the photoionization efficiency (PIE) curves for product N_2^+ and Ar^+ ions formed by the reactions $H_2^+(v_o') + N_2$ and $H_2^+(v_o') + Ar$ at E_{lab} = 20 eV were obtained with the ion beam-horizontal gas cell arrangement described previously.[1] The $H_2^+(v_o')$ ions were formed by photoionization in the photoionization region and deflected through the horizontal cell by adjusting the voltages of grids 1, 2, and 3 at the collision region. Figures 2(a)-(c) show the PIE curves for H_2^+ and product N_2^+ and Ar^+ ions in the region of 750-810 Å measured with a wavelength resolution of 0.28 Å (FWHM). Table 1 lists the values for $n\ell\sigma_{v_o'}(N_2^+)$ $n\ell\sigma_{v_o'}(Ar^+)$, v_o' = 0-4,[4] determined by the analysis (see Ref. 1) of the PIE curves for H_2^+ and product N_2^+ and Ar^+ ions. Since the gas cell used in this study does not allow the collection of all product ions, these values cannot be viewed as absolute total cross sections. The large differences between $n\ell\sigma_0$, $n\ell\sigma_1$ and $n\ell\sigma_2$ and the different trends observed in the vibrational dependence of $n\ell\sigma_{v_o'}(N_2^+)$ and $n\ell\sigma_{v_o'}(Ar^+)$ should provide sensitive detection for the vibrational state distribution of $H_2^+(v'')$ formed by reaction (1).

The values for $n\ell\sigma_m(N_2^+)$ and $n\ell\sigma_m(Ar^+)$ determined using the hori-

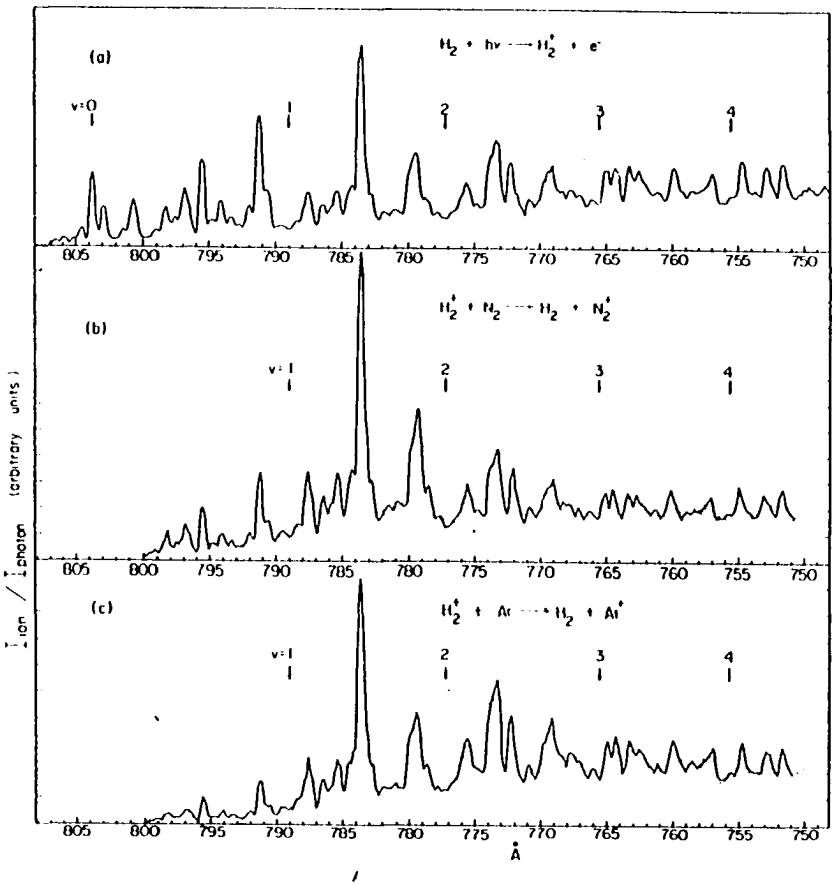

Figure 2. PIE curves in the region of 750-810 Å for a) H_2^+, b) product N_2^+, and c) product Ar^+. The product N_2^+ and Ar^+ ions were formed by the reactions $H_2^+ + N_2$ and $H_2^+ + Ar$, respectively, at E_{lab} = 20 eV using the ion beam-horizontal gas cell arrangement. Wavelength resolution = 0.28 Å (FWHM)

Table 1. Values for $n\ell\sigma_{v_o'}(N_2^+)$[a] and $n\ell\sigma_{v_o'}(Ar^+)$,[a] $v_o' = 0$-4, determined at $E_{lab} = 20$ eV

v_o'	$n\ell\sigma_{v_o'}(N_2^+)$[b,c]	$n\ell\sigma_{v_o'}(Ar^+)$[b,c]
0	0.01305	0.00780
1	0.03344	0.03010
2	0.02001	0.03566
3	0.01482	0.02580
4	0.01471	0.01838

[a] $\sigma_{v_o'}(N_2^+)$ and $\sigma_{v_o'}(Ar^+)$ represent the total cross sections for the reactions, $H_2^+(v_o') + N_2 \rightarrow H_2 + N_2^+$ and $H_2^+(v_o') + Ar \rightarrow H_2 + Ar^+$, respectively. n is the density for N_2 or Ar and ℓ is the effective length of the gas cell.

[b] The standard deviations due to counting statistics are $\leq 3\%$.

[c] $n\ell\sigma_3(N_2^+)$, $n\ell\sigma_4(N_2^+)$, $n\ell\sigma_3(Ar^+)$, and $n\ell\sigma_4(Ar^+)$ are not used in the calculations.

zontal gas cell are listed in Table 2. The photon wavelength of 792 Å was used to produce reactant H_2^+ at $v_o' = 0$. At 784 Å, which coincides with the position of the strongest autoionization peak in the H_2^+ spectrum, H_2^+ ions are formed predominantly in the $v_o' = 1$ state. The values for $v_o' = 1$ shown in Table 2 are obtained from values measured at 784 Å and corrected for the minor contribution of $H_2^+(v_o' = 0)$.

Using the values listed in Tables 1 and 2, the fractions of product H_2^+ formed in $v'' = 0$, 1, and 2 have been calculated by solving appropriate 3x3 linear equations. These fractions are listed in Table 3.

Table 2. Values for $n\ell\sigma_m(N_2^+)^a$ and $n\ell\sigma_m(Ar^+)^a$ determined at E_{lab} = 20 eV[b]

v_o'[c]	$E_{c.m.}$ (eV)[d]	$n\ell\sigma_m(N_2^+)$[e]	$n\ell\sigma_m(Ar^+)$[e]
0	2	0.01282	0.00860
	4	0.01430	0.01020
	6	0.01509	0.01066
	8	0.01529	0.01100
	12	0.01611	0.01175
	16	0.01659	0.01187
1	2	0.02916	0.02542
	4	0.02711	0.02510
	6	0.02505	0.02403
	8	0.02524	0.02297
	12	0.02434	0.02154
	16	0.02250	0.02032

[a] $\sigma_m(N_2^+)$ and $\sigma_m(Ar^+)$ are the total cross sections for the reactions $H_2^+(v'') + H_2 \rightarrow H_2 + N_2^+$ and $H_2^+(v'') + Ar \rightarrow H_2 + Ar^+$, respectively. n is the density of N_2 or CO and ℓ is the effective length of the gas cell.

[b] E_{lab} is defined to be the difference in potential between the collision region and the horizontal gas cell.

[c] Vibrational state of the reactant H_2^+ ions.

[d] Center-of-mass collisional energies of the reaction $H_2^+(v_o') + H_2 \rightarrow H_2(v') + H_2^+(v'')$.

[e] The standard deviations due to counting statistics are $\leq$ 3%.

Table 3. Vibrational state distributions of product $H_2^+(v'')$ formed by the charge transfer reaction $H_2^+(v_o' = 0 \text{ or } 1) + H_2(v_o'' = 0) \rightarrow H_2(v') + H_2^+(v'')$ in the center-of-mass ($E_{c.m.}$) collisional energy range of 2-16 eV

$E_{c.m.}$ (eV)	v_o'	X_0 [a,b]	X_1 [a,b]	X_2 [a,b]
2	0	1.00	0.00	0.00
	1	0.21	0.79	0.00
4	0	0.91	0.04	0.05
	1	0.25	0.66	0.09
6	0	0.88	0.09	0.03
	1	0.31	0.54	0.15
8	0	0.86 (0.92)	0.10 (0.07)	0.04 (0.01)
	1	0.34 (0.17)	0.57 (0.76)	0.09 (0.07)
12	0	0.83	0.14	0.03
	1	0.40	0.53	0.07
16	0	0.82 (0.87)	0.17 (0.12)	0.01 (0.01)
	1	0.46 (0.39)	0.43 (0.50)	0.11 (0.11)

[a] X_0, X_1, and X_2 are the fractions of product H_2^+ formed in the v'' = 0, 1, and 2 states. The uncertainties of these values are estimated to be 0.05.

[b] The values in the parentheses are theoretical values (Ref. 2).

The uncertainties of the calculated values for X_0, X_1, and X_2 are estimated to be $\sim$ 0.05. The SECT theoretical values obtained by Lee and DePristo at $E_{c.m.}$ = 8 and 16 eV are also included in Table 3.

When the reactant H_2^+ ions are in $v_o' = 0$, nearly all the charge transfer product H_2^+ ions formed at $E_{c.m.}$ = 2 eV are in the v'' = 0 state, indicating that resonance charge transfer is the dominant proc-

ess. As $E_{c.m.}$ changes from 2 to 16 eV, the value for X_1 increases steadily from $\sim$ 0.0 to 0.17. The fractions of product H_2^+ observed in the v" = 2 state in this energy range are small. The values for X_0 and X_1 obtained from $E_{c.m.}$ = 16 eV are consistent with those reported previously.[1] The SECT theoretical values for X_0, X_1 and X_2 at $E_{c.m.}$ = 8 and 16 eV with v_o' = 0 are in fair agreement with the experimental findings.

For the reactant H_2^+ ions prepared in v_o' = 1, the experimental results show that even at $E_{c.m.}$ = 2 eV the inelastic relaxation channel forming v" = 0 is significant. The degree of relaxation also increases as $E_{c.m.}$ increases. At a given $E_{c.m.}$, the value for X_2 observed with v_o' = 1 is comparable to that for X_1 with v_o' = 0. The most interesting observation is that the extent of the relaxation channel is substantially greater than that of the excitation channel. Although the SECT calculations predict such a trend, the theory seems to underestimate the degree of inelastic relaxation. A better agreement between experimental and theoretical results is found at $E_{c.m.}$ = 16 eV. At $E_{c.m.}$ = 8 eV and v_o' = 1, the experimental value for X_0 is twice that of the theoretical value. However, the SECT theoretical study of Lee and DePristo has not taken into account the formation of $H_3^+ + H$ which becomes more important at lower collision energies. This may explain the discrepancy observed between the experimental and theoretical results at v_o' = 1.

References

1. C. L. Liao, C. X. Liao and C. Y. Ng, J. Chem. Phys. 81, 5672 (1984).

2. C. Y. Lee and A. E. DePristo, J. Chem. Phys. 80, 1116 (1984).

3. C. L. Liao, C. X. Liao and C. Y. Ng, J. Chem. Phys. 82, 5489 (1985).

4. The values for $n\ell\sigma_3(N_2^+)$, $n\ell\sigma_4(N_2^+)$, $n\ell\sigma_3(Ar^+)$, and $n\ell\sigma_4(Ar^+)$ are not used in the calculation for X_0, X_1, and X_2. They were obtained to check for possible inconsistency.

SECTION VI. A STATE-TO-STATE STUDY OF THE SYMMETRIC CHARGE TRANSFER REACTION $Ar^+(^2P_{3/2,1/2}) + Ar(^1S_o)$

Abstract

The relative state-to-state total charge transfer cross sections $\sigma_{3/2\to3/2}$, $\sigma_{3/2\to1/2}$, $\sigma_{1/2\to1/2}$, and $\sigma_{1/2\to3/2}$, for the reactions

$$Ar^+(^2P_{3/2}) + Ar(^1S_o) \to Ar(^1S_o) + Ar^+(^2P_{3/2}),$$

$$\to Ar(^1S_o) + Ar^+(^2P_{1/2}),$$

$$Ar^+(^2P_{1/2}) + Ar(^1S_o) \to Ar(^1S_o) + Ar^+(^2P_{1/2}), \text{ and}$$

$$\to Ar(^1S_o) + Ar^+(^2P_{3/2}),$$

respectively, at the laboratory collision energy range of 1-4000 eV, have been determined using the newly constructed crossed ion-neutral beam photoionization apparatus. This apparatus is equipped with a high resolution photoionization ion source for reactant state selections and a charge transfer detector for product state identifications. The measured profile of the kinetic energy dependence for the probability for $^2P_{3/2} \to {}^2P_{1/2}$ fine-structure transitions in $Ar^+(^2P_{3/2}) + Ar(^1S_o)$ charge transfer collisions $(\sigma_{3/2\to1/2}/(\sigma_{3/2\to3/2} + \sigma_{3/2\to1/2}))$ is in general agreement with the theoretical prediction of Johnson. However, the theoretical probabilities are approximately 40% greater than those

observed in this experiment. The total charge transfer cross section for $Ar^+(^2P_{3/2}) + Ar(^1S_o)$ $[\sigma_{3/2\rightarrow3/2} + \sigma_{3/2\rightarrow1/2}]$ were found to be slightly higher than that for $Ar^+(^2P_{1/2}) + Ar(^1S_o)$ $[\sigma_{1/2\rightarrow1/2} + \sigma_{1/2\rightarrow3/2}]$. Furthermore, the experimental values for $(\sigma_{1/2\rightarrow1/2} + \sigma_{1/2\rightarrow3/2})/(\sigma_{3/2\rightarrow3/2} + \sigma_{3/2\rightarrow1/2})$ indicate that the difference in the total charge transfer cross sections for $Ar^+(^2P_{1/2}) + Ar(^1S_o)$ and $Ar^+(^2P_{3/2}) + Ar(^1S_o)$ diminishes at both low and high collision energies, in accordance with the theoretical expectations. Taking into account the experimental uncertainties, the experimental results are also consistent with detailed balance which requires the value for $\sigma_{1/2\rightarrow3/2}$ to be twice that for $\sigma_{3/2\rightarrow1/2}$ at collisional energies substantially higher than the spin-orbit splitting of Ar^+.

Introduction

The symmetric charge transfer reactions between Ar^+ and Ar have been the subject of many experimental studies.[1-17] Most of the previous studies involved measurements of the total charge transfer cross section as a function of collision energy using electron-impact ion sources. Thus, the reactant Ar^+ ions were usually formed in a mixture of the $^2P_{3/2}$ and $^2P_{1/2}$ states. Furthermore, due to the nature of the electron ionization, metastable Ar^+ ions may also have been produced in the electron-impact ion sources. In spite of these difficulties, the kinetic energy dependence of the total symmetric charge transfer cross section for the Ar^+ + Ar system is considered to be one of the most reliably established.[18] Using photoionization to prepare the

reactant Ar^+ ions, the fine-structure effects on the symmetric charge transfer in Ar have recently been examined.[15,17] The photoion-photoelectron coincidence study of Campbell et al.[17] shows that the ratio of the total charge transfer cross sections for $Ar^+(^2P_{1/2}) + Ar(^1S_o)$ and $Ar^+(^2P_{3/2}) + Ar(^1S_o)$ is just measurably smaller than unity over the laboratory collision energy (E_{lab}) range of 5-1000 eV, an observation consistent with the two-state model of Rapp and Francis.[19] The previous experimental studies of the $Ar^+ + Ar$ system are in general agreement with theoretical predictions.[19-21]

Although the theoretical calculation of Johnson,[21] which took into account the Σ and Π energy states of the Ar_2^+ quasi-molecular ion, has provided state-to-state cross sections, $\sigma_{3/2\to3/2}$, $\sigma_{3/2\to1/2}$, $\sigma_{1/2\to1/2}$, and $\sigma_{1/2\to3/2}$, for the four charge transfer processes

$$Ar^+(^2P_{3/2}) + Ar(^1S_o) \to Ar(^1S_o) + Ar^+(^2P_{3/2}) \quad (1)$$

$$\to Ar(^1S_o) + Ar^+(^2P_{1/2}) \quad (2)$$

$$Ar^+(^2P_{1/2}) + Ar(^1S_o) \to Ar(^1S_o) + Ar^+(^2P_{1/2}) \quad (3)$$

$$\to Ar(^1S_o) + Ar^+(^2P_{3/2}) \ , \quad (4)$$

respectively, no experimental state-to-state cross-sectional data have yet been available to compare with the theoretical predictions. McAfee et al.[12] have indirectly derived the probabilities for fine-

structure transitions associated with charge transfer collisions at E_{lab} = 123 eV by means of transformation analysis of the energy and angular distributions of the charge transfer product Ar^+ ions. The fine-structure transitions associated with the direct inelastic channels at the E_{lab} range of 60-1500 eV have been observed recently by Itoh et al.[13] Both of these experiments used electron ionization to prepare the reactant Ar^+ ions. The statistical ratio of 2:1 for the intensities of $Ar^+(^2P_{3/2})$ and $Ar^+(^2P_{1/2})$ formed by electron ionization was assumed in their data analyses.

Photionization is the cleanest method for the preparation of reactant ions with well-characterized distributions of internal states. Reactant ions in their ground electronic, vibrational, and/or rotational states can be produced with 100% purity by the simple photoionization method. The major drawback of a photoionization ion source is its inefficiency. The charge transfer product ion intensity observed in a state-selected experiment using a photoionization ion source such as that used in this study is usually less than 1000 ct/s. Therefore, it is difficult to apply experimental methods such as translational energy measurements and laser-induced fluorescence to probe the internal energy distribution of charge transfer product ions formed in a state-selected experiment using a vacuum ultraviolet photoionization source.

Previous state-selected charge transfer studies[22-34] have revealed dramatic variations in total cross-sections with ion internal and translational energies. We have developed an ion-molecule reaction apparatus

which combines the crossed ion-neutral beam method, high resolution photionization mass spectrometry, and charge transfer detection. As a result of the favorable kinematics in crossed ion-neutral beam studies of charge transfer processes, it is possible to collect nearly all product ions and to probe the final state distribution of these ions by measuring their reactivity for charge exchange with other molecules in a reaction gas cell. This report presents the results on the first state-to-state study of Reactions (1)-(4) using this new apparatus.

Experimental

The experimental arrangement and procedures have been reported recently.[35,36] The crossed ion-neutral beam apparatus has been developed from a high resolution photoionization mass spectrometer.[37] In order to facilitate the description below, the cross-sectional view of the crossed ion-neutral beam apparatus is shown in Figure 1. The apparatus essentially consists of a 3-m near normal incidence vacuum (VUV) monochromator (McPherson 2253 M), a discharge lamp, a VUV light detector, two supersonic beam production systems, two quadrupole mass spectrometers, and two reaction gas cells.

The basic pumping arrangement is similar to that described in Ref. 37. The lower nozzle (1), which is positioned at a distance of $\sim$ 0.65 cm from the photoionization region, has a quartz tip (2) with a nozzle diameter (D_o) of 60 μm. Using an argon stagnation pressure (P_o) of $\sim$ 80 Torr, the pressure in the photoionization chamber was $\sim 5 \times 10^{-6}$ Torr. The Ar^+ reactant ions formed by photoionization at the photo-

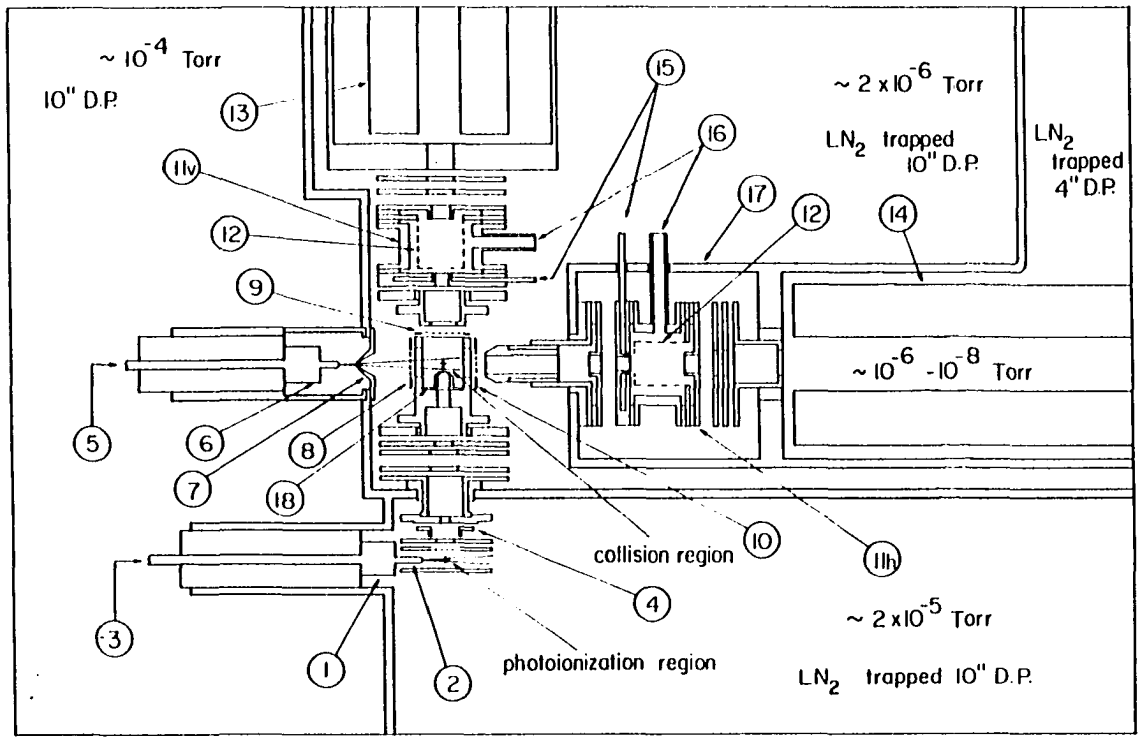

Figure 1. Cross-sectional view of the crossed ion-neutral beam photoionization apparatus. (1) lower nozzle, (2) quartz nozzle tip, (3) Ar inlet, (4) electrostatic deflector, (5) Ar inlet, (6) upper nozzle, (7) skimmer, (8) grid 1, (9) grid 2, (10) grid 3, (11v) vertical gas cell, (11h) horizontal gas cell, (12) platinum grid, (13) vertical quadrupole mass spectrometer, (14) horizontal quadrupole mass spectrometer, (15) gas inlet, (16) to Baratron manometer, (17) horizontal gas cell chamber, (18) aperture.

ionization region were extracted perpendicular to the Ar beam and focused onto another neutral $Ar(^1S_o)$ supersonic beam at an intersecting angle of 90°. In a state-to-state study of $Ar^+(^2P_{3/2,1/2}) + H_2(v = 0)$,[38] there was strong evidence that collisions between $Ar^+(^2P_{3/2})$ initially formed by photoionization and background Ar in the photoionization chamber gave rise to an Ar^+ beam consisting of a mixture of $Ar^+(^2P_{3/2})$ and $Ar^+(^2P_{1/2})$. We found that the purity of the reactant $Ar^+(^2P_{3/2})$ beam was preserved by maintaining a background pressure of $\lesssim 8\times10^{-6}$ Torr in the photoionization chamber. This was achieved by keeping P_o below 100 Tor. The intensity of Ar_2^+ produced under these experimental conditions[39] was negligible in comparison to that of Ar^+. The neutral reactant $Ar(^1S_o)$ beam was produced by a supersonic expansion through the upper stainless steel nozzle (6) with D_o = 120 μm at $P_o \approx 300$ Torr and was then collimated into the scattering chamber by a 0.76 mm diameter conical skimmer (7). The divergence angle of the neutral reactant Ar beam was estimated to be 10°. Accordingly, the width of the neutral beam at the collision center was $\sim$ 0.5 cm. The intensity of the Ar^+ reactant ion beam was monitored with the vertical quadrupole mass spectrometer (13). The intensity of the slow product Ar^+ ions formed in the collisions was measured by the horizontal quadrupole mass spectrometer (14) positioned in the direction of the neutral $Ar(^1S_o)$ reactant beam. The pressures maintained in the beam source chamber and the scattering chamber were $\sim 10^{-4}$ and $\sim 2\times10^{-6}$ Torr, respectively. The vertical and horizontal quadrupole

mass spectrometer chambers were evacuated by a liquid-nitrogen (LN_2) trapped 4-in diffusion pump. With the upper reactant Ar beam off, the base pressure in the mass spectrometer chamber was $\sim 2\times10^{-8}$ Torr. During the crossed ion-neutral beam experiment, the detector chambers were maintained at a pressure of $\sim 8\times10^{-7}$ Torr.

In order to avoid the distortion of the electric field at the photoionization region by field penetration due to adjacent focusing ion lenses, the ion exit aperture of the repeller at the photoionization region was covered by a 90%-transmission gold grid. The collision region was also shielded by a small square ion lens and three 90%-transmission gold grids (8), (9), (10) for a similar reason.

Previous studies[12,16] show that because of inelastic charge transfer channels, the charge transfer product Ar^+ ions can be scattered more than ± 10° away from the neutral reactant Ar beam direction. For accurate measurements of the total charge transfer cross sections, it is important to have high collecting efficiency for inelastic charge transfer product Ar^+ ions scattered at wide angles. Based on the geometric angle sustained by grid 1 at the collision center, the ion lens system of the horizontal mass spectrometer is capable of accepting product Ar^+ ions scattered ± 25° away from the neutral $Ar(^1S_o)$ beam direction. The actual transmission through the horizontal mass spectrometer may depend on the scattering angle. A simple analysis based on the Newton diagram of the scattering, involving a 5 eV $Ar^+(^2P_{3/2})$ ion beam and a supersonic $Ar(^1S_o)$ beam intersecting at 90°, predicts

that charge transfer product $Ar^+(^2P_{1/2})$ ions can be scattered $\sim 15°$ away from the neutral $Ar(^1S_o)$ beam direction. The scattering angles for inelastic charge transfer product Ar^+ ions become smaller as E_{lab} increases. At low collision energies, the scattering angles for inelastic charge transfer product Ar^+ ions are expected to be large. However, since resonance charge transfer is the dominant charge transfer channel at low E_{lab}, it should not be a problem here.

The charge transfer Ar^+ product angular distribution measured at E_{lab} = 200 eV[16] reveals that nearly all charge transfer product Ar^+ ions are scattered within $\pm 4°$ with respect to the neutral reactant Ar beam direction. According to the energy analysis of the charge transfer product Ar^+ ions at a laboratory scattering angle of 4°,[14] a significant fraction of Ar^+ products are produced with high kinetic energies in the range of 1-5 eV. Since these ions have velocity components perpendicular to the neutral reactant Ar beam direction, it is desirable to apply an extraction electrostatic field between grids 1 and 3 to maximize the collection and detection efficiencies of such ions. The extraction electrostatic field maintained between grids 1 and 3 varies from $\sim$ 0.5 V/cm at E_{lab} = 1 eV to $\sim$ 10 V/cm at $E_{lab} \geq$ 100 eV. The product Ar^+ ion intensity as monitored with the horizontal mass spectrometer was found to remain essentially constant for extraction fields $\geq$ 10 V/cm at $E_{lab} \geq$ 100 eV. After the product Ar^+ ions emerged from grid 3, strong focusing fields were used to accelerate these ions towards the horizontal gas cell which is approximately 6 cm

from the collision region. For an entrance aperture of $\sim$ 0.6 cm for the horizontal gas cell, a simple calculation[40] shows that an extraction field of $\sim$ 10 V/cm is more than sufficient to collect the high energy product Ar^+ ions formed at E_{lab} = 200 eV and scattered initially towards grid 3 into the horizontal gas cell. The collection of product Ar^+ ions moving towards grid 1, although less favorable, should still be adequate.[41] Based on the above analysis, we believe that the collection and detection efficiencies for in-plane and near in-plane scattered charge transfer product Ar^+ ions achieved in this experiment is very good. Nevertheless, discriminative effects against product ions scattered out-of-plane with high kinetic energies are to be expected. This is a problem for most of the previous state-selected total cross-sectional studies which used a similar arrangement as that used in this experiment. In this case, one should realize that high energy product Ar^+ ions formed at high E_{lab} and scattered at wide laboratory angles usually represent a small fraction of the total charge transfer product ions.

The laboratory collision energy is defined by the difference in potential between the photoionization and collision regions. The kinetic energy resolution depends on the repeller field at the photoionization region and the extraction field at the collision region. Since the voltage arrangements used in this experiment are similar to those in the $H_2^+ + H_2$ study,[35,36] the kinetic energy resolution achieved here and in the latter experiment should be comparable. In the E_{lab}

range of interest in this study, the values for $\Delta E/E_{lab}$ are estimated to be better than 0.03. ΔE represents the kinetic energy spread for a given value of E_{lab}.

The gold-coated tube-like aperture (18) extends the exit hole for the reactant Ar^+ ions in the square ion lens to 0.3 cm from the collision center. It was shown in the previous study[36] that as a result of a better defined collision volume due to this aperture, the intensity of background ions arising from elastically scattered reactant ions at $E_{lab} \leq 2$ eV, as observed by the horizontal mass spectrometer was minimized. The previous study also indicated that at $E_{lab} \geq 4$ eV, the intensity of background ions due to elastically scattered reactant ions was negligible compared to that of the charge transfer product ions. The extent of surface charging effects on the amount of background ions observed at low E_{lab} is unknown.

The intensity of the charge transfer product Ar^+ ions is directly proportional to that of the reactant Ar^+ beam at the collision region. The electrostatic deflector (4) is helpful in optimizing the transportation of reactant Ar^+ ions from the photoionization region to the collision region at low E_{lab}. The obtainable intensity of the reactant Ar^+ ions at the collision region depends on E_{lab}. Using a wavelength resolution of 1.4 Å (FWHM), the intensities observed between the thresholds of $Ar^+(^2P_{3/2})$ and $Ar^+(^2P_{1/2})$ were > 10^5 ct/s. The ratio of the intensity for the product Ar^+ ions to that of the unattenuated reactant Ar^+ ion beam was ≤ 0.02.[41] The relative standard deviations

due to counting statistics for all PIE data presented here are less than 5%.

The reaction gas cells (11) associated with the ion lens systems of the vertical and horizontal mass spectrometers are referred to here as the vertical and horizontal gas cells, (11v) and (11h), respectively. The two reaction gas cells have an identical design. Each cell consists of a front and a back ion lens, a cylindrical platinum grid (12) and a cylindrical wall. The probing gas entered through the gas inlet (15) connected to the front ion lens and emerged into the gas cell from a circular opening on the front ion lens. The gas flow was regulated by a Granville-Phillips variable leak valve and the absolute pressure in the gas cell was monitored with a MKS Baratron manometer (Model 370 HS-1). The reaction volume of the gas cell was defined by the platinum grid. Product ions formed in the gas cell can be trapped inside the platinum grid by applying a high positive potential to the cylindrical wall of the cell. The front lens and the platinum grid were at the same potential, whereas the potential of the back ion lens was slightly lower than the grid so that the product ions were extracted and sampled by the mass spectrometer.

To illustrate the principle of product state identification by the charge transfer detection method, we shall focus on the detection of product ions of Reactions (1) and (2) in the discussion below. After the formation of $Ar^+(^2P_J)$ via Reactions (1) and (2) in the collision region, the $Ar^+(^2P_J)$ ions were collected and guided through

the horizontal reaction gas cell in which $Ar^+(^2P_J)$ ions further reacted with H_2 according to the reaction

$$Ar^+(^2P_J) + H_2 \rightarrow Ar + H_2^+ . \tag{5}$$

Reaction (5) was selected as the probing reaction because of the substantial difference in the state-selected total cross sections[23,29] for $Ar^+(^2P_{3/2})$ $[\sigma_{3/2}(H_2^+)]$ and $Ar^+(^2P_{1/2})$ $[\sigma_{1/2}(H_2^+)]$. For thin target conditions, the measured ion intensity of H_2^+ $[i(H_2^+)]$ formed at a given kinetic energy of the product $Ar^+(^2P_J)$ ions in the horizontal gas cell is related to the intensities of $Ar^+(^2P_{3/2})$ $[I_{3/2}]$ and $Ar^+(^2P_{1/2})$ $[I_{1/2}]$ produced by Reactions (1) and (2), the density of H_2 [n], the effective length of the reaction gas cell (ℓ), and $\sigma_{3/2}(H_2^+)$ and $\sigma_{1/2}(H_2^+)$ measured at the same kinetic energy by the equation

$$I_{3/2}\, n\ell\sigma_{3/2}(H_2^+) + I_{1/2}\, n\ell\sigma_{1/2}(H_2^+) = i(H_2^+) . \tag{6}$$

Using Eq. (6) and the relations

$$I_{3/2} + I_{1/2} = I_T \tag{7}$$

$$i(H_2^+) = I_T\, n\ell\sigma_m(H_2^+) , \tag{8}$$

it can be shown that

$$X_{3/2}\, n\ell\sigma_{3/2}(H_2^+) + X_{1/2}\, n\ell\sigma_{1/2}(H_2^+) = n\ell\sigma_m(H_2^+) \tag{9}$$

$$X_{3/2} + X_{1/2} = 1 \ . \qquad (10)$$

Here, I_T is the total intensity for $Ar^+(^2P_J)$ measured when the reaction gas cell is empty; $\sigma_m(H_2^+)$ represents the total cross section for the Reaction (5) characteristic of product $Ar^+(^2P_J)$; and $X_{3/2}$ and $X_{1/2}$ are the fractions of $Ar^+(^2P_{3/2})$ and $Ar^+(^2P_{1/2})$ product ions formed in the charge transfer reaction of $Ar^+(^2P_{3/2}) + Ar(^1S_o)$. Since $n\ell\sigma_{3/2}(H_2^+)$, $n\ell\sigma_{1/2}(H_2^+)$, and $n\ell\sigma_m(H_2^+)$ can be measured, Eqs. (9) and (10) allow the calculation of $X_{3/2}$ and $X_{1/2}$. The calculation of $X_{3/2}$ and $X_{1/2}$ need not involve the determination of the absolute values for $\sigma_{3/2}(H_2^+)$ and $\sigma_{1/2}(H_2^+)$, and $\sigma_m(H_2^+)$ provided that they are measured at the same collision energy using the same or identical gas cell and a constant value of n. In the preparation of this paper, we found that a similar method as described above was used recently by Tanaka et al.[42] to analyze the ionic state distribution of N_2^+ formed in autoionization.

The vertical reaction gas cell can be used to measure the values for $n\ell\sigma_{3/2}(H_2^+)$ and $n\ell\sigma_{1/2}(H_2^+)$. We found that the reactant Ar^+ ions formed at the photoionization region could be deflected through the horizontal gas cell with moderate loss in intensity by adjusting the voltages of grids 1, 2, and 3. Therefore, the parameters $n\ell\sigma_{3/2}(H_2^+)$, $n\ell\sigma_{1/2}(H_2^+)$, and $n\ell\sigma_m(H_2^+)$ were all measured using the horizontal gas cell with the neutral reactant beam off.

The horizontal reaction gas cell and the ion lens system of the horizontal mass spectrometer were enclosed by the horizontal gas cell

chamber (17). In this experiment, the gas cell chamber was connected with the horizontal mass spectrometer chamber and evacuated by the same LN_2-trapped 4-in diffusion pump. For a pressure of 5×10^{-4} Torr in the horizontal gas cell, the pressure in the mass spectrometer chamber was maintained at $\sim 3 \times 10^{-6}$ Torr.

The major background of this experiment arose from H_2^+ ions formed at the collision region due to H_2 that diffused from the gas cell to the collision region and reacted with the reactant Ar^+ ions. By the proper design of the gas inlet and differential pumping, we reduced the intensity of the H_2^+ background ions to approximately 30% of the charge transfer product H_2^+ ions formed in the horizontal gas cell. The intensity of the background H_2^+ ions was measured by turning the neutral reactant $Ar(^1S_o)$ beam off, and the actual intensity for the charge transfer product H_2^+ ions was obtained by subtracting the background H_2^+ intensity from the total H_2^+ intensity observed by the horizontal mass spectrometer. The ratio of the intensities for $Ar^+(^2P_J)$ formed by Reactions (1) and (2) and H_2^+ produced in the gas cell via Reaction (5) was generally less than 0.005.[43] Long counting times were used such that the standard deviations due to counting statistics for the charge transfer H_2^+ ions were less than 5%.

After the product Ar^+ ions formed at a given E_{lab} passed through grid 3, these ions were accelerated and focused into the horizontal gas cell by the ion lenses between grid 3 and the horizontal gas cell with the same voltage arrangement regardless of E_{lab}. The average

kinetic energy for Ar^+ traveling through the ion lenses is $\sim$ 50 eV. The total charge transfer cross section for $Ar^+ + Ar$ at 50 eV is $\sim$ 35 $Å^2$.[2,4,6,8] A realistic estimate for the average neutral beam density due to the neutral reactant Ar beam in the region between the collision region and the horizontal gas cell is $< 5 \times 10^{-5}$ Torr. Therefore, we estimate that in a distance of $\sim$ 6 cm less than 4% of the primary product Ar^+ ions will undergo secondary charge transfer. The errors for state-to-state data due to secondary charge transfer should be well within the stated error limits of ± 10%. In fine-structure-selected total cross section measurements, the product Ar^+ ions have to travel a longer distance to reach the horizontal quadrupole mass spectrometer. However, they also traveled through the horizontal ion lens system at a greater average kinetic energy ($\sim$ 200 eV). Stemming from the expectation that a large fraction of secondary charge transfer product ions will still be observed by the horizontal mass spectrometer, secondary charge transfer should have a lesser effect on state-selected total cross-sectional data.

Results and Discussion

The fine-structure effect on the total charge transfer cross section for $Ar^+ + Ar$

Figure 2(a) compares the PIE curves for the reactant Ar^+ and the charge transfer product Ar^+ ions measured at E_{lab} = 9.4 eV. The wavelength resolution used was 0.28 Å (FWHM). The PIE curve for the

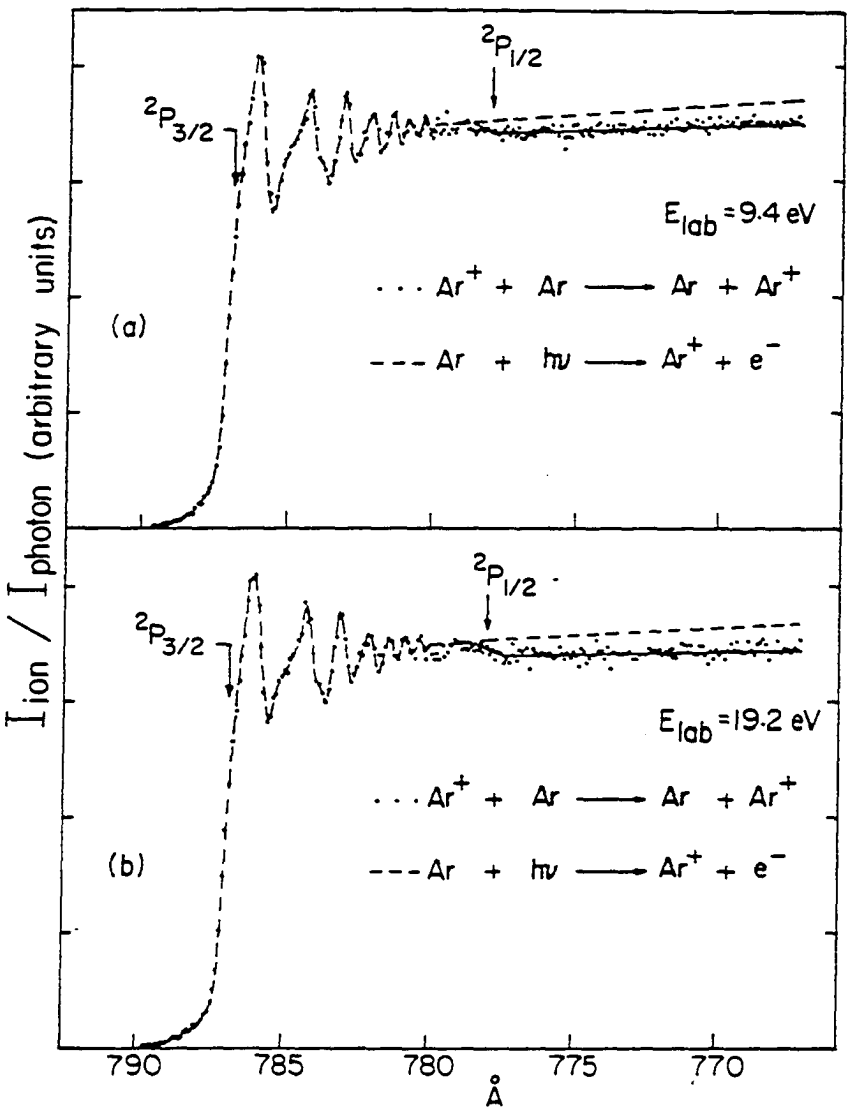

Figure 2. The comparisons of PIE curves for the Ar^+ product ions in the region of 767-790 Å (···) formed at E_{lab} equal to (a) 9.4 eV and (b) 19.2 eV with that for the Ar^+ reactant ions (---) obtained using a wavelength resolution = 0.28 Å (FWHM)

reactant Ar^+ ions was obtained with the neutral reactant $Ar(^1S_o)$ beam off. Since the standard deviations for the PIE data for the reactant Ar^+ were better than 1%, the PIE data were connected by a dashed line. The PIE data for the reactant and product ions were normalized to have the same value at photon energies below the ionization energy (IE) for $Ar^+(^2P_{1/2})$[778 Å]. The PIE curve for the product Ar^+ ions above the IE for $Ar^+(^2P_{1/2})$ is clearly lower than the corresponding PIE curve for the reactant Ar^+ ions. A similar comparison for the PIE curves for the reactant and product Ar^+ ions measured at E_{lab} = 19.2 eV is made in Figure 2(b). The differences in PIE curves for the product and reactant Ar^+ ions at wavelengths shorter than 778 Å found in Figure 2(b) are greater than those in Figure 2(a).

At wavelengths longer than 778 Å, the reactant Ar^+ ions are formed solely in the $^2P_{3/2}$ state, while at shorter wavelengths, a mixture of $Ar^+(^2P_{3/2})$ and $Ar^+(^2P_{1/2})$ should be formed. Using a spherical retarding potential analyzer, Samson and Cairns[44,45] have measured $I_{3/2}/I_{1/2}$ produced by photoionization as a function of excess energy beyond the ionization threshold for $Ar^+(^2P_{1/2})$. Their results indicate that $I_{3/2}/I_{1/2}$ has the same value of 1.98 throughout the photon energy range of $\sim$ 16-21 eV. The quoted uncertainties of their measurements are less than 6%. Similar measurements at 584 Å (HeI) by other workers[46-48] are in agreement with the results of Samson and Cairns. Since the observed values for $I_{3/2}/I_{1/2}$ are essentially identical to the statistical ratio of 2, a value of 2 will be used in the data analysis.

The lower PIEs for the product Ar^+ ions, as compared to those for the reactant Ar^+ above the IE for $Ar^+(^2P_{1/2})$, as shown in Figures 2(a) and 2(b), show unambiguously that the total cross sections for Reactions (1) and (2) ($\sigma_{3/2} = \sigma_{3/2\rightarrow 3/2} + \sigma_{3/2\rightarrow 1/2}$) are higher than those for Reactions (3) and (4) ($\sigma_{1/2} = \sigma_{1/2\rightarrow 1/2} + \sigma_{1/2\rightarrow 3/2}$) at E_{lab} = 9.4 and 19.2 eV. The fact that the ratio for the PIEs for the product and reactant Ar^+ ions, k, at wavelengths shorter than 778 Å for a given E_{lab} remains constant is consistent with the finding of Samson and Cairns that $I_{3/2}/I_{1/2}$ has the same value at photon energies above the IE for $Ar^+(^2P_{1/2})$. It can be shown that $\sigma_{3/2}$ and $\sigma_{1/2}$ are related to k by the equation

$$k = (\frac{2}{3}\sigma_{3/2} + \frac{1}{3}\sigma_{1/2})/\sigma_{3/2} = \sigma_m/\sigma_{3/2} \qquad (11)$$

or

$$\sigma_{1/2}/\sigma_{3/2} = 3\sigma_m/\sigma_{3/2} - 2 \; . \qquad (12)$$

The sum, $\frac{2}{3}\sigma_{3/2} + \frac{1}{3}\sigma_{1/2}$, which is defined to be σ_m here, can be viewed as the total charge transfer cross section characteristic of reactant Ar^+ ions produced at photon energies higher than the IE for $Ar^+(^2P_{1/2})$. Equation (12) allows the calculation of $\sigma_{1/2}/\sigma_{3/2}$ at a given E_{lab} when the value for $\sigma_m/\sigma_{3/2}$ (or k) is known.

Figure 3 shows the values for $\sigma_m/\sigma_{3/2}$ measured in the E_{lab} range of 1-4000 eV. Since the value for $\sigma_m/\sigma_{3/2}$ is constant at wavelengths shorter than 778 Å, the values for $\sigma_m/\sigma_{3/2}$ shown in Figure 3 were ob-

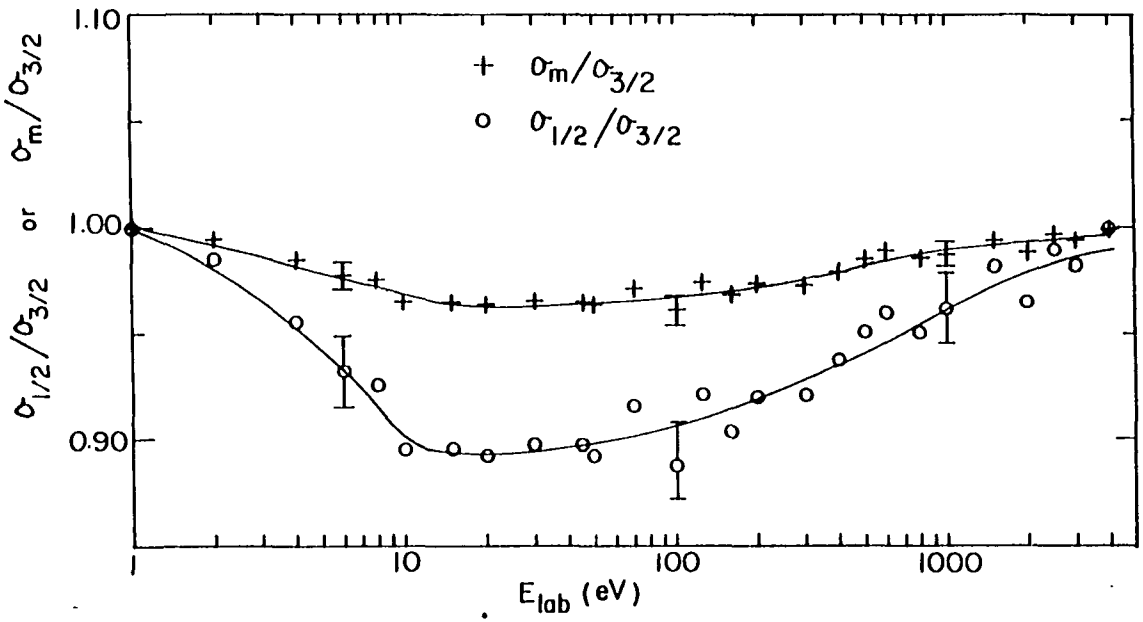

Figure 3. Values for $\sigma_{1/2}/\sigma_{3/2}$ and $\sigma_m/\sigma_{3/2}$ plotted as a function of E_{lab} in the range of 1-4000 eV

tained by measuring the ratio, [i(775 Å)/I(775 Å)]/[i(782 Å)/I(782 Å)]. Here, i(782 Å) and i(775 Å) are the intensities for the charge transfer product Ar^+ ions observed at 782 and 775 Å, respectively; I(782 Å) and I(775 Å) are the corresponding intensities for the reactant Ar^+ ions formed at 782 and 775 Å. The values for I(782 Å) and I(775 Å) were measured by the vertical mass spectrometer when the neutral reactant $Ar(^1S_o)$ beam was off. The wavelength resolution used in these measurements was $\sim$ 2 Å (FWHM). Each datum point is the average of several measurements. Typical standard deviations for the $\sigma_m/\sigma_{3/2}$ values, as shown in Figure 3, are $\leq$ 1%.

The values for $\sigma_{1/2}/\sigma_{3/2}$ in the E_{lab} range of 1-4000 eV calculated by using Eq. (12) are also plotted in Figure 3. The standard deviations for $\sigma_{1/2}/\sigma_{3/2}$ are $\leq$ 2%. These experimental measurements of $\sigma_{1/2}/\sigma_{3/2}$ show that $\sigma_{1/2}/\sigma_{3/2}$ approaches unity smoothly at both low and high collision energies, from a broad minimum of 0.89 at 10-50 eV. The values for $\sigma_{1/2}/\sigma_{3/2}$ being less than unity agree with recent measurements of Campbell et al.,[17] but they did not observe the structure of the kinetic energy dependence for $\sigma_{1/2}/\sigma_{3/2}$.

The impact parameter calculation of Johnson[21] gave a value of 1.00±0.05 for $\sigma_{1/2}/\sigma_{3/2}$ at $E_{lab} \geq 5$ eV. This prediction is higher than experimental values of 0.89–0.94 for $\sigma_{1/2}/\sigma_{3/2}$ in the E_{lab} range of $\sim$ 6–400 eV. Although the calculation indicates that $\sigma_{1/2}/\sigma_{3/2}$ is essentially independent of E_{lab}, the profiles of the kinetic energy dependences for the ratios of the total charge transfer cross sections

for the $^2P_{1/2}$ and $^2P_{3/2}$ states obtained for the $Kr^+ + Kr$ and $Xe^+ + Xe$ systems in similar calculations[49] resemble that observed for the $Ar^+ + Ar$ system shown in Figure 3. The calculated total cross sections for Kr^+ and Xe^+ in the $^2P_{3/2}$ and $^2P_{1/2}$ states have been found to change their slope going from the low energy region where (J_a,J_b) coupling dominates to higher energy where (Λ,S) coupling dominates.[50] The changes in slope occur roughly over the energy region where the velocity goes from a value equal to the spin-orbit splitting in atomic units to half that value. This energy region also corresponds to the location of the broad minimum for the ratio of the total charge transfer cross sections for the $^2P_{1/2}$ and $^2P_{3/2}$ states. Since the spin-orbit splitting for Ar^+ is substantially smaller than those for Kr^+ and Xe^+, the position of the broad minimum for $\sigma_{1/2}/\sigma_{3/2}$ is expected to be at a lower E_{lab} region. Based on the known spin-orbit splitting of 0.178 eV for Ar^+, the E_{lab} region predicted for the location of the minimum for $\sigma_{1/2}/\sigma_{3/2}$ is $\sim$ 40 eV, in agreement with the experimental observation.

As the collision energy increases, the nonadiabatic transitions between a quasi-molecular state derived from $Ar^+(^2P_{3/2})$ to that derived from $Ar^+(^2P_{1/2})$ become more important. These nonadiabatic transitions lead to the increase in $\sigma_{1/2}/\sigma_{3/2}$ as a function of collision energy at $E_{lab} > 50$ eV. At sufficiently high E_{lab}, the charge transfer cross section is expected to be independent of the initial J state of the ion. Johnson[49] pointed out that at high collision

energies the value for $\sigma_{1/2}/\sigma_{3/2}$ depends strictly on the ionization potentials for the $^2P_{3/2}$ and $^2P_{1/2}$ states and would be predicted correctly by the theory of Rapp and Francis.[19] The simple two-state model of Rapp and Francis gives a value of 0.98 for $\sigma_{1/2}/\sigma_{3/2}$ in good agreement with experimental value measured at $E_{lab} \geq 1500$ eV.

The conditions of the collision become more adiabatic as the collision energy decreases from $E_{lab} \approx 20$ eV. At very low collision energies, the cross section should be determined solely by the polarizability of the neutral Ar atom[51] and E_{lab} and thus should be independent of the ionic state. The observation that the value for $\sigma_{1/2}/\sigma_{3/2}$ approaches unity at low E_{lab} is in accord with this theoretical expectation.

Relative state-to-state total charge transfer cross sections for Reactions (1)-(4)

In order to illustrate the difference in reactivity of $Ar^+(^2P_{3/2})$ and $Ar^+(^2P_{1/2})$ with H_2, PIE data for H_2^+ formed via Reaction (5) at $E_{lab} = 45$ eV in the region of $\sim$ 767-790 Å were plotted in Figure 4(b) and compared with the PIE spectrum for Ar^+ shown in Figure 4(a). The PIE curve for the product H_2^+ ion was obtained in a separate study[38] using the crossed ion-neutral beam arrangement and a wavelength resolution of 0.28 Å (FWHM). The increase in PIE for H_2^+ above the $Ar^+(^2P_{1/2})$ threshold indicates that $\sigma_{1/2}(H_2^+)$ is substantially greater than $\sigma_{3/2}(H_2^+)$ at $E_{lab} = 45$ eV. From the ratio of the step heights measured in the H_2^+ spectrum, together with the known distribution of $Ar^+(^2P_{3/2})$

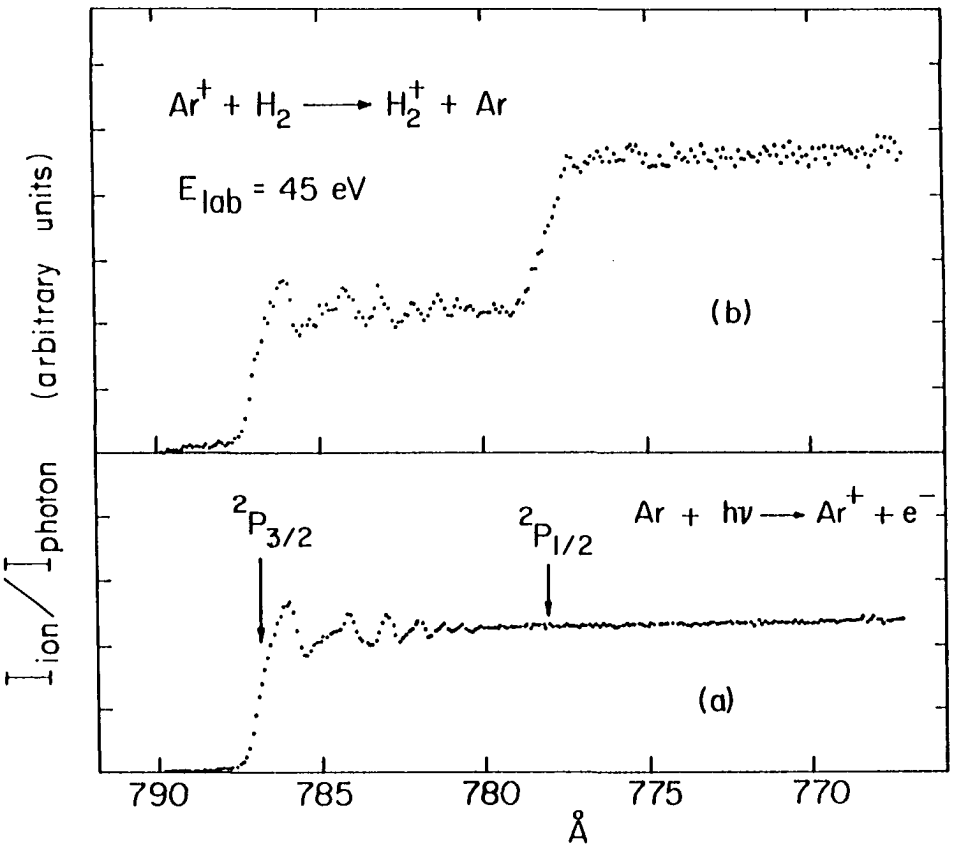

Figure 4(a). PIE curve for the Ar^+ in the region of 766-790 Å (wavelength resolution = 0.28 Å (FWHM)

Figure 4(b). PIE curve for the H_2^+ product ion in the region of 766-790 Å obtained using the crossed ion-neutral beam arrangement (wavelength resolution = 0.28 Å (FWHM))

and $Ar^+(^2P_{1/2})$ formed at wavelengths shorter than 778 Å, the ratio of $\sigma_{1/2}(H_2^+)$ to $\sigma_{3/2}(H_2^+)$ [R] at 45 eV can be deduced from an equation similar to Eq. (12). The ratio R has been found to increase as E_{lab} decreases.[23,29,38]

A similar PIE curve for the product H_2^+ ion can be obtained by using the horizontal gas cell. This involved guiding a beam of reactant Ar^+ ions formed at the photoionization region through the horizontal gas cell filled with a known pressure of H_2 and measuring the intensity of the product H_2^+ ions with the horizontal mass spectrometer. We found that the ratio R determined at a given collision energy using the horizontal gas cell depends slightly on the pressure of H_2 in the cell. As mentioned above, since a constant value for the pressure of H_2 was used for the measurements of $n\ell\sigma_{3/2}(H_2^+)$, $n\ell\sigma_{1/2}(H_2^+)$, and $n\ell\sigma_m(H_2^+)$, the slight dependence of R should not affect the results derived in this experiment. The collision energy for the probing Reaction (5) was fixed at E_{lab} = 20 eV, and the pressure of H_2 in the horizontal gas cell was maintained at 5×10^{-4} Torr. Under these conditions, a value of 6.10 was obtained for R. A value of 1.75 for $n\ell\sigma_{3/2}(H_2^+)$ was determined by measuring $i(H_2^+)/I_o[Ar^+(^2P_{3/2})]$, where $I_o[Ar^+(^2P_{3/2})]$ is the intensity of a pure $Ar^+(^2P_{3/2})$ beam prepared by photoionization at 782 Å and measured by the horizontal mass spectrometer when the horizontal gas cell was emtpy. Combining the values for $n\ell\sigma_{3/2}(H_2^+)$ and R, the value for $n\ell\sigma_{1/2}(H_2^+)$ at E_{lab} = 20 eV was found to be 10.68.

Typical values for $n\ell\sigma_m(H_2^+)[i(H_2^+)/I_T]$ in the E_{lab} range of 10-800

eV measured at 782 Å are listed in Table 1. The values for $n\ell\sigma_m(H_2^+)$ at E_{lab} = 10, 20, and 30 eV are very close to the value of 1.75. This indicates that at these collision energies, $\sigma_{3/2\to1/2}$ is negligibly small in comparison with $\sigma_{3/2\to3/2}$. As E_{lab} increases, a steady increase is seen in the value for $n\ell\sigma_m(H_2^+)$. For example, the value for $n\ell\sigma_m(H_2^+)$ at 100 eV is 2.25. Values of $X_{3/2}$ = 0.944 and $X_{1/2}$ = 0.056 at E_{lab} = 100 eV were obtained by solving the linear equations:

$$1.75\ X_{3/2} + 10.68\ X_{1/2} = 2.25 \tag{13}$$

$$X_{3/2} + X_{1/2} = 1\ , \tag{14}$$

The values for $\sigma_{3/2\to3/2}/\sigma_{3/2}(= X_{3/2})$ and $\sigma_{3/2\to1/2}/\sigma_{3/2}(= X_{1/2})$ calculated for other E_{lab} are summarized in Table 2.

Table 1 also includes the values for $n\ell\sigma_m(H_2^+)$ measured at 775 Å. Since 2/3 of the reactant Ar^+ ions formed at 775 Å are $Ar^+(^2P_{3/2})$ and 1/3 are $Ar^+(^2P_{1/2})$, the ratio of $n\ell\sigma_m(H_2^+)$ measured at 775 and 782 Å $[(n\ell\sigma_m(H_2^+;775\ Å)/[n\ell\sigma_m(H_2^+;782\ Å)]$ is related to R, $\sigma_{3/2\to3/2}$, $\sigma_{3/2\to1/2}$, $\sigma_{1/2\to1/2}$, and $\sigma_{1/2\to3/2}$ by the relation,

$$\frac{n\ell\sigma_m(H_2^+;775\ Å)}{n\ell\sigma_m(H_2^+;782\ Å)} = \frac{\frac{2}{3}\ (\sigma_{3/2\to3/2} + R\sigma_{3/2\to1/2}) + \frac{1}{3}(R\sigma_{1/2\to1/2} + \sigma_{1/2\to3/2})}{\sigma_{3/2\to3/2} + R\sigma_{3/2\to1/2}}. \tag{15}$$

Combining the relation

$$r = \frac{\sigma_{1/2\to1/2} + \sigma_{1/2\to3/2}}{\sigma_{3/2\to3/2} + \sigma_{3/2\to1/2}} , \tag{16}$$

Eq. (15) can be rewritten

$$\frac{n\ell\sigma_m(H_2^+;775\ \text{Å})}{n\ell\sigma_m(H_2^+;782\ \text{Å})} = \frac{(\frac{2}{3}+\frac{Rr}{3})\sigma_{3/2\to3/2} + (\frac{2R}{3}+\frac{Rr}{3})\sigma_{3/2\to1/2} + (\frac{1}{3}-\frac{R}{3})\sigma_{1/2\to3/2}}{\sigma_{3/2\to3/2} + R\sigma_{3/2\to1/2}} . \tag{17}$$

Dividing the numerator and denominator on the right-hand side of Eq. (17) by $\sigma_{3/2}$, we have

$$\frac{n\ell\sigma_m(H_2^+;775\ \text{Å})}{n\ell\sigma_m(H_2^+;782\ \text{Å})} = \frac{(\frac{2}{3}+\frac{Rr}{3})X_{3/2} + (\frac{2R}{3}+\frac{Rr}{3})X_{1/2} + (\frac{1}{3}-\frac{R}{3})(\sigma_{1/2\to3/2}/\sigma_{3/2})}{X_{3/2} + RX_{1/2}} . \tag{18}$$

Since R, r, $X_{3/2}$, $X_{1/2}$, $n\ell\sigma_m(H_2^+;782\ \text{Å})$, and $n\ell\sigma_m(H_2^+;775\ \text{Å})$ are known, Eq. (18) can be used to compute the value for $\sigma_{1/2\to3/2}/\sigma_{3/2}$. Assuming the validity of detailed balance, $2\sigma_{3/2\to1/2} = \sigma_{1/2\to3/2}$, Eq. (18) can further be simplified as

$$\frac{n\ell\sigma_m(H_2^+;775\ \text{Å})}{n\ell\sigma_m(H_2^+;782\ \text{Å})} = \frac{(\frac{2}{3}+\frac{Rr}{3})}{X_{3/2} + RX_{1/2}} . \tag{19}$$

In order to examine the consistency between the experimental data and the condition of detailed balance, one can either compute both $\sigma_{3/2\to1/2}/\sigma_{3/2}$ and $\sigma_{1/2\to3/2}/\sigma_{3/2}$ or compare the values for $n\ell\sigma_m(H_2^+;775\ \text{Å})$/

$n\ell\sigma_m(H_2^+;782\ \text{Å})$ and $(2/3 + Rr/3)/(X_{3/2} + RX_{1/2})$. We have adopted the latter approach. Taking into account the experimental uncertainties, the corresponding values for $n\ell\sigma_m(H_2^+;775\ \text{Å})/n\ell\sigma_m(H_2^+;782\ \text{Å})$ and $(2/3 + Rr/3)/(X_{3/2} + RX_{1/2})$ in the E_{lab} range of 10-800 eV, shown in Table 1, are found to be in good agreement. Therefore, we conclude that the experimental results are consistent with detailed balance.

Table 2 lists the values found for $\sigma_{1/2}/\sigma_{3/2}$, $\sigma_{3/2\to1/2}/\sigma_{3/2}$, $\sigma_{3/2\to3/2}/\sigma_{3/2}$, and $\sigma_{1/2\to1/2}/\sigma_{3/2}$ in the E_{lab} range of 1-4000 eV. The values for $\sigma_{1/2\to1/2}/\sigma_{3/2}$ were deduced using the known values for r, $X_{3/2}$ and $X_{1/2}$ and the condition of detailed balance, $\sigma_{1/2\to3/2} = 2\sigma_{3/2\to1/2}$. Since $\sigma_{1/2\to1/2}/\sigma_{3/2} = r-2X_{1/2}$, the value for $\sigma_{1/2\to1/2}/\sigma_{3/2}$ decreases from 1.00 at E_{lab} = 1 eV to 0.47 at E_{lab} = 3000 eV where $X_{1/2}$ reaches the maximum value of 0.26. Values for $\sigma_{3/2\to1/2}/\sigma_{3/2}$ obtained by scaling the theoretical plots shown in Figures 4 and 5 of Ref. 21 are also included in the table. The experimental values for $\sigma_{3/2\to1/2}/\sigma_{3/2}$ are approximately 40% lower than those predicted by the calculation with the inclusion of rotational couplings (RC), and slightly higher than the theoretical results obtained by neglecting rotational couplings (NR). Nevertheless, the theoretical prediction of the profile for the probability of fine-structure transitions as a function of E_{lab} is in good accord with the experimental results (Figure 5). Both the experimental and RC theoretical results show that $\sigma_{3/2\to1/2}/\sigma_{3/2}$ reaches a maximum at $E_{lab} \sim$ 2000-3000 eV.

Johnson[21] points out that the greatest uncertainty in the calcula-

Table 1. Typical values for $n\ell\sigma_m(H_2^+)$ [a] determined at E_{lab} = 20 eV [b]

E_{lab}(eV) [c]	$n\ell\sigma_m(H_2^+;782\ Å)$ [d]	$n\ell\sigma_m(H_2^+;775\ Å)$ [e]	$\frac{n\ell\sigma_m(H_2^+;775\ Å)}{n\ell\sigma_m(H_2^+;782\ Å)}$ [f]	$\frac{(3/2 + Rr/3)}{(X_{3/2} + RX_{1/2})}$ [f]
10	1.80	4.58	2.54	2.50
20	1.76	4.57	2.60	2.48
30	1.74	4.62	2.66	2.50
45	1.82	4.65	2.55	2.40
70	1.90	4.38	2.31	2.30
100	2.25	4.38	1.95	1.90
123	2.40	4.27	1.78	1.87
160	2.70	4.10	1.52	1.60
200	3.10	4.13	1.33	1.44
300	3.29	4.10	1.25	1.36
400	3.45	4.15	1.20	1.31
500	3.50	4.25	1.21	1.29
600	3.58	4.10	1.15	1.26
800	3.58	4.22	1.18	1.25

[a] $\sigma_m(H_2^+)$ is the total cross section for the reaction, $Ar^+(^2P_J) + H_2 \rightarrow Ar + H_2^+$. n is the density and ℓ is the effective length of the gas cell.

[b] The value of 20 eV for E_{lab} of the probing reaction is the difference in potential between the collision region and the horizontal gas cell.

[c] Laboratory collision energies of the reactions $Ar^+(^2P_{3/2,1/2}) + Ar(^1S_o) \rightarrow Ar(^1S_o) + Ar^+(^2P_J)$.

[d] The values for $n\ell\sigma_m(H_2^+)$ measured at 782 Å. The standard deviations due to counting statistics are $\leq$ 5%.

[e] The values for $n\ell\sigma_m(H_2^+)$ measured at 775 Å. The standard deviations due to counting statistics are $\leq$ 5%.

[f] See text and Eq. (19). R is equal to 6.10 which is the value for $\sigma_{1/2}(H_2^+)/\sigma_{3/2}(H_3^+)$ at E_{lab} = 20 eV measured with the horizontal gas cell. $r = \sigma_{1/2}/\sigma_{3/2}$. The values for $\sigma_{3/2\rightarrow 3/2}/\sigma_{3/2}(X_{3/2})$ and $\sigma_{3/2\rightarrow 1/2}/\sigma_{3/2}(X_{1/2})$ are listed in Table 2.

Table 2. Relative state-to-state total cross sections for the charge transfer reaction $Ar^+(^2P_{3/2,1/2}) + Ar(^1S_o)$ in the laboratory collision energy (E_{lab}) range of 1-4000 eV

E_{lab} (eV)	Experimental[a]				$\sigma_{3/2\to1/2}/\sigma_{3/2}$ (theoretical)[b]	
	$\sigma_{1/2}/\sigma_{3/2}$	$\sigma_{3/2\to1/2}/\sigma_{3/2}$[c]	$\sigma_{3/2\to3/2}/\sigma_{3/2}$[d]	$\sigma_{1/2\to1/2}/\sigma_{3/2}$	RC	NR
1	1.00	0.00	1.00	1.00	0.00	0.00
2	0.99	0.00	1.00	0.99	0.00	0.00
4	0.96	0.00	1.00	0.96	0.00	0.00
6	0.93	0.00	1.00	0.93	0.00	0.00
8	0.93	0.00	1.00	0.93	0.00	0.00
10	0.90	0.00	1.00	0.90	0.00	0.00
15	0.90	0.00	1.00	0.90	0.00	0.00
20	0.89	0.00	1.00	0.89	0.00	0.00
30	0.90	0.00	1.00	0.90	0.01	0.00
45	0.90	0.01	0.99	0.88	0.03	0.01
50	0.90	0.01	0.99	0.88	0.03	0.01
70	0.92	0.02	0.98	0.88	0.06	0.02
100	0.89	0.06	0.94	0.77	0.11	0.04
123	0.92	0.07[e]	0.93	0.78	0.14[f]	0.05
160	0.90	0.11	0.89	0.68	0.18	0.07
200	0.92	0.15	0.85	0.62	0.23	0.10
300	0.92	0.17	0.83	0.58	0.28	0.12

400	0.94	0.19	0.81	0.56	0.31	0.15
500	0.95	0.20	0.80	0.55	0.32	0.16
600	0.96	0.21	0.79	0.54	0.33	0.18
800	0.95	0.21	0.79	0.53	0.34	0.19
1000	0.96	0.23	0.77	0.50	0.35	0.20
1500	0.98	0.25	0.75	0.48	0.36	0.22
2000	0.97	0.25	0.75	0.47	0.36	0.24
2500	0.99	0.26	0.74	0.47	0.37	0.24
3000	0.98	0.26	0.74	0.46	0.36	0.24
4000	1.00	0.24	0.76	0.52	0.36	0.23

[a]This work. The experimental uncertainties are estimated to be $\leq$ 10%.

[b]Reference 21. RC, with rotational coupling; NR without rotational coupling.

[c]$\sigma_{3/2\to1/2}/\sigma_{3/2} = X_{1/2}$. The values for $\sigma_{1/2\to3/2}/\sigma_{3/2}$ are twice those for $\sigma_{3/2\to1/2}$ according to detailed balance.

[d]$\sigma_{3/2\to3/2}/\sigma_{3/2} = X_{3/2}$.

[e]An estimate value of 0.35 was reported in Ref. 12.

[f]A value of 0.11 was quoted in Ref. 12.

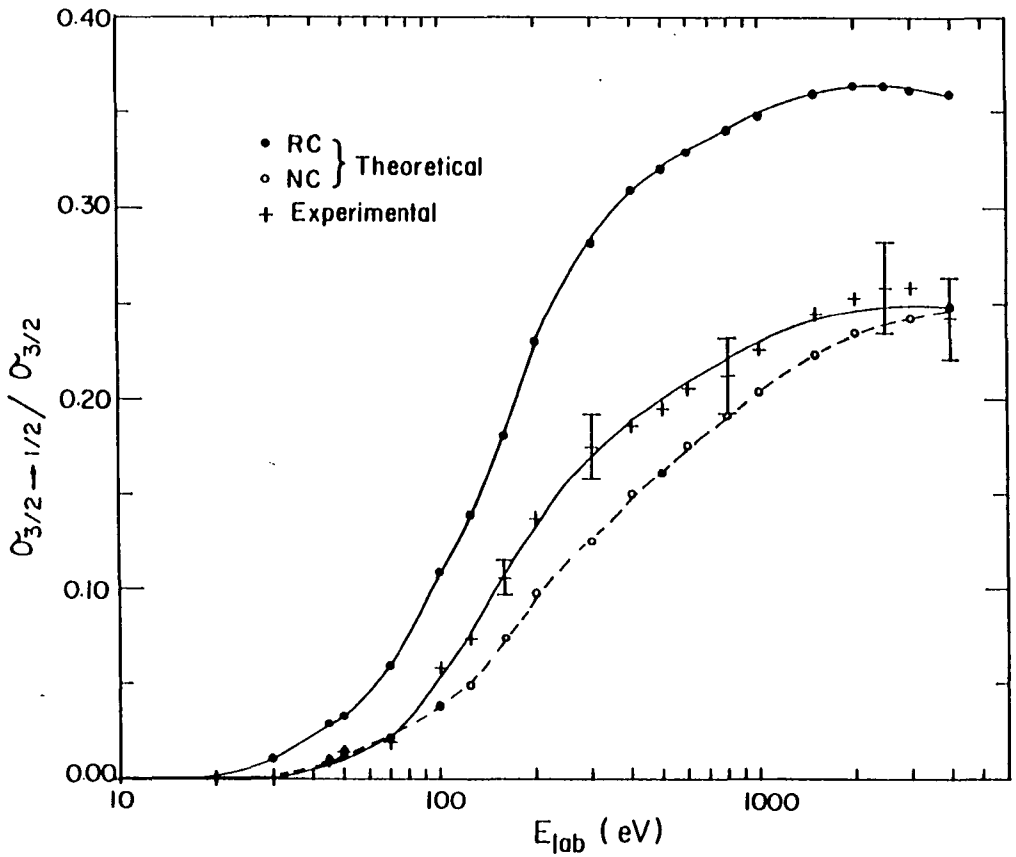

Figure 5. Values for $\sigma_{3/2 \rightarrow 1/2}/\sigma_{3/2}$ plotted as a function of E_{lab} in the range of 1-4000 eV. Experimental values: (+++). Theoretical values: (···) with rotational coupling; (ooo) without rotational coupling

tion of the cross sections is due to the potentials. An overall uncertainty of 20% in the potential for the important internuclear distances can give rise to a shift in the calculated excitation cross sections in the $\log_{10}E_{lab}$ scale by ± 0.2. In addition to the possibility of being shfited, the magnitudes of the calculated transition cross sections in the vicinity of the maximum were estimated to have an uncertainty of $\sim$ ± 20%. Since the uncertainties of the experimental results are estimated to be within ± 10%, we conclude that the RC theoretical values for $\sigma_{3/2\rightarrow 1/2}/\sigma_{3/2}$ are too high. Recent measurements[13] of the fine-structure transitions for the direct channel in the $Ar^+(^2P_J)$ + $Ar(^1S_o)$ collisions find that the RC theoretical values are higher than the experimental results by a factor of two. Since accurate ab initio potential energy curves for Ar_2^+ [51-55] are now available, a calculation using the more accurate potentials should improve the agreement with the experimental results.

As mentioned previously, the horizontal ion lens system is likely to discriminate against charge transfer product Ar^+ ions scattered out-of-plane with high kinetic energies. If these energetic product Ar^+ ions are mainly produced by the inelastic charge transfer channel, the experimental results for $\sigma_{3/2\rightarrow 1/2}/\sigma_{3/2}$ may represent a lower bound. Quantitative assessments of these effects on the value of $\sigma_{3/2\rightarrow 1/2}/\sigma_{3/2}$ can be made in a future experiment where angular and final product state distributions are measured.

The change in momentum of the captured electron, polarization ef-

fects and coupling to higher states are neglected in the calculation of Johnson. In the deduction of experimental results, we have also assumed that the only states involved are $Ar^+(^2P_{3/2})$, $Ar^+(^2P_{1/2})$, and $Ar(^1S_o)$. Although the excitations to other electronic states are expected to be small in comparison to the resonance and near resonance channels [Reactions (1)-(4)], the cross sections for the excitations to higher electronic states might be more significant at high collision energies.

Conclusion

Combining the crossed ion-neutral beam method, high resolution photoionization mass spectrometry, and charge transfer detection, we have performed a state-to-state study of the symmetric charge transfer reactions $Ar^+(^2P_{3/2,1/2}) + Ar(^1S_o)$ in the E_{lab} range of 1-4000 eV. The fine-structure effects on the charge transfer cross sections were found to be negligible at very low and very high collision energies, in accord with the theoretical expectations. The profile for the probability of fine-structure transitions as a function of E_{lab} is in agreement with the RC theoretical prediction of Johnson. However, the RC theoretical values for $\sigma_{3/2\rightarrow 1/2}/\sigma_{3/2}$ are $\sim$ 40% higher than the experimental values. Taking into account the experimental uncertainties, the experimental results are consistent with detailed balance.

This experiment has demonstrated that the charge transfer detection method is a highly sensitive method for the measurements of the

final state distributions of charge transfer product ions. The charge transfer detection method can be extended to meaure product electronic state and/or vibrational state distributions involving more than two states provided relative state-to-state cross sections for the selected probing reactions are known.

References

1. R. C. Amme and H. C. Hayden, J. Chem. Phys. 42, 2011 (1965).
2. W. H. Cramer, J. Chem. Phys. 30, 641 (1959).
3. I. P. Flaks and E. S. Solov'ev, Sov. Phys.-Tech. Phys. 3, 564 (1958).
4. J. B. Hasted, Proc. R. Soc. A205, 421 (1951).
5. R. M. Kushmir, B. M. Polynkh, and L. A. Sena, Bull. Acad. Sci. USSR, Phys. Ser. 23, 995 (1959).
6. P. Mahadevan and G. D. Magnuson, Phys. Rev. 171, 103 (1968).
7. J. B. Nichols and F. C. Witteborm, NASA Tech. Note NASA TN D-3265 (1966).
8. R. F. Potter, J. Chem. Phys. 22, 974 (1954).
9. B. Ziegler, Z. Physik 136, 108 (1953).
10. R. H. Neynabar, S. M. Trujillo, and E. W. Rothe, Phys. Rev. 157, 101 (1967).
11. K. Birkinshaw, A. J. Masson, D. Hyatt, L. Matus, I. Opauszky, and M. J. Henchman, in E. Kendrick, ed., "Advances in Mass Spectrometry" (Institute of Petroleum, London, 1968) Vol. 4, p. 379.
12. K. B. McAfee, Jr., W. E. Falconer, R. S. Hozack, and D. J. McClure, Phys. Rev. A21, 827 (1980).
13. Y. Itoh, N. Kobayashi, and Y. Kaneko, J. Phys. Soc. Japan 50, 3541 (1981).

14. K. B. McAfee, Jr., R. S. Hozack, and R. E. Johnson, Phys. Rev. Lett. 44, 1247 (1980).

15. H. Hishinuma, J. Phys. Soc. Japan 32, 227 (1972).

16. E. W. Kaiser, A. Crowe, and W. E. Falconer, J. Chem. Phys. 61, 2720 (1974).

17. F. M. Campbell, R. Browning, and C. J. Latimer, J. Phys. B14, 1183 (1981).

18. M. Henchman, in J. L. Franklin, ed., "Ion-Molecule Reactions" (Plenum, New York, 1972) Vol. 1, p. 183.

19. D. Rapp and W. E. Francis, J. Chem. Phys. 37, 2631 (1962).

20. I. Pepscu Iovitsu and N. Ionescu-Pallas, Soviet Phys.-Tech. Phys. 4, 781 (1960).

21. R. E. Johnson, J. Phys. B3, 539 (1970).

22. W. A. Chupka, in J. L. Franklin, ed., "Ion-Molecule Reactions" (Plenum, New York, 1972) Vol. 1, p. 1.

23. K. Tanaka, J. Durup, T. Kato, and I. Koyano, J. Chem. Phys. 74, 5561 (1981).

24. K. Tanaka, T. Kato, and I. Koyano, J. Chem. Phys. 75, 4941 (1981).

25. T. Kato, K. Tanaka, and I. Koyano, J. Chem. Phys. 77, 837 (1982).

26. K. Tanaka, T. Kato, P.-M. Guyon, and I. Koyano, J. Chem. Phys. 77, 4441 (1982).

27. T. Kato, K. Tanaka, and I. Koyano, J. Chem. Phys. 79, 5969 (1983).

28. F. M. Campbell, R. Browning, and C. J. Latimer, J. Phys. B14, 3493 (1981).

29. C. J. Latimer and F. M. Campbell, J. Phys. B15, 1765 (1982).

30. F. M. Campbell, R. Browning, and C. J. Latimer, J. Phys. B13, 4257 (1980).

31. S. L. Anderson, F. A. Houle, D. Gerlich, and Y. T. Lee, J. Chem. Phys. 75, 2153 (1981).

32. F. A. Houle, S. L. Anderson, D. Gerlich, T. Turner, and Y. T. Lee, Chem. Phys. Lett. 82, 392 (1981).

33. F. A. House, S. L. Anderson, D. Gerlich, T. Turner, and Y. T. Lee, J. Chem. Phys. 77, 748 (1982).

34. S. L. Anderson, T. Turner, B. H. Mahan, and Y. T. Lee, J. Chem. Phys. 77, 1842 (1982).

35. C. L. Liao, C. X. Liao, and C. Y. Ng, Chem. Phys. Lett. 103, 418 (1984).

36. C. L. Liao, C. X. Liao, and C. Y. Ng, J. Chem. Phys. in press.

37. Y. Ono, S. H. Linn, H. F. Prest, M. E. Gress, and C. Y. Ng, J. Chem. Phys. 73, 2523 (1980).

38. C. L. Liao, C. X. Liao, and C. Y. Ng, to be published.

39. The main mechanism for the production of Ar_2^+ in the wavelength region of interest here is by the direct photoionization of Ar_2 formed in the supersonic expansion. Due to the low stagnation pressure used in this experiment, the concentration of Ar_2 is negligibly small in comparison to that of Ar.

40. The entrance aperture for the horizontal gas cell is $\sim$ 0.6 cm. The distance between the collision region and the entrance aperture is $\sim$ 6 cm. As a product of Ar^+ ion arrives at the horizontal gas cell and the transverse distance resulted from the transverse velocity component is less than 0.3 cm, it is considered to be collected. For the Ar^+ ions initially scattered at a laboratory angle of 4° with a kinetic energy of 5 eV moving towards grid 3 and an extraction electrostatic field of 10 V/cm, the time required for these ions to reach the horizontal gas cell is estimated to be $< 4.7 \times 10^{-6}$ sec. In arriving at the latter value, we have assumed that the Ar^+ ions traveled through the region between grid 3 and the horizontal gas cell with an average kinetic energy of $\sim$ 50 eV. The transverse velocity of the Ar^+ ions is $\sim 3.4 \times 10^4$ cm/sec. Therefore, the corresponding transverse distance is $\sim$ 0.16 cm. Since this value is substantially less than 0.3 cm, the collection efficiency for these energetic ions is expected to be excellent. In the worst case when the Ar^+ ions are scattered towards grid 1 with a kinetic energy of 5 eV, the ions will first be stopped by the extraction field and will then be accelerated towards the horizontal gas cell. The traveling time for the ions to arrive at the horizontal gas cell is $\sim 8.8 \times 10^{-6}$ sec. Thus, a transverse distance of $\sim$ 0.30 cm is expected. The fact that this latter value is equal to the radius of the aperture of the horizontal gas cell indicates that the extraction field of 10 V/cm is still adequate for the collection of product Ar^+ scattered towards grid 1. The above consideration has not taken into account the focusing effect of the horizontal ion lenses.

41. Since the transmissions through the vertical and the horizontal mass spectrometers are different, this number must be considered to be a crude estimate.

42. K. Tanaka, T. Kato, and I. Koyano, Chem. Phys. Lett. 97, 562 (1983).

43. This value has been corrected for background H_2^+ ion formed at the collision region.

44. J. A. R. Samson and R. B. Cairns, Phys. Rev. 173, 80 (1968).

45. Similar measurements were made by Comes and Salzer (F. J. Comes and H. G. Salzer, Z. Naturforsch. 192, 1230 (1964). Samson and Cairns (Ref. 44) pointed out that the results of Comes and Salzer were suffered from the discrimination of the lower-energy electron group.

46. D. C. Frost, C. A. McDowell, and D. A. Vroom, Proc. R. Soc. (London) 296, 566 (1967).

47. D. W. Turner and D. P. May, J. Chem. Phys. 45, 471 (1966).

48. J. W. Rabalais and J. P. Debies, Electron Spectrosc. and Related Phenomena 5, 847 (1974).

49. R. E. Johnson, J. Phys. Soc. Japan 32, 1612 (1972).

50. G. Herzberg, "Molecular Spectra and Molecular Structure, 1. Spectra of Diatomic Molecules" (Van Nostrand Reinhold, New York, 1950).

51. S. Sinha and J. N. Bradsley, Phys. Rev. A 14, 104 (1976).

52. W. J. Stevens, M. Gardner, P. Julienne, and A. Karo, J. Chem. Phys. 67, 2860 (1977).

53. T. L. Gilbert and A. C. Wahl, J. Chem. Phys. 55, 5247 (1971).

54. V. Sidis, M. Barat, and D. Dhuicq, J. Phys. B8, 474 (1975).

55. W. R. Wadt, J. Chem. Phys. 68, 402 (1978).

GENERAL SUMMARY

Photoionization efficiency studies of high temperature vapors (S_2, Hg_2, HgKr, HgXe) have been performed using the supersonic oven beam method. These studies have yielded precise values of ionization energies (IE). The measured appearance energy (AE) for the dissociative ionization process, combined with the IE's of S_2 and S, allow the calculations of the dissociation energies (D_o) of S_2^+ and S_2. Two Rydberg series converging to the $\tilde{b}^4\Sigma_g^-$ state of S_2^+ have been observed. Window resonances resolved in the region of 650-850 Å have been assigned as members of Rydberg series converging to the $\tilde{c}^4\Sigma_u^-$ and $^2\Pi_u$ (or $^2\Sigma_u^-$) states of S_2^+, respectively.

Using the measured IE's of HgM (M = Hg, Kr, Xe), the known D_o's of HgM and the IE of Hg, D_o's of HgM^+ have been deduced. By analyzing the shifts in energy between corresponding autoionization peaks observed in the M^+ and HgM^+ spectra, and by assuming the charge induced-dipole interaction to be the dominant interaction at the equilibrium bond distance for HgM, the equilibrium bond distances have been deduced. These values are in excellent agreement with values determined by spectroscopic studies.

A new ion-neutral reaction apparatus, which combines high resolution photoionization mass spectrometry, crossed ion-neutral beam method and charge transfer detection, has been used to examine the energy effects on the total charge transfer cross sections for the reaction

$H_2^+ + H_2$. The vibrational energy dependences for total charge transfer cross sections in the kinetic energy range of $E_{c.m.}$ = 8-200 eV have been found to be in good agreement with calculations based on the semi-classical trajectory formulation. The vibrational energy effects on charge and proton transfers at low collision energies have been directly observed. The observations are in accord with qualitative predictions based on the accessibility of the avoided crossing seam on the ground state potential energy surface and trajectory surface hopping calculation. The kinetic energy dependences for total charge transfer cross sections ($\sigma_{v_o'}(H_2^+)$, v_o' = 0 and 1) show broad peaks at $E_{c.m.} \approx 35$ and 16 eV, respectively. These broad features are attributed to the strongly coupled multistate nature in the dynamics of charge transfer reaction. The vibrational state distributions of product $H_2^+(v'')$ in collision energy range $E_{c.m.}$ = 2-16 eV have been probed by the charge exchange method. When reactant H_2^+ ions are prepared in v_o' = 0, the majority (> 80%) of product $H_2^+(v'')$ ions are formed in v'' = 0. The vibrational relaxation channel for forming $H_2^+(v'' = 0)$ is found to be more efficient than the vibrational excitation for producing $H_2^+(v'' = 1)$ in the $H_2^+(v_o' = 1) + H_2(v_o'' = 0)$ charge transfer collisions. A better agreement between experiment and theoretical calculation is observed at $E_{c.m.}$ = 16 eV. The discrepancy observed at $E_{c.m.}$ = 8 eV with v_o' = 1 might be due to the neglect of the $H_3^+ + H$ channel in the theoretical study.

A state-to-state study of the symmetric charge transfer reactions

$Ar^+(^2P_{3/2,1/2}) + Ar(^1S_o)$ in the energy range of E_{lab} = 1-4000 eV has been performed. The kinetic energy dependence for the probability of fine-structure transitions ($^2P_{3/2} \rightarrow {}^2P_{1/2}$) in $Ar^+(^2P_{3/2}) + Ar(^1S_o)$ charge transfer collisions is in general agreement with the theoretical prediction. However, the theoretical probabilities are $\sim$ 40% higher than the experimental values. The fine-structure effects on the charge transfer cross sections are found to diminish at both low and high collision energies, in accordance with the theoretical expectations. Taking into account the experimental uncertainties, the experimental results are consistent with detailed balance which requires the value for the state-to-state charge transfer cross sections $\sigma_{1/2\rightarrow 3/2}$ to be twice that for $\sigma_{3/2\rightarrow 1/2}$ at collision energies substantially greater than the spin-orbit splitting of Ar^+.

The experiments have demonstrated that the charge transfer detection method is a highly sensitive method for measurements of final state distributions of charge transfer product ions.

REFERENCES

1. J. Berkowitz, "Photoabsorption, Photoionization, and Photoelectron Spectroscopy" (Academic, New York, 1979).

2. C. Y. Ng, in I. Prigogine and S. A. Rice, eds., "Advances in Chemical Physics" (Wiley, New York, 1983) Vol. 52, p. 263.

3. G. V. Marr, "Photoionization Process in Gases" (Academic Press, New York, 1967).

4. P. W. Dehmer and W. A. Chupka, J. Chem. Phys. 65, 2243 (1906).

5. M. G. Liverman, S. M. Beck, and R. E. Smalley, J. Chem. Phys. 70, 192 (1979).

6. G. R. Parr and J. W. Taylor, Rev. Sci. Instrum. 44, 1578 (1973).

7. G. R. Parr and J. W. Taylor, Int. J. Mass Spectrom. Ion Phys. 14, 467 (1974).

8. C. Y. Ng, B. H. Mahan, and Y. T. Lee, J. Chem. Phys. 65, 1965 (1976).

9. C. Y. Ng, D. J. Trevor, B. H. Mahan, and Y. T. Lee, J. Chem. Phys. 65, 4327 (1976).

10. C. Y. Ng, D. J. Trevor, B. H. Mahan, and Y. T. Lee, J. Chem. Phys. 66, 446 (1977).

11. C. Y. Ng, P. W. Tiedemann, B. H. Mahan, and Y. T. Lee, J. Chem. Phys. 66, 3985 (1977); 66, 5737 (1977).

12. C. Y. Ng, D. J. Trevor, P. W. Tiedemann, S. T. Ceyer, P. L. Kronebush, B. H. Mahan, and Y. T. Lee, J. Chem. Phys. 67, 4235 (1977).

13. G. G. Jones and J. W. Taylor, J. Chem. Phys. 68, 1768 (1978).

14. W. M. Trott, N. C. Blais, and E. A. Walter, J. Chem. Phys. 69, 3150 (1978); 71, 1692 (1979).

15. S. T. Ceyer, P. W. Tiedemann, B. H. Mahan, and Y. T. Lee, J. Chem. Phys. 70, 14 (1979).

16. S. T. Ceyer, P. W. Tiedemann, C. Y. Ng, B. H. Mahan, and Y. T. Lee, J. Chem. Phys. 70, 2138 (1979).

17. P. W. Tiedemann, S. L. Anderson, S. T. Ceyer, T. Hirooka, C. Y. Ng, B. H. Mahan, and Y. T. Lee, J. Chem. Phys. 71, 605 (1979).

18. M. E. Gress, S. H. Linn, Y. Ono, H. F. Prest, and C. Y. Ng, J. Chem. Phys. 72, 4244 (1980).

19. Y. Ono, S. H. Linn, H. F. Prest, M. E. Gress, and C. Y. Ng, J. Chem. Phys. 73, 2523 (1980).

20. Y. Ono, S. H. Linn, H. F. Prest, C. Y. Ng, and E. Miescher, J. Chem. Phys. 73, 4855 (1980).

21. S. L. Anderson, T. Hirooka, P. W. Tiedemann, B. H. Mahan, and Y. T. Lee, J. Chem. Phys. 73, 4779 (1980).

22. Y. Ono, S. H. Linn, H. F. Prest, M. E. Gress, and C. Y. Ng, J. Chem. Phys. 74, 1125 (1981).

23. Y. Ono, E. A. Osuch, and C. Y. Ng, J. Chem. Phys. 74, 1645 (1981).

24. S. H. Linn, Y. Ono, and C. Y. Ng, 74, 3342, 3348 (1981).

25. Y. Ono and C. Y. Ng, J. Chem. Phys. 74, 6985 (1981).

26. J. Erickson and C. Y. Ng, J. Chem. Phys. 75, 1650 (1981).

27. S. H. Linn, J. M. Brom, Jr., W. B. Tzeng, and C. Y. Ng, J. Chem. Phys. 78, 37, 50 (1983); 82, 648 (1985).

28. H. S. W. Massey and R. A. Smith, Proc. R. Soc. London Ser. A 142, 142 (1933).

29. O. B. Firsov, J. Exp. Theor. Phys. U.S.S.R. 21, 1001 (1951).

30. H. S. W. Massey and E. H. S. Burhop, "Electronic and Ion Impact Phenomena" (Oxford University, Oxford, 1952).

31. A Dalgarno and H. N. Yadav, Proc. Phys. Soc. London Ser. A 66, 173 (1953).

32. D. R. Bates, H. S. W. Massey, and A. L. Stewart, Proc. R. Soc. London Ser. A 216, 436 (1953).

33. E. F. Gurnee and J. L. Magee, J. Chem. Phys. 26, 1237 (1957).

34. D. R. Bates and R. McCarrol, Proc. R. Soc. London Ser. A 245, 175 (1958).

35. I. Popescu-Iovitsu and N. Ionescu-Pallas, Soviet Phys.-Tech. Phys. 4, 781 (1960).

36. D. Rapp and W. E. Francis, J. Chem. Phys. 37, 2631 (1962).

37. D. R. Bates and R. McCarroll, Philos. Mag. Suppl. 11, 39 (1962).

38. D. R. Bates, "Atomic and Molecular Processes," ed. by D. R. Bates (Academic, New York, 1962).

39. F. J. Smith, Phys. Lett. 20, 271 (1966).

40. F. J. Smith, Planet. Space Sci. 14, 929 (1966).

41. R. A. Mapleton, "Theory of Charge Exchange" (Wiley-Interscience, New York, 1972).

42. J. J. Leventhal, T. F. Moran, and L. Friedman, J. Chem. Phys. 46, 4666 (1967).

43. D. R. Bates and R. H. G. Reid, Proc. R. Soc. London Ser. A 310, 1 (1969).

44. R. N. Stocker and H. Neumann, J. Chem. Phys. 61, 3852 (1974).

45. K. J. McCann, M. R. Flannery, J. V. Hornstein, and T. F. Moran, J. Chem. Phys. 63, 4998 (1975).

46. T. F. Moran, M. R. Flannery, and D. L. Albritten, J. Chem. Phys. 62, 2869 (1975).

47. C. Y. Lee and A. E. DePristo, J. Chem. Phys. 80, 1116 (1984).

48. I. Koyano and K. Tanaka, J. Chem. Phys. 72, 4858 (1980).

49. S. L. Anderson, F. A. Houle, D. Gerlich, and Y.-T. Lee, J. Chem. Phys. 75, 2153 (1981).

50. W. A. Chupka, "Ion-Molecule Reactions," ed. by J. L. Franklin (Plenum, New York, 1972), Vol. 1, p. 33.

51. F. M. Campbell, R. Browning, and C. J. Latimer, J. Phys. B 14, 3493 (1981).

52. W. A. Chupka and J. Berkowitz, J. Chem. Phys. 48 5226 (1968).

53. W. A. Chupka and J. Berkowitz, J. Chem. Phys. 51, 4244 (1969).

54. J. Berkowitz and W. A. Chupka, J. Chem. Phys. 51, 2341 (1969).

55. P. M. Dehmer and W. A. Chupka, J. Chem. Phys. 65, 2243 (1976).

ACKNOWLEDGMENTS

I would like to express my deepest appreciation to Professor C.-Y. Ng for his support, understanding, and assistance throughout the course of this research. His physical insight, encourgement, and patience have made my graduate studies to be one of the most exciting and fruitful periods of time in my life. I am indebted to Mr. C.-X. Liao for his skillful assistance, advice and helpful suggestions during the last two years. I would also like to thank my many colleagues, Dr. S. H. Linn, Dr. Y. Ono, Dr. H. F. Prest, Mr. W.-B. Tzeng, Mr. J.-D. Shao and Mr. R. Xu for their assistance, friendship, and enlightening discussion.

Sincere thanks to the members of many service groups at Ames Laboratory, and special thanks to E. Ness, G. Steinbrenner and J. Sauke of the Chemistry Department Machine Shop.

Finally, I would like to thank my wife Lisa for her love, support and deep understanding and encouragement.